# Determination of nuclear forensic signatures from lead ratios and REEs in uranium ore samples using ICP-MS and LIBS

**D Madzunya**

**orcid.org/0000-0001-5221-7787**

Dissertation accepted in fulfilment of the requirements for the degree *Master of Science in Applied Radiation Science and Technology* at the North-West University

Supervisor: Prof M Mathuthu

Co-supervisor: Miss ND Mokhine

Graduation: May 2021

Student number: 24791679

**DECLARATION**

I, Dakalo Madzunya, hereby declare that this dissertation is the result of my investigation and that this has not been submitted in part or full for any other degree at any other University. Any information taken from other sources have been referenced.

Student Signature: 

Student number: 24791679

**Acknowledgements**

Firstly, I would like to acknowledge the Almighty God who has given me wisdom, health and power to conquer life's difficulties without Him this study would not have been possible. My heartfelt thanks go to my mom and dad, who have stood by me through their financial support, prayers, emotional and moral support. They never stopped quoting the scriptures from the Bible to motivate me not to give up, but to continue working on my studies. I will never forget my sisters and grandma for their endless prayers and encouragement. My appreciation goes to my best friend Bongumusa Thabethe for always forcing me to work on my thesis, even when I did not feel like it.

I would like to express my sincere gratitude to Prof. Mathuthu, my supervisor, for the immense effort he has put in place to help me through my studies, and for not giving up on me, without his support, this work could not have been possible. Many thanks go to Ms Dikeledi Mokhine for her technical assistance during the ICP-MS sample analysis of all my samples and to Vera Uushona for assisting with the statistical analysis. I also extend my thanks to Prof Damian Onwudiwe who gave me access to use the laser equipment at the Chemistry Department.

I would also like to acknowledge the CSIR/DSI inter-bursary support and the Faculty of Natural and Agricultural Sciences for supporting my research, the completion of this study would not have been possible without funding.

Finally, I would also like to express my gratitude to the Center for Applied Radiation Science and Technology at North-West University for allowing me the opportunity to do my research at their facility.

**Abstract**

The aim of this study was to determine nuclear forensic signatures from lead ratios and resolve rare earth elements (REE) signatures in uranium samples and water using inductively coupled plasma mass spectroscopy (ICP-MS) and laser induced breakdown spectroscopy (LIBS), as well as comparing resolved REEs and lead isotopic ratios from South Africa with the Namibian results.

A set of water samples were collected from underground in the Namibian area and another set of uranium ore samples were collected in the mine tailings from both South Africa and Namibia. The uranium ore samples were digested in a microwave and diluted with distilled water. Both the water and uranium ore samples were analyzed using the ICP-MS and LIBS. For ICP-MS, the instrument was set to isotopic ratio method, operated in the collision mode for mass energy discrimination and filtration against interferences and it was also set to total quantitative method to analyze REEs. For LIBS, no sample preparation was required so the sample was directly ablated by the laser to analyze REEs. Principal component analysis (PCA) was performed using the results obtained from both techniques in order to identify patterns in the samples.

Enriched light rare earth elements and depleted heavy rare earth elements were exhibited in both samples analyzed using the LIBS and ICP-MS. $^{206}Pb/^{204}Pb$ isotope ratio was greater than 20 thus, indicating a uranium rich ore. However, lead ratios from South Africa exhibited a uranium rich ore compared to lead ratios of Namibia. The PCA displayed identical patterns for samples analyzed by ICP-MS whereas distinct patterns were observed in the samples analyzed by LIBS.

These characteristics can be used as a fingerprint and this study will promote and improve nuclear safety in the fight against theft of nuclear material, thereby promoting the non-violent use of nuclear material. That is why nuclear forensic signatures of uranium or nuclear materials need to be established and stored in a nuclear forensic library database.

# Table of Contents

**List of figures**

**List of tables**

**List of Abbreviations**

| | |
|---|---|
| REE | Rare earth element |
| LREE | Light rare earth element |
| HREE | Heavy rare earth element |
| IAEA | International Atomic Energy Agency |
| ICP-MS | Inductively coupled plasma mass spectroscopy |
| LIBS | Laser induced breakdown spectroscopy |
| PCA | Principal component analysis |
| NIST | National Institute of Standard and Technology |
| NPT | Non-proliferation treaty |
| PUREX | Plutonium and uranium extraction |
| TIMS | Thermal ionization mass spectrometry |
| GPS | Global positioning system |
| NNFL | National nuclear forensic library |
| NFL | Nuclear forensic library |
| NFKMS | Nuclear forensics knowledge management |
| ISL | In-situ leaching |
| MC-ICP-MS | Multi-collector inductively coupled plasma spectroscopy |
| SEM | Scanning electron microscopy |
| XRD | X-ray diffraction |

| | |
|---|---|
| LASER | Laser amplification by simulated emission of radiation |
| DDG | Digital delay generator |
| PPM | Parts per minute |
| CCD | Charge coupled device |
| CSIR | Council for scientific and industrial research |

# Chapter 1: Introduction and Problem statement

## 1.1 Background

At the beginning of the 1990s, a kilogram of highly enriched uranium (HEU) was costly to produce within the framework of a well-established enrichment program, resulting in theft and sale of developed nuclear materials. Since then, cases of nuclear materials trafficking have been reported and these incidents continued to increase gradually, therefore the science of nuclear forensics began to develop with the aim of determining the origin of any nuclear materials found (Reading, 2016, Mayer et al., 2005). Nuclear forensic is a scientific discipline, which has been evolving for about few decades. The purpose of nuclear forensics is to assist criminal investigations of nuclear material or other radioactive material to determine the origin or proposed use of the material confiscated.

The investigated material is usually nuclear material such as yellowcake ($U_3O_8$), uranium and plutonium (Glossary, 2002). Nuclear forensics focuses primarily on the analysis of measurable or characteristic parameters referred to as nuclear forensic signatures or fingerprints. In this study, these parameters refers to lead isotopic ratios and rare earth elements patterns. These parameters will be determined by inductively coupled plasma spectrometry (ICP-MS) and laser induced breakdown spectrometry (LIBS). Many of the techniques used in nuclear forensics are based on techniques that are frequently used in geology or in other fields such as age dating and rare earth elements analysis (Cheong et al., 2015, Lobato et al., 2015). The purpose of this research is to identify nuclear forensic signatures of uranium ore samples from two uranium mines in South Africa and Namibia and to differentiate REE signatures or fingerprints or patterns using statistical analysis such as principal component analysis (PCA) and dendrogram clusters. All these concepts will be discussed further in the next sections of this study.

### 1.1.1 Historical Background

In, 1938 the theoretical description invented by Lise Meitner and Otto Frisch was that the neutron irradiation divides the uranium atom into two nuclei of approximately identical size and that energy is released in the process (Vesterlund, 2019). Fission was invented and soon after that, it was found that a chain reaction could be caused by the neutrons formed in the fission. Rudolf Peierls and Otto Frisch wrote a paper in 1940 on the probability of establishing "super bombs" using uranium enriched in $^{235}U$ (Arnold, 2003), and the first nuclear experiment, called the "Trinity" experiment, was carried out on July 16, 1945. Shortly thereafter, the atomic bombs over

Hiroshima and Nagasaki followed. Then, the Soviet Union implemented the nuclear weapons technology in 1949, after technical information on the structure of the atomic bomb leaked to the Soviet Union and then the nuclear missiles became a part of the cold war (Vesterlund, 2016).

In 1957, IAEA was established following the "Atoms for Peace" initiative by the 34$^{th}$ president of the United States (Dwight D. Eisenhower) to promote the peaceful use of nuclear energy and to obstruct the use of nuclear material for military intentions (Arnold, 2003). The goal was that the IAEA would function as a nuclear material repository. This safety measure organization was formed to make sure that nuclear material did not fall into the wrong hands. Nevertheless, the cold war prohibited the execution of the IAEA as a nuclear material protector. While nuclear technology was spreading around the planet for peaceful uses, nuclear weapons technology was also distributed (IAEA, 2015a). Five nations around the world had nuclear weapons technology by 1968 and in addition, performed nuclear weapons experimental tests. It became evident that it was necessary to stop the spread of this skill and technology so the nuclear Non-Proliferation Treaty (NPT) came into force in 1970 (Mayer and Glaser, 2015).

Few countries created and tested nuclear weapons after the execution of the NPT. There were immediately three new nuclear weapons nations after the Soviet Union separation. Furthermore, these three nations namely, Belarus, Kazakhstan and Ukraine, (Reed and Stillman, 2010), shortly moved their nuclear weapons inventory to the Russian Federation. However, following the Soviet Union's separation, seizures of illicit radioactive and nuclear material at borders began to rise quickly. Between 1993 and 2011, the IAEA reported over 2150 cases involving illicit trafficking of radioactive material. Over 400 of these cases were involved with depleted uranium, natural uranium or low-enriched uranium, and about 16 were involved with highly-enriched uranium and plutonium (Hutcheon et al., 2013).

Countries such as Namibia, South Africa, Egypt and others, export uranium ore for additional processing into fuel for the nuclear reactor. All these countries comply with the Non-Proliferation treaty which (Mathuthu and Khumalo, 2017) seeks to safeguard nuclear materials and to deter nuclear terrorism as a result of the illegal trafficking of materials. South Africa was able to process, enrich its own uranium and it had a nuclear program (Albright, 1994, Mathuthu and Khumalo, 2017). This program then ended after the end of cold war when it signed an agreement to the Nuclear Non-Proliferation Treaty (NPT) on July 10, 1991 (Initiative, 2016).

### 1.1.2 Nuclear forensics

For nearly 60 years, nuclear material has been kept under strict control. The IAEA safeguards agencies in each country (e.g. NECSA in South Africa), have the primary duty to ensure that government retains accountability for its nuclear material inventory. Nevertheless, cases have occurred where nuclear material has been discovered out of regulatory control (Wallenius et al., 2006, Wallenius et al., 2007). Trafficking was the key element, however there have been cases, where nuclear material theft was also reported While the organisation of safeguards is intended to avoid incidents concerning nuclear material, it is also necessary to enforce charges on people who have unlawfully handled nuclear material (UNSCR, 2004). Legal cases may have two goals, namely deterrence and retribution. Deterrence is directed at both citizens and the state. The complicated processing of nuclear material makes the involvement of the state and the state information of the existence of nuclear material production unavoidable. The seizure of nuclear material identified outside regulatory control would mean that the state has failed to comply with international nuclear material law. This strengthens the state's willingness to control nuclear materials and thus prevent both carelessness and proliferation. In order to help in such legal cases, it is necessary for forensics to enhance existing evidence focused on the information obtained from nuclear material.

Investigations of nuclear forensic may be grouped into the following components:

#### 1.1.2.1 Categorization

According to (IAEA, 2006), categorization is used to deal with threat caused by a certain case. The purpose of this is to define the security threat to first victims and the public and to assess if the event is part of illegal activity or a danger to national security. The interception of uranium at a border control is an illustration of categorization. At this point, the categorization carried out may include gamma spectrometric measurements of the substance identified. Assessing uranium enrichment will include details on how to continue with confiscation or even whether a crime was committed.

#### 1.1.2.2 Characterization

Characterization determines certain features of the material. Crucial nuclear forensic features involve isotope, elementary composition and physical characteristics. Based on the sample size (Ramebäck et al., 2012), the isotopic composition analysis may be performed using alpha or

gamma spectrometry or any of the mass spectrometric techniques such as Inductively coupled plasma mass spectrometry (ICP-MS). The isotopic composition contains information on the intended use of nuclear material, but it can also indicate whether the material is being recycled (Zsigrai et al., 2015). Elemental composition, or impurity assessment, is the measurement of remaining metal impurities and can be used to describe the nuclear material production process or the geographical origin of the source material (Button et al., 2013, Varga et al., 2010b). This can be performed by laser induced breakdown spectroscopy (LIBS) and ICP-MS. Physical characterization is used to describe the grain size or chemical stage of a material and is primarily conducted using surface characterization methods such as scanning electron microscopy (SEM) and X-ray diffraction (XRD) but also other fundamental methods such as weight and density measurements (Sweet et al., 2013). The age of a nuclear material, especially the time that has passed since the last chemical separation of isotopes, is another helpful characteristic (Gehrke et al., 2000, Eppich et al., 2013, Varga et al., 2011).

#### 1.1.2.3 Nuclear Forensic Interpretation

In addition to the analysis of nuclear and other radioactive materials, another crucial part of nuclear forensics is the interpretation of analytical results. Nuclear forensic analysis can be broken down into two groups; relative and prognostic analysis (Hutcheon et al., 2013). Based on the question, a measuring technique can be used for relative and prognostic analysis. The relative analysis may be used to answer the questions "Do these materials have the same origin?" or "Does this material correlate to any material in the database or to any material we know about?" On the contrary, the prognostic analysis can be used to identify the material's origin and proposed use. For instance, the isotopic composition can be used to compare various samples to see if they are likely to come from the same place, nevertheless the composition could also be used to describe the material's proposed use and perhaps the production process (Mayer and Glaser, 2015). Hence, the nuclear forensic interpretation is used to relate materials and incidents with each other as well as to determine the purpose of the nuclear safety cases.

### 1.1.3 National nuclear forensics libraries (NNFL)

The IAEA has suggested that each member States develop a national record of nuclear material and radioactive sources to certify that nuclear material and radioactive sources are distinguishable and traceable, or where this is not feasible, certify that there are alternative processes to detect and

trace sources (IAEA, 2015). Nuclear forensics knowledge management systems (NFKMS) is a term that tackles these problems, ranging from experts to databases providing data of regional nuclear and other radioactive materials, sometimes referred to as the national nuclear forensics libraries (NNFL) (IAEA, 2019). The library's purpose is to provide data to determine the origin and history of radioactive or nuclear material that has been taken from regulatory control, to promote nuclear safety and non-proliferation. A library may be used to determine the probability that, for example, a seized nuclear material originates from the country in which it is found or it belongs to another country (IAEA, 2018). The library may contain information on analysis, which can be used to compare data from nuclear forensic investigations analysis, as well as the producer's information.

### 1.1.4 Cases of Illicit trafficking of nuclear materials

The first cases of nuclear smuggling took place in Switzerland and Italy in 1991 (Švedkauskaite-LeGore et al., 2007). Thereafter a rapid increase of nuclear or radioactive materials incidents around central Europe followed (Wallenius et al., 2006).

This first incident was also preceded by a few other cases. Most materials were seized in central and eastern European countries and most cases of the seizures were related to the former Soviet Republics. In 1994, 560 g of weapons-usable Pu (87% $^{239}$Pu) mixed with low enriched uranium was seized at Munich airport together with 210 g Li-metal (Wallenius et al., 2007) and in 1994-1995 seizures of highly enriched uranium powders were reported in the Czech Republic (Wallenius et al., 2006). Afterwards, incidents involving uranium and plutonium bearing material continued, but on a smaller scale (Krajko, 2016, Straub et al., 2020).

### 1.1.5 Nuclear forensics signatures

Nuclear forensic signatures are a set of data features of a particular sample of nuclear or other radioactive material capable of identifying the sample as consistent with, or inconsistent with, specific nuclear or other radioactive material used, produced or stored in a country. Such signatures can help to determine the processes that produced the material and its history (Reading, 2016).

Each nuclear material carries a signature of the materials from which it was made or the process to which it was exposed. Such signatures may be related to chemical processes (such as extraction, ion exchange, precipitation), or may be due to physical processes. They can also be

from source material inherited. For instance, signature can be made up of isotopic composition, chemical impurities, age and morphology (Mayer et al., 2011).

Three kinds of signatures exist, which are chemical, physical and radiological. The decision to use them relies on the type of substance you are investigation. There is chemical signatures which refers to signatures associated with their geological origin or their process of production. The next signature is a physical signature related to the process of handling, use or production. Radiological signature gives rise to essential details regarding the origin, in case of minerals, nuclear reactors, and isotope enrichment plants and reprocessing plants (Sarkis and Rosa, 2011). More details on these nuclear forensic signatures will be discussed in Chapter 2.

## 1.2 Problem statement

There were a couple of incidents that took place a while ago, such as, the seizures of uranium yellowcake in August 2011 in Namibia, uranium yellowcake from a Sierra Leonean attempting to sell it to Iran in August 2013 and a kilogram of uranium in Durban which raised concerns over a surge of yellowcake trafficking and uranium yellowcake in Africa. (Mutua, 2015) speculates that the increase in trafficking of these nuclear materials in Africa could be attributed to social-economic conditions, which may have created unsophisticated smugglers motivated by profit but unaware of the inconsiderable financial benefits associated with the scale of primary uranium products.

Although recent seizures containing inconsiderable amounts of yellowcake, such as 1 kg of uranium yellowcake seizure in the November 2013 Durban incident, do not appear to pose a severe danger to proliferation and there is, however, the possibility that the trivial quantities of yellowcake being smuggled may be accumulated to obtain a large stock for the development of nuclear weapons (Zwane, 2018). Even then, the probability of non-state actors seeking the tedious path of conversion-enrichment-manufacturing yellowcake in obtaining crude nuclear weapons seems minimal.

Such incidents related to nuclear security are mostly linked to the end of the cold war and the fallout of the former Soviet Union, leaving important nuclear manufacturing and research facilities in the successor countries without proper regulation and security measures (Moody et al., 2014).

In general, radioactive materials such as actinides are held under strict physical supervision with constant monitoring, but the malicious intent of the outlaws cannot be excluded. It is important to control the presence of radiation-emitting materials in various biological and environmental samples, because they are hazardous to human health even though they enter the human body at extremely low levels (Aggarwal, 2016).

Critically developing signatures for a certain nuclear or radioactive material that are then kept in a nuclear forensics library (NFL) can be used to resolve nuclear security cases. A national library of nuclear forensics maintains a record of nuclear or radioactive material generated by a nation. This data helps in discriminating nuclear or radioactive material according to each other's characteristics and the library includes data on how the material was produced, how it is deposited and how it is designed to be used, it makes it simpler to resolve instances of illegal nuclear material use (Mathuthu and Khumalo, 2017).

South Africa and Namibia are major exporters of uranium yellowcake. Hence, there is a need to develop nuclear signatures in case of interdictions of nuclear material. Rare earth elements (REE) and lead isotopic ratios are normally used as signatures. The data obtained from these REE and lead isotopic ratios may be used as nuclear fingerprint for source attribution. This analysis proves to be a strong analytical tool that can help resolve nuclear security and non-proliferation problems.

One of the tactics used to prevent illicit trafficking of nuclear material is by the identification and characterization of nuclear material by each nation and compiling that data in the nuclear forensic library (Fuchs et al., 2016).

This study is focused mainly in determining nuclear forensics signatures such as the isotopic ratios, elemental composition and rare earth elements (REE) in uranium samples found in uranium mines in South Africa and Namibia using inductively coupled plasma mass spectroscopy (ICP-MS) and laser induced breakdown spectroscopy (LIBS).

## 1.3 Aim and objectives

### 1.3.1 Aim

The aim of this study was to determine nuclear forensic signatures from lead isotopic ratios and rare earth elements in uranium ore samples from Namibia and South Africa using Perkin Elmer

NexION 2000 inductively coupled plasma mass spectrometry (ICP-MS) and (EKSPLA NT342B-SH-10-AW, Lithuania) Q-switched Nd:YAG laser induced breakdown spectroscopy (LIBS).

### 1.3.2 Objectives

The objectives of the research are to:

- Identify the rare earth elements and elemental composition in uranium ore from South Africa and Namibia using ICP-MS and LIBS.
- Determine lead isotopic ratios in uranium ore from South Africa and Namibia using ICP-MS.
- Resolve the nuclear forensic signatures from REE and lead isotopic ratios results.
- Compare the results obtained from ICP-MS and LIBS.

## 1.4 Study area and justification

The study area is located near the West Wits line (Far West Rand) in South Africa's Gauteng province, near Carletonville, about 70 km southwest of Johannesburg. This ranges from latitude 26 ° 18 'S-26 ° 26 'S to longitude 27 ° 23'E-27 ° 31'E. The area's gold discovery dates back to 1898. This area is part of the Witwatersrand Basin, the world's largest gold and uranium mining basin covering an area of 1,600 $km^2$ (Winde and Stoch, 2010). The basin has produced some 400 $km^2$ of mine tailings dams consisting 6 billion tons of pyrite tailings and 600 000 tons of low-grade uranium (Winde and Stoch, 2010). The study area has certain shaft systems with surface reserves defined by rock dumps and mine tailings that have been gathered everywhere in the mine's operating history. The mine tailings studied in this research are shown in Figure 4.

The other study area of interest is the Erongo region in Namibia. The Erongo region is situated in the central western part of Namibia and covers an area of 63,549 $Km^2$ and is occupied by the Namib Desert, which extends parallel to the coast from 120 km to 150 km inland to study sites (Njinga et al., 2016). This area has two uranium mining operations, two uranium mines under care and maintenance and five active uranium exploration companies. There are two types of uranium deposits in the area. Primary alaskite and secondary calcrite deposits. These deposits and radionuclides leached from uranium mining tailings are potential sources of uranium in ground water (Mathuthu et al., 2020). The samples were collected from a uranium mine in the Erongo region, whose identity cannot be revealed due to confidentiality agreements.

In the case of nuclear material trafficking in the uranium mines of Witwatersrand and Erongo region, there should be a nuclear forensic database containing information on nuclear material from each country. This information should include nuclear forensic signatures such as REE patterns, Pb isotopic ratios, age of nuclear material, date of production, etc. This may be used to identify the origin of the nuclear material. Since Witwatersrand is the largest gold/uranium mine in South Africa and the Erongo region in Namibia has many uranium mines, nuclear forensic signatures need to be developed. This is the main objective of this study.

Chapter 1 consists of sections providing a brief discussion on nuclear forensics, incidents involving the trafficking of nuclear materials, and the investigation of nuclear materials after their discovery. This section also described how nuclear forensic science was developed, the concept of nuclear forensic signatures and also presented initiatives that force states to use nuclear materials for peaceful purposes and to account for their nuclear material. The purpose, the study area, the problem statement and the justification of the study were also presented. The importance of each country or state storing nuclear forensic signatures (lead isotopic ratios and rare earth elements (REEs)) and information for each nuclear material into a database was stated. The next section will discuss the concept of nuclear forensic signatures, starting from the front end of the nuclear fuel cycle to the determination of nuclear forensics signatures and the techniques that will be employed to identify them. This section will also describe why lead isotopic ratios and rare earth elements are used as signatures to identify the origin of uranium samples.

# Chapter 2: Literature study

The process of extracting natural uranium from the mine will be presented through the nuclear fuel cycle as shown in Figure 1. This figure shows the basic stages from mining of uranium to the transformation of nuclear energy into electricity and lastly, the reprocessing of the spent fuel. Detailed literature on nuclear forensic signatures, such as lead isotopic ratios, impurities (rare earth elements) and age or date of production, as well as the techniques used for analysis (ICP-MS and LIBS) will be presented in this section.

## 2.1 Nuclear fuel cycle

Uranium is an element which is spread extensively throughout the earth's crust. It is used as a main fuel in the nuclear power plant and it consists of 99.3% $^{238}U$, 0.7% $^{235}U$ and negligible amounts of $^{234}U$. Most of the development of nuclear forensic signatures are presently focused on natural uranium materials. A short introduction to the front end of the nuclear fuel cycle will be provided to better understand the word "natural uranium" (Ho, 2015) The front end of the fuel cycle will be emphasized more than the back end cycle because of easier access to materials from the front end of the fuel cycle see Figure 1.

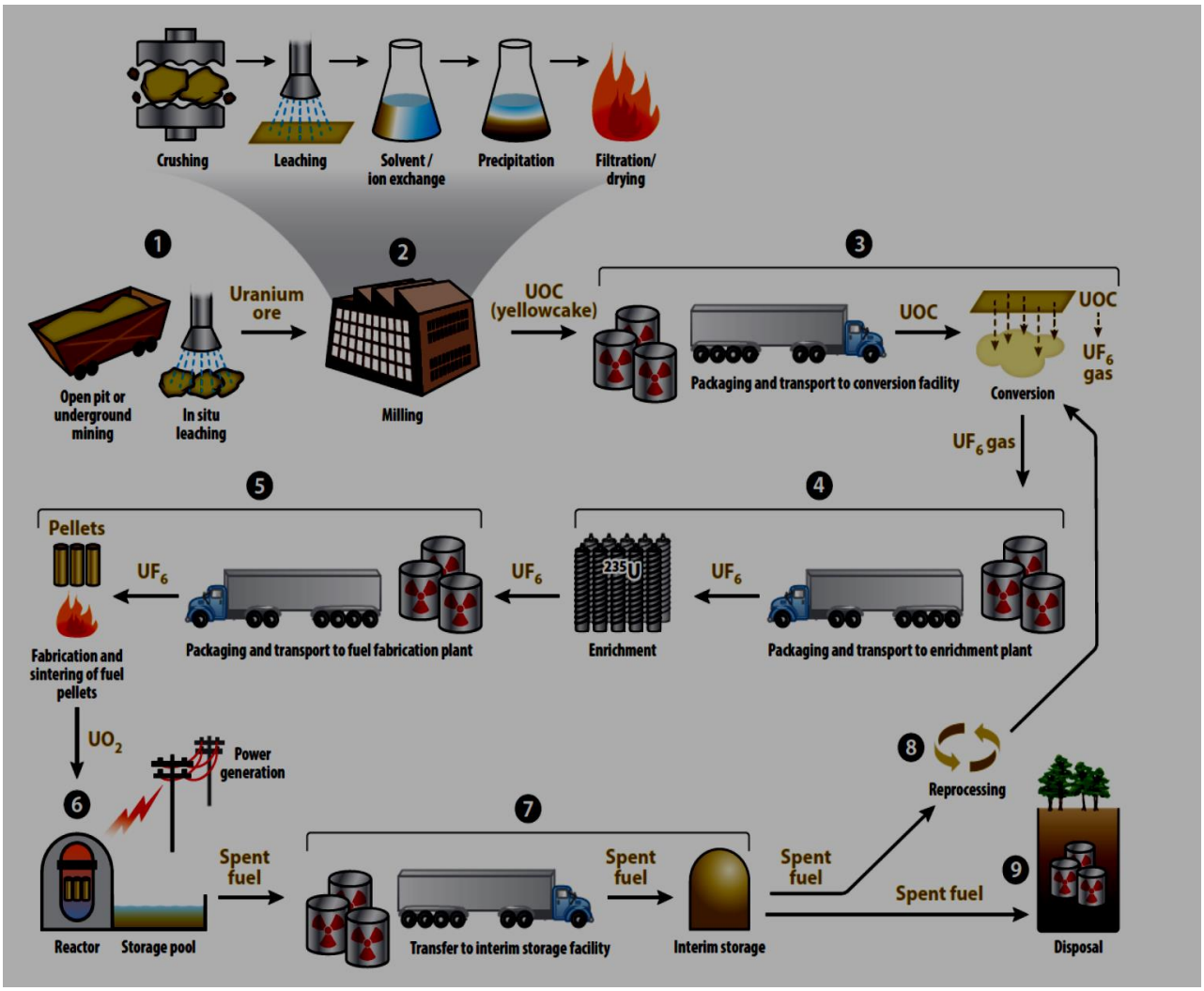


**Figure 1:** Nuclear fuel cycle (Kristo et al., 2016).

### 2.1.1 Mining

The front end starts with uranium mining from the different ores discovered on earth. Uraninite (also known as pitchblende) is the most prevalent. Uranium is mainly mined using three techniques: open pit, deep mines or *in-situ* leaching (ISL) and the selection depends mainly on the depth of uranium deposits (Ho, 2015). The ore containing uranium are mined underground or open pit mining and transported to a distinct milling facility where the real dissolution of uranium takes place as shown on the first stage of the nuclear fuel cycle in Figure 1. ISL, on the other hand, leaches uranium without the need to dig the ore.

### 2.1.2 Milling

Following the extraction (mining) process, comes the ore milling process (see Figure 1). The milling facility is generally situated near mines. Weighing, sorting, crushing, sampling and grinding are components of the milling operation (Reading et al., 2016). Comminution is essential for the reduction of the particle size of the mined ore, so that uranium can be easily obtained through leaching. When alkali treatment is used, the efficient extraction of uranium involves a finer grinding process (Connelly, 2008). In order to increase the solubility of essential components and improve the physical properties of the ores, certain uranium ores containing vanadium must be burnt (Švedkauskaitė-Le Gore, 2008, Edwards and Oliver, 2000).

### 2.1.3 Conversion

Natural uranium comprises of mainly two isotopes, namely $^{238}U$ and $^{235}U$ as discussed earlier in the introduction of this section. The fission process that releases thermal energy in a nuclear reactor occurs mainly in $^{235}U$. A percentage of 3-5% $^{235}U$ is needed in many nuclear power plants, thus uranium must be enriched in order to raise the concentration of $^{235}U$. As enrichment occurs in gaseous form, yellowcake is transformed to uranium hexafluoride gas ($UF_6$) at a conversion plant, thereafter, $UF_6$ gas is loaded into large cylinders where it solidifies (IAEA, 2011). The cylinders are then packed into heavy metal containers and transported to an enrichment plant.

### 2.1.4. Enrichment

Uranium is enriched in $^{235}U$ by the application of gas into fast-spinning cylinders, where heavier isotopes are forced out of the cylinder walls. Uranium can also be enriched with older technology by pumping $UF_6$ gas through permeable membranes that make it easier for $^{235}U$ to pass through than heavier isotopes such as $^{238}U$ (IAEA, 2009).

### 2.1.5 Fabrication

Enriched uranium ($UF_6$) cannot be used straight in reactors because it does not withstand high temperatures. It thus becomes uranium oxide ($UO_2$) and in order to achieve high density and stability, fuel pellets are formed by pressing $UO_2$, which is sintered at temperatures above 1400 °C. The pellets are cylindrical and usually have a diameter of 8 – 15 mm and 10 – 15 mm long (IAEA, 2011). They are packed to form fuel rods in lengthy metal pipes, which are clustered into ' fuel assemblies ' for introduction into a reactor.

### 2.1.6 Generation of electricity

Controlled fission happens once the fuel is loaded inside a nuclear reactor and that implies that the atoms of the $^{235}U$ are bombarded and fissioned by neutrons to release energy (heat) and 2 or 3 neutrons. Then Borinated control rods are used to control the rate of heat production. During this fission (splitting), heat energy used for heating water and generating high-pressure steam vapour is released (Reading, 2016) as shown in Figure 1 above. The steam turns the turbine generators connected which then produce electricity. The fuel can be used for 3–6 years in the reactor.

### 2.1.7 Spent fuel storage

Around one third of the spent fuel is removed and replaced with a new fuel in order to maintain a successful reactor efficiency. When the spent fuel is removed from the reactor, it is hot and highly radioactive, so it is then cooled and safeguarded from humans and it is placed in the reactor site's storage pools (Zakariya, 2016). Spent fuel can be stored safely in these pools for long periods. It can also be stored dry, cooled by air, in engineered installations (IAEA, 2018). The longer it is stored, the easier it is to deal with the decay of radioactivity. There are two alternatives for spent fuel: reprocessing for recovery of the usable portion and vitrification. However, reprocessing does not take place in South Africa due to the NPT she signed (IAEA, 2015a).

### 2.1.8 Reprocessing

Reprocessing is the process by which the unexploited energy content of the spent fuel is retrieved for future reuse or where different components of spent fuel are separated for waste management purposes. About 3% of the fuel used includes waste products and the remaining 1% is plutonium (Pu) produced while the fuel is in the reactor and not "burnt." Around 97% of the spent fuel can therefore be recycled for further use (Ho, 2015). Reprocessing divides uranium and plutonium from waste products by means of a chemical process called plutonium and uranium extraction (PUREX). For conversion to $UF_6$ and subsequent re-enrichment, recovered uranium can be returned to the conversion plant.

## 2.2 Investigations of nuclear forensic signatures

To date, research of uranium ore concentrate signatures has included analyses of uranium isotopic composition, trace elemental impurities, organic impurities; analyses of stable and radiogenic isotopic lead composition, morphology; as well as the use of age dating and multivariate analysis

(Keegan et al., 2016). In this section, we examine how techniques have been used to determine the geological origin, the history of processing, and perhaps the age of uranium ore concentrates and to discuss signatures that are essential to nuclear forensic investigations with emphasis on the characterization of uranium ore.

### 2.2.1 Lead isotope ratios

Lead isotopic signatures have proved to be an outstanding illustration of useful impurities in nuclear forensic studies. Numerous studies address the use of lead signatures to identify the origin of uranium samples (Švedkauskaitė-LeGore et al., 2008, Fahey et al., 2010, Švedkauskaite-LeGore et al., 2007, Stanley et al., 2013). Each of these reports gives insight into the nature of the sample material based on the disturbance of naturally occurring lead isotopic abundances; the distribution of lead isotopes in uranium products differs dramatically from general sources (Stanley et al., 2013).

Since three lead isotopes ($^{206}$Pb, $^{207}$Pb and $^{208}$Pb) are generated by the decay of uranium or thorium, it suggests that uranium-bearing materials such as uranium ores and uranium ore concentrates would demonstrate natural variability that is large enough to differentiate between materials of distinct origins (Reading et al., 2016). Investigating uranium ores from two different deposits and uranium ore concentrates from a couple of mills, the lead isotopic composition was found to be suitable for the fingerprinting of several natural uranium materials. The isotopic structure of the measured lead is a function of the age of the ore body and the concentration of uranium and thorium (Švedkauskaite-LeGore et al., 2007, Varga et al., 2012). However, the possible overlap of lead isotopic signatures for materials from varying geo-locations requires the use of extra chemical impurity information. Mayer *et al*. 2013 investigation proved that in several cases, high variations in lead isotopic composition can take place within the mine locations and in uranium ore concentrate, from the same location. This concept, together with the likelihood of introducing natural lead as a technological contaminant reduces the applicability of lead isotopic ratio as a unique signature. However, using the radiogenic ratio $^{207}$Pb/$^{206}$Pb, the age of the raw ore material can be calculated and is found to be directly linked to the source deposit type.

Lead is widely dispersed across the planet and it does not only exist as the radiogenic progeny of uranium and thorium. It has four stable isotopes, but only $^{204}$Pb is not radiogenic. The decay of long-lived radioactive isotopes of uranium ($^{235}$U and $^{238}$U) and the radioactive isotope of $^{232}$Th

yields three radiogenic isotopes of lead ($^{206}$Pb, $^{207}$Pb and $^{208}$Pb), see Table 5 (Švedkauskaite-LeGore et al., 2007). Lead bearing material has a time dependent isotopic Pb composition, which demonstrates the relative abundance and decay cycle of the three main parent isotopes. As a result of radioactive decay, the abundance of the Pb isotopes is increased, with $^{232}$Th forming $^{208}$Pb, $^{235}$U decaying to $^{207}$Pb, and $^{238}$U producing $^{206}$Pb. About half the capacity of $^{238}$U has decayed to $^{206}$Pb and over 90 percent of the $^{235}$U has decayed to $^{207}$Pb on a geological time scale. Standard chemical or physical processes do not fractionate Pb isotopes easily. Pb isotopes are mainly changed by radioactive decay or by combining typical non-radiogenic lead with a mixture of four isotopes (Nuclear, 2001).

Consequently, Lead-204, which is not generated by radioactive decay, provides a measure of "natural" lead. It is found that the proportion of lead isotopes in natural lead is almost constant for most minerals, so the $^{204}$Pb can be used to determine the non-radiogenic concentrations of $^{206}$Pb and $^{207}$Pb (Švedkauskaite-LeGore et al., 2007). Lead is a widely dispersed material that can be found in all kinds of rock as a trace element. Pb's isotopic composition in layers of rock and ore provides details on the geological past of the rocks the Pb exists in. The higher the difference between the radiogenic lead from natural lead composition, the higher the deposition age and higher uranium and thorium content in source material (Varga et al., 2009). Standard ranges of Pb isotope ratios found in natural materials are: 14–30 for $^{206}$Pb/$^{204}$Pb, 15–17 for $^{207}$Pb/$^{204}$Pb and 35–50 for $^{208}$Pb/$^{204}$Pb, even though values beyond these ranges are not unusual (Cheng and Hu, 2010).

### 2.2.2 Impurities or trace elements

Valuable information on nuclear material's history can be found on the following parameters: the characteristics of the main element of a nuclear material, the minor elements and trace elements. These trace elements, mostly known as impurities, may be present at constantly changing concentrations. Impurities may have been deliberately added to the material in order to obtain certain material properties or may have inadvertently entered the material as residues from the process material (Mayer and Glaser, 2015). Therefore, the type and level of concentration of such impurities is representative of the material type, origin (hydrometallurgical processes) and anticipated use of the material.

Various patterns have been studied for their utility as a characteristic signature in nuclear forensics, the concentration of trace elements, the isotopic structure of minor elements and the isotopic structure of some trace elements. In addition, the concentration of anionic impurities has also been presented to indicate the chemical processes used in the production of uranium ore concentrate (Reading, 2016).

#### 2.2.2.1 Metallic impurities (rare earth elements)

Rare earth elements (REE) (also known as lanthanides) are a set of seventeen metallic elements on the periodic table, specifically in addition to scandium and yttrium we have the fifteen lanthanides (lanthanum, cerium, praseodymium, neodymium, promethium, samarium, europium, gadolinium terbium dysprosium, holmium, erbium, thulium, ytterbium and lutetium). These elements were discovered in extensively varying levels in unusual types of igneous rocks. A huge quantity of uranium is in rare earth deposits and can be extracted as a by-product. REE is also present in nuclear material (such as uranium and plutonium) created by nuclear fission in the reactor. Lanthanides can be present in negligible concentrations in these products either as process contamination or as raw material residues. Measurements of REEs are used for the quality control and development of nuclear fuel products or for the examination of discovered illegal nuclear materials. REE in uranium compounds can therefore be used as proof of the origin of uranium (Sarkis and Rosa, 2011).

The patterns of REEs existence differ with the kind of deposit of the uranium ore. Even after the milling process, these patterns remains largely unchanged and thus provide strong proof of the origin of the interdicted uranium ore concentrate or uranium ore (Keegan et al., 2008, Keegan et al., 2014). These patterns are therefore an extremely important signature for providing information on the type of material used to generate the uranium ore (Varga et al., 2010a).

**REE CI-chondrite normalized patterns**

In petro-genetic studies of igneous rocks, rare earth elements are extremely effective because they are all geochemically similar. REE concentrations in rocks are typically normalized to a common reference standard, which mainly contains the chondritic meteorite values. The REEs are usually demonstrated in a concentration versus atomic number figure where concentrations are normalized to the chondritic reference value, illustrated as graphs and are connected by a straight

line (Kanyan 2015). If the plotted structure is above the general trend, then the anomaly is defined as positive and the anomaly is said to be negative if it is below the trend. Europium anomalies can be analyzed by comparing the observed concentration (Eu) to the anticipated concentration acquired by inserting between the normalized Sm and Gd (Eu *) values. Cerium anomalies can be analyzed by comparing the observed concentration (Ce) to the anticipated concentration acquired by inserting between the normalized La and Pr (Ce*) values. The ratio Eu/Eu* is therefore a measure of europium and a value greater than 1 (>1) implies a positive anomaly whereas a value less than 1 (<1) is a negative anomaly, the same applies to a cerium anomaly ratio.

The REE can be grouped into two sub-groups, namely the light rare earth elements (LREE) and heavy rare earth elements (HREE). Some ratios such as ($Gd_N/Yb_N$), ($La_N/Yb_N$), Eu/Eu* and Ce/Ce* may be used to define the fractionation characteristics. These parameters were measured in the following way:

$$\left(\frac{Gd_N}{Yb_N}\right) = \frac{Gd/Gd_N}{Yb/Yb_N} \tag{2.1}$$

$$\left(\frac{La_N}{Yb_N}\right) = \frac{La/La_N}{Yb/Yb_N} \tag{2.2}$$

$$\left(\frac{Eu}{Eu}*\right) = \frac{Eu/Eu_N}{\sqrt{\left(\frac{Sm}{Sm_N}\right)\times\left(\frac{Gd}{Gd_N}\right)}} \tag{2.3}$$

$$\left(\frac{Ce}{Ce}*\right) = \frac{Ce/Ce_N}{\sqrt{\left(\frac{La}{La_N}\right)\times\left(\frac{Pr}{Pr_N}\right)}} \tag{2.4}$$

where, the constant (N) means chondrite normalized REE material.

Apart from cerium (Ce) and europium (Eu), the REE exists in trivalent form. Cerium stays in the trivalent state under conditions without oxygen but its solubility decreases under conditions with oxygen and it precipitates as $Ce(IV)O_2$ causing a positive anomaly compared to the other REEs. However, Europium is trivalent in oxygenated environments but may be present in a reducing environment as a divalent ion. In addition, it can be substituted for plagioclase and other Ca-bearing minerals as it has the same charge and ionic radii as $Ca^{2+}$. Eu would therefore be enriched in the plagioclase relative to the other REE but depleted compared with the other minerals created by the magma or mineralizing fluids (Kanyan 2015).

During the formation of ores like apatite, garnet, monazite, sphene and zircon, the light rare earth (La-Gd) may be fractionated from the heavy rare earths (Dy-Lu). Ce and Eu's geochemical signature and fractionation level are maintained so long as no further diagenetic modification occurs (Mercadier et al., 2011). The fractionation and relative enrichment or depletion of Ce or Eu together with the relative elemental REE concentration present in a sample could even act as a forensic tool in the identification of a possible geological setting of origin. This signature is one of the major distinctive parameter of uranium ore and along with other isotopic, elemental, or morphological data may assist in determining the origin of these materials. For instance, if the REE signature showed no fractionation or anomaly, the sample would likely come from a deposit derived from synmetamorphic deposits or sandstone (Donard et al., 2015). A negative Eu anomaly will be the identification of a quartz-pebble conglomerate (Varga et al., 2010b) due to REE mineralizing fluids associated with granitic melt or weathered granitic deposits. Igneous or intrusive deposits will typically exhibit light rare earth elements (LREE) enrichment over heavy rare earth elements (HREE) by fractionation of HREE in minerals such as garnet and pyroxene throughout partial melting of the source materials.

### 2.2.3 Age or production date

In the subject of nuclear forensics, the age of a sample corresponds to the date of production since the last separation of the daughter isotopes from the radioactive parent. Separation processes set the clock to 0, the subsequent growth of the daughter isotope allows measurement of the sample age through daughter to parent ratio measurement and assessment relying on radioactive decay equations. Age measurement is an incredibly valuable nuclear forensic signature, it does not require any correlation with other material in a database (Keegan et al., 2016). Nonetheless, it must be carefully applied. Very delicate techniques such as inductively coupled plasma mass spectrometry (ICP-MS) (Varga and Surányi, 2007), thermal ionization mass spectrometry (TIMS) or alpha spectrometry are usually used for this type of study (Morgenstern et al., 2002).

## 2.3 Nuclear forensic techniques

This section provides an overview of the primary and analytical techniques used in nuclear forensics. The intention is to provide the reader with an overview of the technique’s fundamental principles and offer information limitation and benefits of the tools used in nuclear forensics.

### 2.3.1 Background of techniques used

The sections below provides explanation how LIBS works, LIBS concept and other factors related to the instrument. It also involves a description and principle of the LIBS technique. Furthermore, it also provides the literature on ICP-MS and all other factors related to the instrument.

#### 2.3.1.1 Literature of Lasers

The term LASER is an acronym for light amplification by stimulated emission of radiation. The physical process that happens during laser action is stimulated emission which is intensified by the use of mirrors. A laser is a tool used to stimulate atoms or molecules to produce energy as light in a particular way. The light emitted will be at frequencies in either the ultraviolet, visible or infrared areas of the electromagnetic spectrum (Telle et al., 2007).

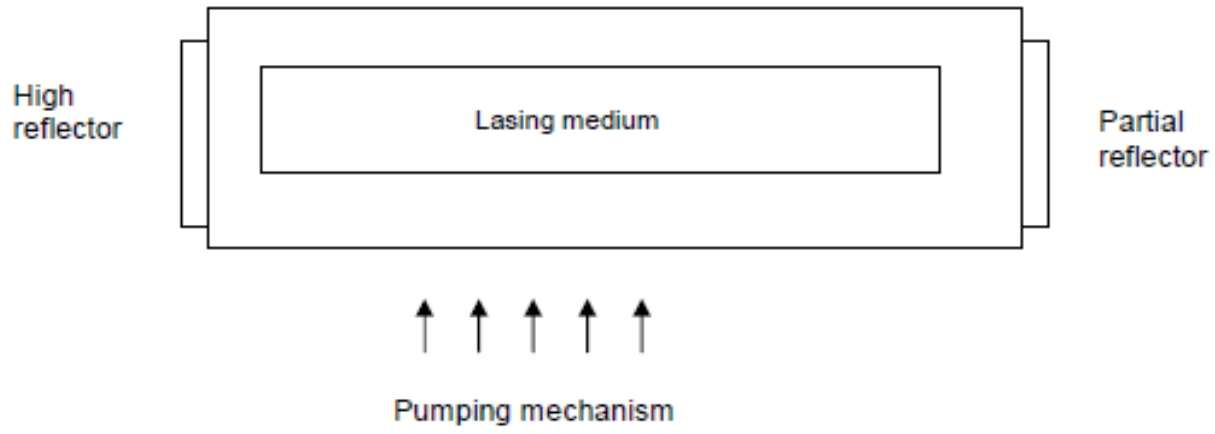


**Figure 2:** Basic laser diagram (Telle et al., 2007).

Most lasers have the following familiar features as shown in Figure 2. They have a laser medium that contains atoms or molecules that can be either solid, liquid, gas or semiconductor material capable of being pumped to an excited energy state; a pump source that pumps energy into the laser medium. This source provides energy from excitation from a lower to a greater level in order to generate population inversion. The source of the pump may be optical, electrical, mechanical or

chemical. There is a resonator which consist of two mirrors. One mirror is fully reflective and the other is partly reflective (Pelle, 2008).

A laser can either be operated in continuous or pulsed mode meaning that the laser production can be constant and continuous or breaks in between pulses. Continuous lasers are effective in many applications, however, some pulsed laser has a very large peak power which is beneficial for this study. Laser spectroscopy is a scientific field whereby lasers can be used in conjunction with spectroscopic methods to supply data about the interaction of coherent light with material and has high resolution and sensitivity in general (Telle et al., 2007). This field has contributed to improvements in the reliability with which spectral line frequencies can be analyzed, and this is important for the basic understanding of atomic processes. There are several types of lasers, namely Nd: YAG laser, excimer-pumped laser, helium neon laser, carbon dioxide laser, dye laser, femtosecond laser and semiconductor diode laser, however, the commercial Nd: YAG laser was selected for this research due to its accessibility and ability to ionize the atoms of concern (Paschotta, 2008).

#### 2.3.1.2 Neodymium: yttrium aluminium garnet (Nd:YAG) laser

The Nd:YAG Neodymium yttrium aluminum garnet laser is a solid state laser that is optically pumped using flash lamps or laser diodes (Telle et al., 2007). The Nd: YAG crystal is used as a lasing medium (Pelle, 2008). Typically, Nd: YAG lasers emit light in the spectrum's infrared region with a wavelength of 1064 nm. The beam of 1064 nm focuses on a doubling crystal to generate both the beams of 1064 nm and 532 nm. The Nd: YAG lasers are normally doubled, tripled or quadrupled in frequency to produce 532 nm (green, visible), 355 nm (UV) and 266 nm (UV) light when such wavelengths are required. Nd: YAG lasers can function both in continuous and pulsed mode. Nd: YAG lasers are used in a variety of applications. It involves cutting, welding and marking of metals and other materials, as well as scientific applications like those of Raman spectroscopy, remote sensing and mass spectroscopy, and also pumping dye lasers.

#### 2.3.1.3 Laser induced breakdown spectroscopy (LIBS)

Focusing a laser pulse on a solid, liquid or gaseous sample with sufficient energy to generate a plasma useful for spectral analysis is what the laser-induced breakdown spectroscopy (LIBS) is about. LIBS has distinctive benefits such as the ability to analyze quickly, in situ, multi-elements

with little or no sample preparation. However, quantitative analysis of LIBS is not a minor task since the spectroscopic emission of the plasma is defined by the characteristics of the plasma itself, which in turn depends on the experimental conditions (Pace et al., 2011).

In order to obtain LIBS features, parameters including temperature and electron density, spectral assessment of the radiation emitted by laser generated plasmas may be used. Nevertheless, it is quite difficult to measure the atom and ion densities from the calculated emission spectra (Aragón and Aguilera, 2008b). There are still some concerns under investigation that are believed to be a major challenge for LIBS. Specifically, self-absorption of spectral lines within the plasma plume, spatial non-uniformity, shielding effects at high laser irradiance and matrix effects. In many practical situations, reference samples are therefore inaccessible (Aragón and Aguilera, 2008a). For instance, when dealing with distinctive samples, samples with a complicated or a sample with an unidentified matrix or samples needing high-cost production, or a mixture of these characteristics.

LIBS has been used for the identification of uranium in fluids for nuclear fuel reprocessing, the identification of impurities in uranium related to nuclear fuel production and the identification of uranium containing vapor. LIBS is suitable for such applications because it can offer non-invasive or minimally invasive analyzes using spectrometer. As an illustration, LIBS typically does not apply to the measurement of isotope ratios for many elements due to small isotope shifts and difficulties in identifying the shifts because of Stark line broadening arising from elevated electron density in laser plasma (Chinni et al., 2009).

LIBS is used to determine a sample's atomic composition. Every element emits light at very distinct wavelengths to form a "fingerprint" spectra for that element. Laser is focused on a material surface to vaporize and ionize the sample in the formation of a plasma plume. The ionized atoms return to their ground states with the emission of characteristic light that can be obtained through an optical setup as the plasma cools. The spectrum of emitted wavelengths can be analysed from this light using a spectrometer. This technique depends on time and the time difference between the firing of laser and detector acquisition (Miziolek et al., 2006). Spectral emissions from the various elements become dominant as the plasma cools. As an outcome, the detector in LIBS is gated in order to block the continuum light to obtain only the preferred spectral data. Intensifying of the gate delay not only lowers the continuum background and the overall intensity, but also

affects the type of spectral lines observed. Normally, ion lines are stronger initially in the plasma lifetime, meanwhile molecular data is only available at longer gate delays. It is therefore prevalent not only to gate the detector, but also to use a particular gate width. A digital delay generator (DDG) coupled with the detector controls both gate delay and gate width.

LIBS applies a high-energy laser pulse as source of vaporization, atomization, and excitation to produce a high-temperature micro-plasma at the target's surface (Cremers and Radziemski, 2006). The initial process begins by the sample reflecting or absorbing energy from the pulsed laser. The absorbed energy is then abruptly transformed into heat, resulting in the melting and vaporization of small quantities of material into ionized gas as the temperature reaches the material's boiling point. The elimination of particulate matter from the surface results to a vapor forming in front of the sample. As this vapor condenses into droplets of a sub-micrometer size, it results to the dispersion and absorption of the laser radiation inducing heat, ionization and plasma creation. This is followed by the rapid expansion of the photo-ablated material, with the emission of characteristic signals for the elements in the sample. The emission lines that resulted were due to electronic transition within the atoms or ions that are excited (El-Deftar, 2014). The plasma temperature reaches 4,000 – 15,000 K, which affects the ionization of the atoms contained in the sample and results in different line intensities formed. The ions and electrons then combine to form neutral atoms or even molecules, with the emission of light of characteristic wavelengths, as the plasma cools and decays.

Each element has a distinctive emission lines which functions as a "signature" of the elements present in the sample. Roman numeral I in front of an emission line refers to an electron transition in the atom, while II refers to a transition in the first ionization state. After the spectra is resolved, the wavelength of the emission lines are used to distinguish each element's presence (El-Deftar, 2014). The peak area at the chosen emission line can be used for quantitative assessments.

The wavelengths of the emission lines are independent of the energy of the incident pulses, yet the intensity of the lines rises with the pulse energy up to the limit of saturation. Each of the emission line peaks detected in the spectra was compared to the LIBS database available from the United States National Institute of Standards and Technology (Abedin et al., 2011).

The wavelength of the spectral line records the identity of an element, while its intensity is equivalent to the number of atoms present. LIBS has the ability to detect and measure multi-elements in any solid, liquid or gas materials or in-situ and in real time. Since LIBS is sensitive to all elements and the plasma emission from a laser shot, offers a broadband spectrum recording the complete chemical fingerprint of a sample that can be utilized to classify elements and applications such as origin determination and natural resource assessment (Harmon et al., 2017). Observing the location and intensity of the emission lines in the LIBS optical spectrum provides knowledge on both the chemical elements and their abundance in the plasma. Chemical composition of the sample can be easily determined by distinguishing the various spectral peaks. Elements on the left side of the periodic table, such as Li, Na and Ca, with relatively low ionization energy , usually exhibit high emissions and can therefore be detected in very small abundances, while non-metallic elements on the right side of the periodic table such as F and Cl are more difficult to identify and have far higher detection limits (Harmon et al., 2017).

Qualitative data about the sample can be derived based on the wavelengths present after the atomic spectrum of the material is acquired. The intensity of the spectral lines can directly be associated to the amount of the element that emitted them. Major challenges take place when performing LIBS with a heavy element, particularly the spectral interferences because of spectral line density. Wachters and Cremers (2010) were amongst the first to research about uranium using LIBS. They studied uranium in nitric acid solution stored in a horizontal vial in order to avoid lens exposure from splashing. Their results indicated that LIBS was able to carry out quantitative analysis in solution on heavy elements (Williams, 2016). Sarkar and his colleague (2008) also researched uranium in a form of a solution. Instead of carrying out the LIBS analysis directly in the liquid, the authors dried the samples onto a substrate before measuring the uranium sample (Sarkar et al., 2008, Sarkar et al., 2012).

Singh and his co-workers ( ) studied uranium (U), plutonium (Pu) and neptunium (Np) in aqueous solutions. In the solution, the Pu and Np were dried on a carbon rod and were detected on the surface using LIBS and the strongest lines were observed. For U, the sample was nebulized using an ultrasonic nebulizer, and a gate delay of 30 us was used to perform LIBS in the aerosol. The results produced a limit of detection of 1,359 ppm U using a line of 409,013 nm (Williams, 2016). These studies showed LIBS ability to detect uranium in aqueous solutions regardless of spectral

interferences and challenges of using liquid samples Actinides were not only measured in solutions using LIBS, but extensive research was performed in other sample structure.

The geographical origin of yellowcake was determined using LIBS in the study of (Sirven et al., 2009). The yellowcake was combined with grease to create a paste in which the LIBS analysis was carried out. The results of their study suggests that the origins of the yellowcake samples can be assessed in all 11 cases. Chinni and colleagues (2009) were able to determine uranium in soils using a stand-off method that showed that uranium can be detected in trace amounts using this method. To measure the uranium and plutonium isotope ratios, several authors used high-resolution spectrometers (Chinni et al., 2009). (Emmert et al., 2011) also researched techniques to improve the measurement of actinide. Depleted uranium samples were studied using nanosecond and femtosecond laser pulses. The results stated that femtosecond laser pulses could help overcome the difficulties of heavy element assessment and could considerably enhance sensitivity.

LIBS technique was selected for this study due to it's the capacity to identify all elements and the capacity to detect multi-elements simultaneously. Any type of material in gas, liquid and solid state can be evaluated in air, under water and under extreme circumstances such as elevated temperature and pressure with simple or even without sample preparation. From an analytical perspective, LIBS performance of qualitative analysis may still be considered as imperfect. The major factor influencing the quantitative of LIBS is the matrix effect. Clearly, such an effect also occurs for other plasma based atomic emission spectroscopy, such as inductively coupled plasma, but is normally more serious for LIBS due to direct laser sampling of materials in different stages. In addition, LIBS is still typically less comparable in respect of the normal analytical merit figures (detection limit, precision, accuracy) than other traditional laboratory-based analytical methods. The existing shortcomings of LIBS can be attributed to several factors from a theoretical perspective. The first factor is the complicated nature of the laser-sample interaction processes, which relies on the laser characteristics and the properties of the sample material. The second factor is the complicated time and space evolution of laser-induced plasma. All of this can induce unacceptable matrix effects. Even though the concept of LIBS procedure is quite straightforward, the physical processes included in laser interaction and ionization of plasma excitation are quite challenging and not yet comprehended. For this reason, ways to mitigate these problems are based on a clear explanation of the processes involved in plasma evolution and the resulting emission

characteristics, which rely primarily on the experimental conditions under which the ablation is performed. In fact, the characteristics of the emission spectrum are associated with the laser pulse's specific interaction with the sample and the dynamics of the plasma generated.

On the other side, not all modern analytical methods actually require considerable research to handle the samples in order to achieve good analytical results. All other common methods are based on strict sample preparation protocols, including ICP and XRF. It is obvious that employing a complicated treatment to the sample tends to give up one of the mist desirable benefits of LIBS technique. However, adequate adaptation of the sample to the LIBS readings could significantly improve the LIBS ability to attain the merits that any excellent analytical instrument should have. Various techniques of sample treatment and preparation have now been used for LIBS in separate analytical applications, such as liquid analysis, loose powder analysis and biological samples.

### 2.3.2 Inductively coupled plasma mass spectrometry (ICP-MS)

The most common analytical method used for elementary analysis is ICP-MS because of its negligible limit of detection, accuracy and high degree of sensitivity. Figure 3 demonstrates a diagram of the ICP-MS scheme. ICP-MS is a destructive analytical technique used for elementary assessment. A more complicated variant of this, ICP-MS (MC-ICP-MS) multi-collector, is a more delicate technique with reduced detection limits that can provide both elemental and isotopic data. This instrumentation can be used to accomplish isotopic ratios and concentration determination via isotope dilution. ICP-MS was used in this research to identify elementary and isotopic nuclear forensic signatures (Meyers, 2013).

The source of ICP-MS is an ionized argon plasma that can achieve around 10,000 K electron temperature. Before being positioned into the plasma, a sample solution is thermally nebulized into small vapor droplets and what makes the sample constituents mainly atomized into individual atoms that are positively charged, is the high plasma temperature. Upon ionization, the atoms are removed from the plasma and positioned through a vacuum pump system with two water cooled nickel metal skimmer cones into a quadrupole mass analyzer. The ions are segregated and distinguished by passing through four circular perpendicular pair rods, interchanging AC and DC potential in reverse pairs of rods, depending on their mass to charge ratio (Skoog et al., 2007).

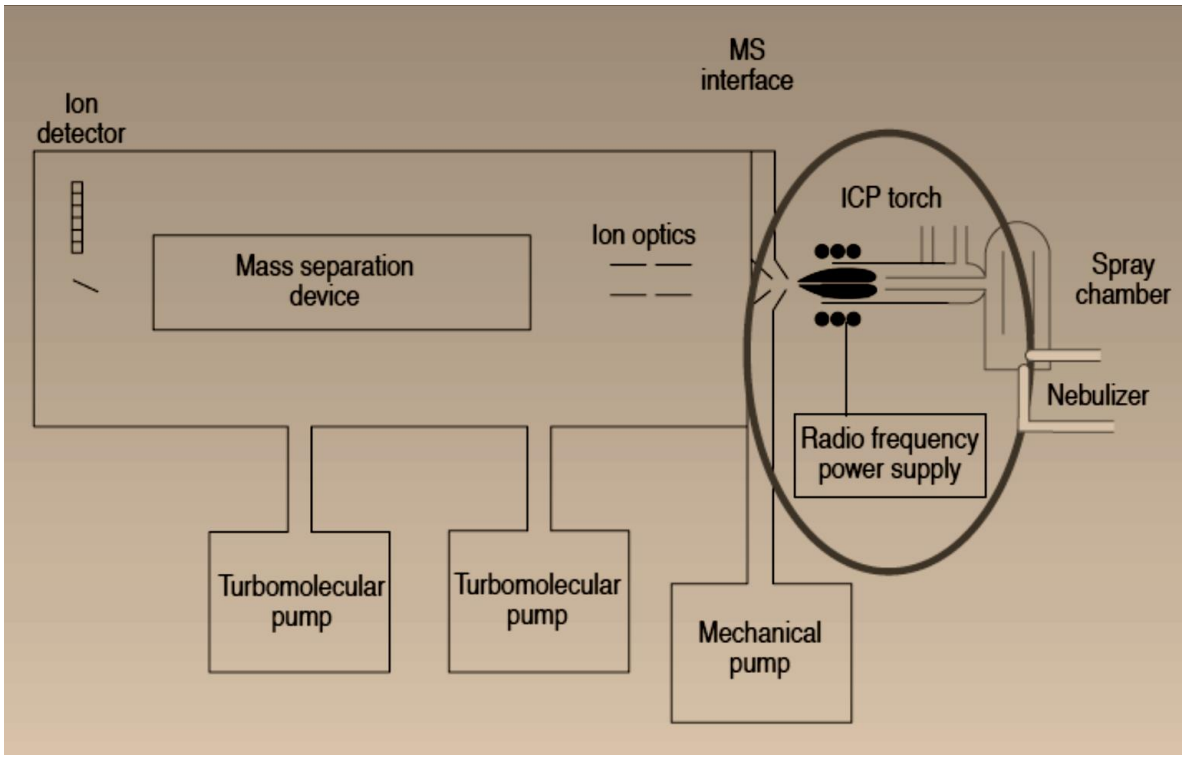


**Figure 3:** An ICP-MS instrument schematics (Thomas, 2013).

Although ICP-MS is a common technique, it also has its disadvantages. One of the main issues related with this technique is the interferences. Isobaric interference can arise when two elements have the same isotopic mass, such as $^{232}Th$ and $^{232}U$. When analyzing radioisotopes, isobaric interference is one of the most important problems that needs to be tackled and to solve this problem, chemical separations should be done before analysis (McMahon, 2020).

Another form of interference, which is also important to address, is interferences with oxide, hydroxide, or hydride molecules, such as $^{233}UH^{+}$ and $^{234}U^{+}$.Such kinds of compound are created by interactions with the sample matrix or plasma gas itself (Argon). Polyatomic interference can occur whenever the elements form a molecular element in the plasma, sample matrix, or in the atmosphere like $^{40}Ar^{+}$ and $^{40}ArH^{+}$. This kind of interference is negligible than isobaric and hydride-forming interference in nuclear or radiological samples during analysis (de Hoffmann and Stroobant, 2007).

ICP-MS technique have a mass resolution of approximately one atomic mass unit, enough for most applications (Meyers, 2013). High resolution or sector field mass spectrometers were used in the event that a higher resolution is required. These kinds of technique help minimize or remove the effects of interference resulting from mass overlap.

The main benefit of ICP-MS is its versatility and it can be used to measure the concentration as well as to determine the isotope ratio of different components. Perkin Elmer NexIon 2000 ICP is a very delicate measuring instrument for nearly all components. The method can be used to define the material type and isotopic data can also be provided (Thomas, 2013). It generally needs less tedious sample preparation compared to thermal ionization mass spectrometry (TIMS) and can also be used for components with high potential for ionization. Since it is a destructive analytical technique, the preparation of samples must be carefully planned, particularly when a restricted quantity of material is accessible (Fedchenko, 2015).

# Chapter 3: Methodology

This chapter presents the methodology performed in this study. It provides the description of the study area, sample collection and analytical techniques used in identifying the samples.

## 3.1 Introduction

This study was conducted in the Witwatersrand area in South Africa as discussed in Chapter 1 study area. Uranium mine tailings identified in this area were Tailing 1 and 2 as shown in Figure 4. Samples were taken from the mine tailings and 22 samples were obtained for laboratory analysis. Another area of study is the Namibia uranium mine in the Erongo region and the identified mine tailings were NAM-T and underground water (UDW). Samples were taken from the mine tailings and underground water and 20 samples were obtained for laboratory analysis.

Elemental composition was studied at the Centre for Applied Radiation Science and Technology (CARST) and the Department of Chemistry, both of which are located at North-West University. For elemental composition, the analysis was done using an inductively coupled plasma mass spectrometer (ICP-MS) and a laser induced breakdown spectroscopy (LIBS).

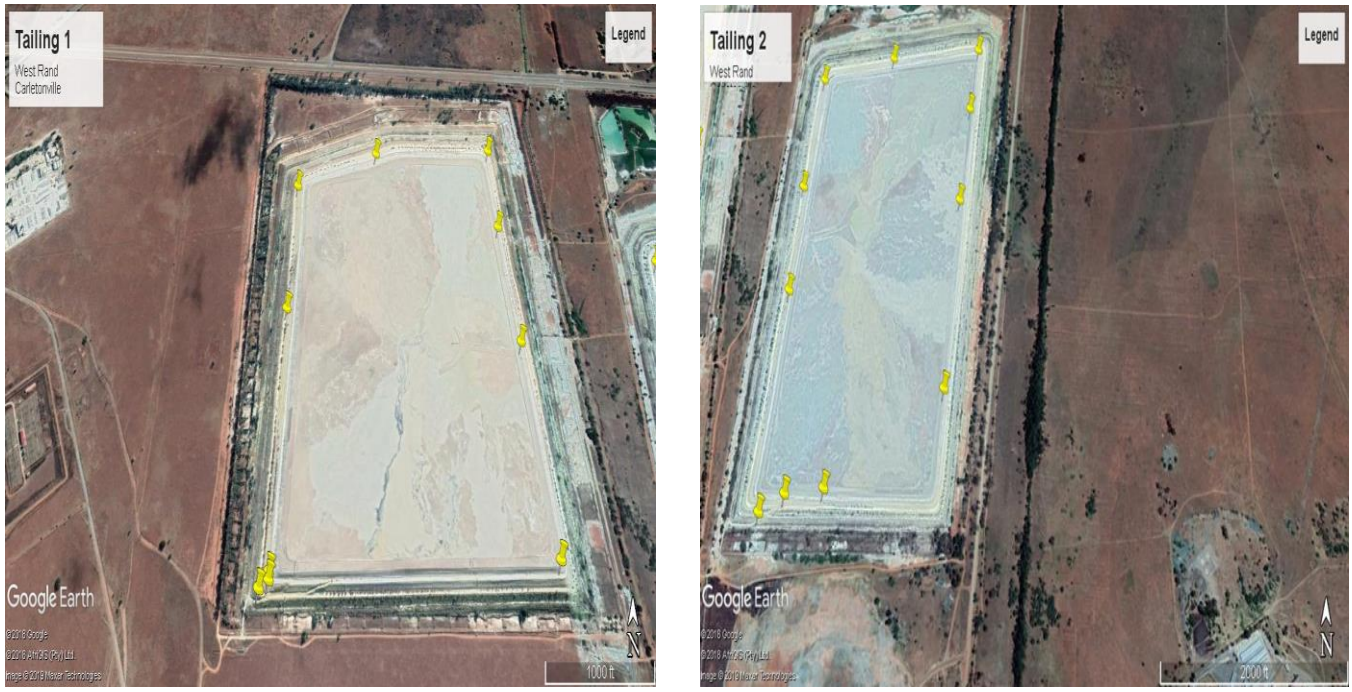


**Figure 4:** Sampling points for uranium (yellow) samples from a uranium mine in South Africa.

### 3.2 Sample collection

Uranium ore and water samples from different locations were collected in this study using random sampling see Figure 4. All the samples collected were properly marked and classified by their sampling positions using Global Positioning System (GPS) for future reference. The samples collected were then transported for further analysis to the CASRT laboratory.

#### 3.2.1 Uranium ore collection

A maximum of 32 uranium ore samples from three mine tailings were collected at a depth of 5 cm and packaged in 4 kg polyethylene bags (Kamunda, 2017).

#### 3.2.2 Water collection

Ten water samples from underground were collected and packaged in 2 L polyethylene bottles. The water was then acidified with $HNO_3$ to avoid elements from sticking on the walls of the bottle (Kamunda, 2017).

### 3.3 ICP-MS methodology

#### 3.3.1 Uranium ore digestion by Perkin Elmer Titan MPS

1 g of uranium ore sample was weighed and transferred into a 75 ml standard digestion vessel. 9 ml of 37% HCl and 3 ml of 70% $HNO_3$ reagents were slowly added into the digestion vessel,

rinsing the sample to the bottom of the vessel. The mixture swirled gently for about 10 minutes before putting the seal in place and closing the vessel. They were then placed inside the Perkin Elmer Titan MPS (Microwave Preparation System) at 180℃, for about 30 minutes. The vessel was then removed from the microwave and allowed to cool, to avoid foaming and sample loss. The digested samples were then transferred into 50 ml vials. The environmental digestion method used in the sample digestion achieves total sample decomposition (Mangum and Shelton, 2015).

### 3.3.2 Sample run

About 1 ml of the digested sample was pipetted into a 15 ml vial and was then diluted to 10 ml with ultra-pure distilled water. The samples were loaded on the auto-sampler. For isotopic ratio, the instrument was set to isotopic ratio method, operated in the collision mode for mass energy discrimination and filtration against interferences (Vilta, 2016). For rare earth element analysis, the instrument was set to total quantitative method.

**Figure 5:** NexION 2000C, ICP instrument.

### 3.3.3 Determination of rare earth elements

The analysis included samples of quality control such as blanks and standard solutions and certified reference material. The Perkin Elmer, NexION 2000C ICP (as shown in Figure 5) calibration utilizes Perkin Elmer multi-element calibration standard, for the assessment of rare earth elements, the requirements are: 10 mg/L of Ag, Al, As, Ba, Be, Bi, Ca, Cd, Co, Cr, Cs, Cu, Fe, Ga, In, K, Li, Mg, Mn, Na, Ni, Pb, Rb, Se, Sr, Ti, U, V and Zn. For quality control, the instrument was set to run a blank and standard check on every ten samples for each set of measurements.

### 3.3.4 Determination of lead isotopic ratios

For uranium isotope ratio, the Perkin Elmer multi-element calibration standard certified reference material was used for the validation of the uranium isotopes and a NIST SMR 981 standard was used for lead isotopic ratios.

## 3.4 Laser induced breakdown spectroscopy (LIBS) methodology

### 3.4.1 Sample preparation

No sample preparation was required for laser induced breakdown spectroscopy to avoid contamination of the original sample.

### 3.4.2 Sample run

The LIBS spectra of the different uranium ore and water samples were recorded using a LIBS experimental setup; a schematic diagram is shown in Figure 6. The setup basically consisted of a laser source, sample stage, and spectrometer equipped with a detector system. The laser source used in the present study was an Nd:YAG Q-switched laser (EKSPLA NT342B-SH-10-AW, Lithuania) operating at 355 nm wavelength and capable of delivering a maximum energy of 30 mJ over a pulse duration of 3.6 ns at a maximum pulse repetition rate of 10 Hz. The samples were placed on a sample stage and the laser beam was focused onto the cross-sectional surface of the uranium ore using a 100 mm focal length lens to create the plasma (Pathak et al., 2012). The light from the plasma was collected using a lens fixed at the tip of fibre bundle and finally fed into the entrance slit of the USB 2000+ spectrometer (Ocean Optics, USA) equipped with charge-coupled device (CCD). The resulting spectra were analysed using Spectra-suite software, with the Spec-line software was used to identify elements in the spectrum.

Since ionization energy increase from the left to right across the periodic table, it can be assumed that the LREE have low ionization energy relative to HREE and therefore they exhibit high emissions and can be detected in very small abundances. REEs of samples from two different locations were analyzed using LIBS and the acquired spectra is shown in Figure 25 - 36. Rare earth elements are observed only when at least three of its non-interfered lines are clearly defined.

The LIBS spectra of uranium ore and water samples were recorded in the spectral range 250 – 800 nm and an average spectrum of 10 laser shots were recorded to enhance the signal-to-noise ratio.

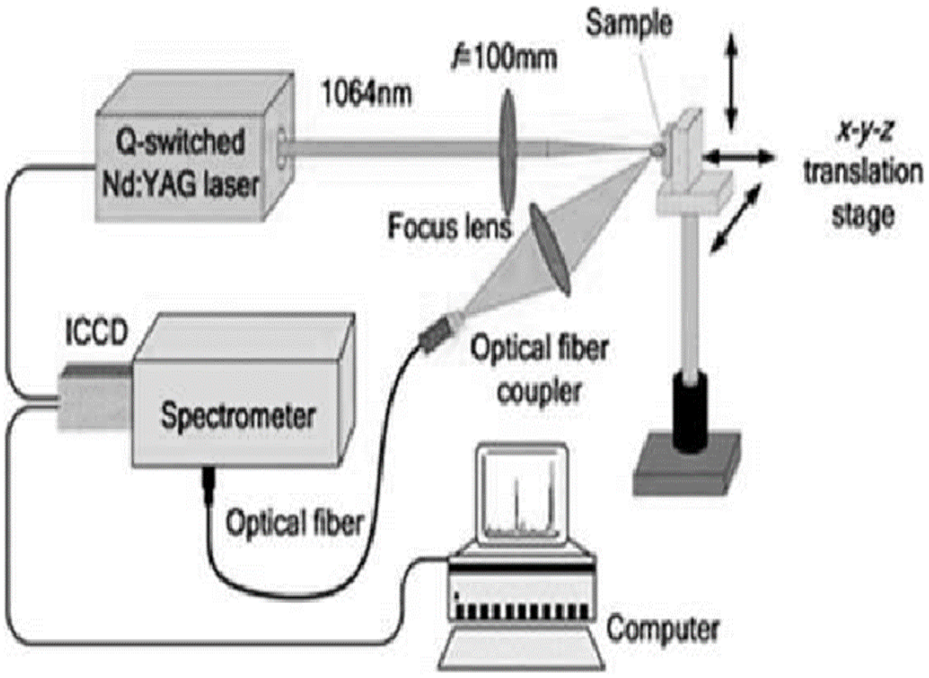


**Figure 6a:** LIBS experimental set-up (Pace et al., 2011).

### 3.4.3 Wavelength calibration of the spectrometer

A light source which produces at least 5 spectral lines in the wavelength region of the spectrometer and a mercury lamp was used to recalibrate the ocean optics USB2000+ spectrometer; an optical fibre and a spreadsheet program like excel for calculation.

A spectrum of the light source (high pressure mercury lamp) was acquired after placing spectra-suite into scope mode. The integration time was adjusted until there were several peaks on the display screen that are not off scale. The cursor was moved to one of the peaks and was carefully positioned so that it was at the point of maximum intensity and the pixel number displayed in the

status bar was recorded. This step was repeated for all the peaks in the spectrum obtained. A spreadsheet was then prepared in the following manner:

The true wavelength of the spectral lines used were placed in the first column. In the second column of the worksheet, the observed pixel number was placed, for the third column the pixel number squared was calculated and in the fourth column, the pixel number cubed was calculated. The created spreadsheet program was used to calculate the calibration coefficients and to perform linear regressions. The true wavelength was selected as the dependent variable. The pixel number, pixel number squared and the pixel number cubed as independent variables. The intercept as well as the first, second and third coefficient were recorded and the value for R squared was obtained as shown in Figure 6. The wavelength calibration was updated within the spectra-suite software. This process was repeated for each channel in the setup.

$$\lambda_p = I + C_1 p + C_2 p^2 + C_3 p^3 \qquad 3.1$$

where $\lambda$ is the wavelength of pixel p, $I$ is the wavelength of pixel 0, $C_1$ is the first coefficient (nm/pixel), $C_2$ is the second coefficient (nm/pixel$^2$), and $C_3$ is the third coefficient (nm/pixel$^3$). The value for $I$ and the three Cs was calculated as described below see Figure 6b.

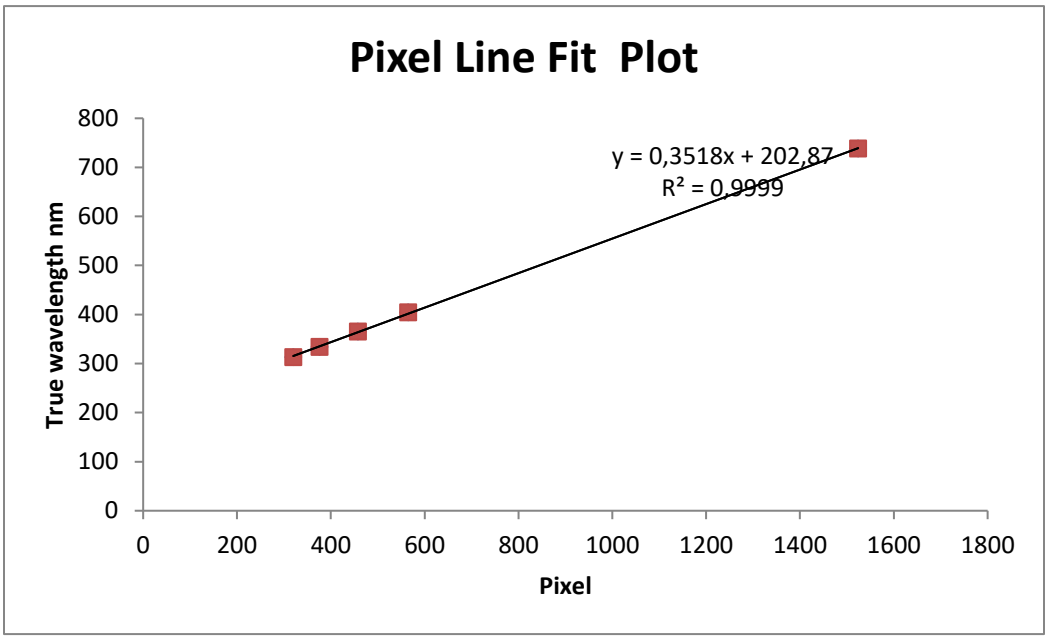


**Figure 6b:** True wavelength versus pixel number plot obtained from the high pressure mercury lamp.

## 3.5 Data analysis

R software v.4.0.2 (Rstudio team 2020, R core Team, 2020) was used for PCA and dendrogram analysis the data in this study. PCA was performed to identify patterns, similarities, differences and grouping in the form of a dendrogram clusters. PCA provided a valuable tool to evaluate whether the samples are the same or different and which variables were responsible for the possible differences (Gottfried et al., 2009). The dendrogram cluster analysis was used to arrange multivariate data and to identify common trends in samples. It started with each sample in a separate cluster. At each stage, two clusters that were the most similar would be joined into a single new cluster. When the samples were combined, they were never isolated. Samples near dendrogram branches exhibited more similarities than samples linked to each other through remote branches. The data analysis procedure was set up in such a way that only chemical elements present in all samples were used to produce clusters.

The PCA is used to identify variations in the data set. These variations are reduced to a smaller set of principal components (PC). Each PC is an abstract expression for the actual eigenvector and the resulting own eigenvalues. PC1 (first PC) provides a definition of the greatest variation, meaning it accounts for more of the overall variance in the data set than any of the original variables. PC2 (second PC) defines the greatest remaining variance and is orthogonal to PC1. When peaks in the plot are much closer to +1 or -1, the more relevant the peaks are to the variation in the spectrum and the variation of the elements in the samples can also be correlated with each peak (Rühlmann et al., 2018).

# Chapter 4: Results and discussion

## 4.1 Data analysis

This work was aimed at applying ICP-MS and LIBS techniques to resolve nuclear forensic signatures from a South African and a Namibian uranium mine and processing plant. It is important to develop nuclear forensic signatures in case of interdiction of nuclear materials. Signatures consists of elemental impurities such as rare earth elements, isotopic composition chemical composition, physical and trace elements. Such data may be stored in a nuclear forensic library and may be used as a nuclear fingerprint for source attribution.

The results of this work are divided into four categories:

- REE CI-chondrite normalized patterns analysis using ICP-MS
- Lead isotopic ratio analysis
- REE concentrations analysis using LIBS
- Comparison of ICP-MS and LIBS

**Determination of REE concentrations from a South African uranium mine**

Table1 and Table 2 provide REE concentrations of the analyzed tailings in South Africa. The REE patterns of different mine tailings were distinguished in this section. Tailing 1 had REE (∑REE) concentrations which were significantly higher compared to tailing 2, with the total number of REE (∑REE) which ranged between 30.035 and 39.908 ppm (parts per million) in tailing 1 and for tailing 2 it ranged between 27.751 and 38.731 ppm. All these were lower than the coarse and fine sediments reported by (Silva et al., 2016) which contains ∑REE ranging between 48.35 to 95.23 ppm and 125.38 to 320.81 ppm respectively. These values were also lower than the fine sand and coarse sand which ranged from 12.5 to 63.6 ppm and 126.2 to 877.6 ppm reported by (Sako et al., 2009). The sum of the LREEs (∑LHREE) and HREEs (∑HREE) ranged between 26.815 to 35.896 and 1.754 to 4.012 ppm respectively for tailings one and for tailing two it ranged between 24.643 to 35.688 and 1.854 to 4.945. LREE (∑LHREE) contributed about 91.76% and HREE (∑HREE) contributed 8.24% of the total REEs for the tailing one. For tailing two, LREE (∑LHREE) contributed about 89.95% and HREE (∑HREE) contributed 10.05% of the total REEs.

Total quant method was used to discriminate the rare earth elements on each tailing sample. The concentration of all REEs present were distinguished in ppm. The statistical analysis of this this results was done using excel. The  sum of REES, the standard deviation, the error, the sum of LREE and HREE, the LREE and HREE content (represented by equation 2.1 and 2.2) and the anomaly represent by the equation 2.3 were calculated. The standard error found in Table 1 and 2 was lower than 3%. The concentration of rare earth elements in natural uranium are low, so we expect the REE concentration to be low. Low REE concentration also proves that the REE remain unchanged and can be used as a signature as described in the literature (Chapter 2 metallic impurities section).

**Table 1:** REE concentration for tailing 1 (mineT1) in ppm.

| Sample ID | La | Ce | Pr | Nd | Sm | Eu | Gd | Tb | Dy | Ho | Er | Tm | Yb | Lu | ∑REE | ±∑REE | LaN/YbN | GdN/YbN | ∑LREE | ∑HREE | Ce/Ce* |
|---|---|---|---|---|---|---|---|---|---|---|---|---|---|---|---|---|---|---|---|---|---|
| **T1E1** | 13.248 | 0.205 | 2.573 | 9.513 | 1.703 | 0.447 | 1.436 | 0.198 | 1.048 | 0.176 | 0.457 | 0.066 | 0.43 | 0.062 | 31.562 | 4.002 | 21.332 | 2.760 | 29.125 | 2.437 | 0.008 |
| **T1E3** | 10.785 | 6.007 | 2.122 | 7.768 | 1.332 | 0.337 | 1.067 | 0.143 | 0.771 | 0.126 | 0.324 | 0.046 | 0.301 | 0.043 | 31.172 | 3.416 | 24.808 | 2.930 | 29.418 | 1.754 | 0.301 |
| **T1E4** | 15.84 | 0.205 | 3.184 | 11.558 | 2.078 | 0.57 | 1.805 | 0.251 | 1.3 | 0.217 | 0.557 | 0.08 | 0.518 | 0.076 | 38.239 | 4.808 | 21.172 | 2.880 | 35.24 | 2.999 | 0.007 |
| **T1E5** | 5.191 | 0.205 | 3.515 | 13.033 | 2.27 | 0.634 | 1.967 | 0.27 | 1.373 | 0.236 | 0.608 | 0.087 | 0.564 | 0.082 | 30.035 | 3.474 | 6.373 | 2.883 | 26.815 | 3.22 | 0.012 |
| **T1E6** | 16.127 | 0.205 | 3.157 | 11.503 | 2.059 | 0.527 | 1.72 | 0.237 | 1.221 | 0.204 | 0.534 | 0.077 | 0.499 | 0.075 | 38.145 | 4.868 | 22.377 | 2.849 | 35.298 | 2.847 | 0.007 |
| **T1E7** | 15.455 | 0.205 | 2.965 | 11.343 | 2.216 | 0.53 | 1.74 | 0.237 | 1.242 | 0.206 | 0.534 | 0.078 | 0.491 | 0.073 | 37.315 | 4.701 | 21.794 | 2.929 | 34.454 | 2.861 | 0.007 |
| **T1E8** | 11.069 | 0.205 | 3.406 | 12.359 | 2.219 | 0.58 | 1.834 | 0.251 | 1.286 | 0.211 | 0.555 | 0.078 | 0.506 | 0.075 | 34.629 | 4.040 | 15.146 | 2.996 | 31.672 | 2.957 | 0.008 |
| **T1E9** | 16.337 | 0.205 | 3.152 | 11.616 | 2.016 | 0.544 | 1.757 | 0.246 | 1.278 | 0.221 | 0.565 | 0.085 | 0.529 | 0.081 | 38.632 | 4.923 | 21.382 | 2.745 | 35.627 | 3.005 | 0.007 |
| **T1E10** | 12.001 | 0.205 | 2.443 | 8.973 | 1.689 | 0.466 | 1.593 | 0.247 | 1.427 | 0.242 | 0.634 | 0.091 | 0.579 | 0.082 | 30.672 | 3.636 | 14.351 | 2.274 | 27.37 | 3.302 | 0.009 |
| **T1E11** | 15.597 | 0.205 | 3.127 | 11.823 | 2.286 | 0.658 | 2.2 | 0.317 | 1.742 | 0.292 | 0.742 | 0.109 | 0.707 | 0.103 | 39.908 | 4.755 | 15.274 | 2.572 | 35.896 | 4.012 | 0.007 |
| **T1E12** | 13.485 | 0.205 | 2.554 | 9.091 | 1.587 | 0.42 | 1.297 | 0.169 | 0.85 | 0.139 | 0.369 | 0.052 | 0.351 | 0.053 | 30.622 | 4.014 | 26.600 | 3.054 | 28.639 | 1.983 | 0.008 |
| **Average** | 13.194 | 0.732 | 2.927 | 10.780 | 1.950 | 0.519 | 1.674 | 0.233 | 1.231 | 0.206 | 0.534 | 0.077 | 0.498 | 0.073 | 34.630 | 4.240 | 19.146 | 2.807 | 31.778 | 2.852 | 0.035 |
| **STD** | 3.350 | 1.749 | 0.440 | 1.661 | 0.322 | 0.095 | 0.315 | 0.048 | 0.268 | 0.047 | 0.117 | 0.018 | 0.110 | 0.016 | 3.882 | 0.586 | 5.797 | 0.220 | 3.603 | 0.622 | 0.088 |
| **STD ERR** | 0.922 | 2.044 | 0.257 | 0.506 | 0.230 | 0.132 | 0.243 | 0.099 | 0.242 | 0.103 | 0.161 | 0.063 | 0.156 | 0.059 | 0.660 | 0.285 | 1.325 | 0.131 | 0.639 | 0.368 | 0.475 |
| **Min** | 5.191 | 0.205 | 2.122 | 7.768 | 1.332 | 0.337 | 1.067 | 0.143 | 0.771 | 0.126 | 0.324 | 0.046 | 0.301 | 0.043 | 30.035 | 3.416 | 6.373 | 2.274 | 26.815 | 1.754 | 0.007 |
| **Max** | 16.337 | 6.007 | 3.515 | 13.033 | 2.286 | 0.658 | 2.200 | 0.317 | 1.742 | 0.292 | 0.742 | 0.109 | 0.707 | 0.103 | 39.908 | 4.923 | 26.600 | 3.054 | 35.896 | 4.012 | 0.301 |

**Table 2:** REE concentrations for tailing 2 (mine T2) in ppm.

| Sample ID | La | Ce | Pr | Nd | Sm | Eu | Gd | Tb | Dy | Ho | Er | Tm | Yb | Lu | ∑REE | ±∑REE | LaN/YbN | GdN/YbN | ∑LREE | ∑HREE | Ce/Ce* |
|---|---|---|---|---|---|---|---|---|---|---|---|---|---|---|---|---|---|---|---|---|---|
| **T2E1** | 0.217 | 0.205 | 4.705 | 17.106 | 3.184 | 0.925 | 2.958 | 0.418 | 2.108 | 0.365 | 0.936 | 0.131 | 0.861 | 0.126 | 34.245 | 4.448 | 0.175 | 2.840 | 29.3 | 4.945 | 0.049 |
| **T2E3** | 5.049 | 0.205 | 3.513 | 12.774 | 2.269 | 0.632 | 2.03 | 0.279 | 1.501 | 0.26 | 0.675 | 0.096 | 0.627 | 0.093 | 30.003 | 3.393 | 5.575 | 2.676 | 26.472 | 3.531 | 0.012 |
| **T2E4** | 15.972 | 0.205 | 3.113 | 11.421 | 2.008 | 0.545 | 1.709 | 0.242 | 1.312 | 0.213 | 0.544 | 0.077 | 0.49 | 0.071 | 37.922 | 4.821 | 22.569 | 2.883 | 34.973 | 2.949 | 0.007 |
| **T2E5** | 4.94 | 0.205 | 3.252 | 11.897 | 2.08 | 0.544 | 1.725 | 0.247 | 1.317 | 0.225 | 0.587 | 0.087 | 0.561 | 0.084 | 27.751 | 3.183 | 6.097 | 2.542 | 24.643 | 3.108 | 0.012 |
| **T2E6** | 0.217 | 0.205 | 4.278 | 15.521 | 2.721 | 0.74 | 2.274 | 0.319 | 1.65 | 0.283 | 0.736 | 0.105 | 0.688 | 0.106 | 29.843 | 4.045 | 0.218 | 2.732 | 25.956 | 3.887 | 0.051 |
| **T2E7** | 13.208 | 0.205 | 2.505 | 9.108 | 1.625 | 0.401 | 1.3 | 0.186 | 1.007 | 0.17 | 0.436 | 0.062 | 0.408 | 0.058 | 30.679 | 3.946 | 22.414 | 2.634 | 28.352 | 2.327 | 0.009 |
| **T2E8** | 16.605 | 0.205 | 3.097 | 11.492 | 2.042 | 0.55 | 1.697 | 0.235 | 1.281 | 0.221 | 0.586 | 0.084 | 0.552 | 0.084 | 38.731 | 4.962 | 20.828 | 2.541 | 35.688 | 3.043 | 0.007 |
| **T2E9** | 5.499 | 0.205 | 3.599 | 13.001 | 2.235 | 0.583 | 1.827 | 0.258 | 1.383 | 0.237 | 0.62 | 0.09 | 0.575 | 0.088 | 30.2 | 3.492 | 6.621 | 2.626 | 26.949 | 3.251 | 0.011 |
| **T2E10** | 6.001 | 0.205 | 4.097 | 14.996 | 2.589 | 0.699 | 2.179 | 0.307 | 1.598 | 0.28 | 0.725 | 0.103 | 0.67 | 0.1 | 34.549 | 4.001 | 6.201 | 2.688 | 30.766 | 3.783 | 0.010 |
| **T2E12** | 13.163 | 0.205 | 2.462 | 8.954 | 1.535 | 0.392 | 1.207 | 0.157 | 0.789 | 0.131 | 0.345 | 0.051 | 0.331 | 0.05 | 29.772 | 3.933 | 27.534 | 3.014 | 27.918 | 1.854 | 0.009 |
| **T2E13** | 15.1 | 0.2 | 3.087 | 11.484 | 2.188 | 0.564 | 1.928 | 0.29 | 1.649 | 0.273 | 0.694 | 0.097 | 0.62 | 0.088 | 38.262 | 4.620 | 16.863 | 2.570 | 34.551 | 3.711 | 0.007 |
| **Average** | 8.725 | 0.205 | 3.428 | 12.523 | 2.225 | 0.598 | 1.894 | 0.267 | 1.418 | 0.242 | 0.626 | 0.089 | 0.580 | 0.086 | 32.905 | 4.077 | 12.281 | 2.704 | 29.597 | 3.308 | 0.017 |
| **STD** | 6.209 | 0.002 | 0.706 | 2.541 | 0.473 | 0.151 | 0.480 | 0.070 | 0.351 | 0.062 | 0.158 | 0.022 | 0.143 | 0.021 | 3.984 | 0.585 | 9.897 | 0.152 | 3.885 | 0.823 | 0.017 |
| **STD ERR** | 2.102 | 0.003 | 0.381 | 0.718 | 0.317 | 0.196 | 0.349 | 0.135 | 0.294 | 0.126 | 0.200 | 0.072 | 0.187 | 0.073 | 0.695 | 0.290 | 2.824 | 0.092 | 0.714 | 0.452 | 0.128 |
| **Min** | 0.217 | 0.200 | 2.462 | 8.954 | 1.535 | 0.392 | 1.207 | 0.157 | 0.789 | 0.131 | 0.345 | 0.051 | 0.331 | 0.050 | 27.751 | 3.183 | 0.175 | 2.541 | 24.643 | 1.854 | 0.007 |
| **Max** | 16.605 | 0.205 | 4.705 | 17.106 | 3.184 | 0.925 | 2.958 | 0.418 | 2.108 | 0.365 | 0.936 | 0.131 | 0.861 | 0.126 | 38.731 | 4.962 | 27.534 | 3.014 | 35.688 | 4.945 | 0.051 |

The REE patterns are enriched with LREE, as the LaN/YbN ratio for tailing 1 varied from 6.373 to 26.6 ppm and 0.175 to 27.534 ppm for tailing 2. These values were consistent with the ones reported by (Silva, Pinto et al. 2016). The GdN/YbN ratios ranged from 2.572 to 2.996 ppm for tailing 1 and 2.541 to 3.014 ppm for tailing 2. Tailings one and two exhibited HREE patterns that were almost flat with no fractionation. All the samples displayed a consistently strong negative cerium (Ce) anomalies with Ce/Ce* ratios ranging between 0.007 to 0.301 and 0.007 to 0.051 for tailing 1 and tailing 2 respectively. Ce/Ce* ratios is less than 1 (<1). This indicated a negative cerium anomaly. In Chapter 2, Cerium was discussed as element that stays in the trivalent state under conditions without oxygen but its solubility decreases under conditions with oxygen and it precipitates, thus, causing a positive anomaly compared to the other REEs. In this case a negative Cerium was obtained this could be mean that Cerium solubility was increased thus causing a negative Cerium. The enrichment or depletion of Ce acts as a tool in the identification of origin as discussed in chapter 2.

Four REEs were found to be a fingerprint of both mines T1 and T2. These were La, Pr, Nd, Sm. Tailing 1 had higher concentrations of La than all other REEs and in tailing two, Nd had a higher concentration than all other REEs. This suggested an enrichment of the LREEs, indicating a large concentration of uranium. The proportion of these REEs could be used for geochronology and fossil dating, as their rock concentrations were modified slowly by geochemical processes (Khumalo and Mathuthu, 2018).

### 4.1.1 Signatures of REE relative to CI-chondrite

Figure 7 and 8 displays a strong negative Ce anomaly, showing no HREE (Tb-Lu) fractionation. This were possibly due to the geo-tectonic activity related with the mining area. The HREE were flat, clearly indicating that the uranium processing or geological factors did not change them. The LREE exhibits La, Pr, Nd, Sm, Eu and Gd enrichment with an exception of La that looked slightly depleted in samples T2E1 and T2E3. The REE patterns of the two tailings are however similar in general, demonstrating the characteristic signature for this mine.

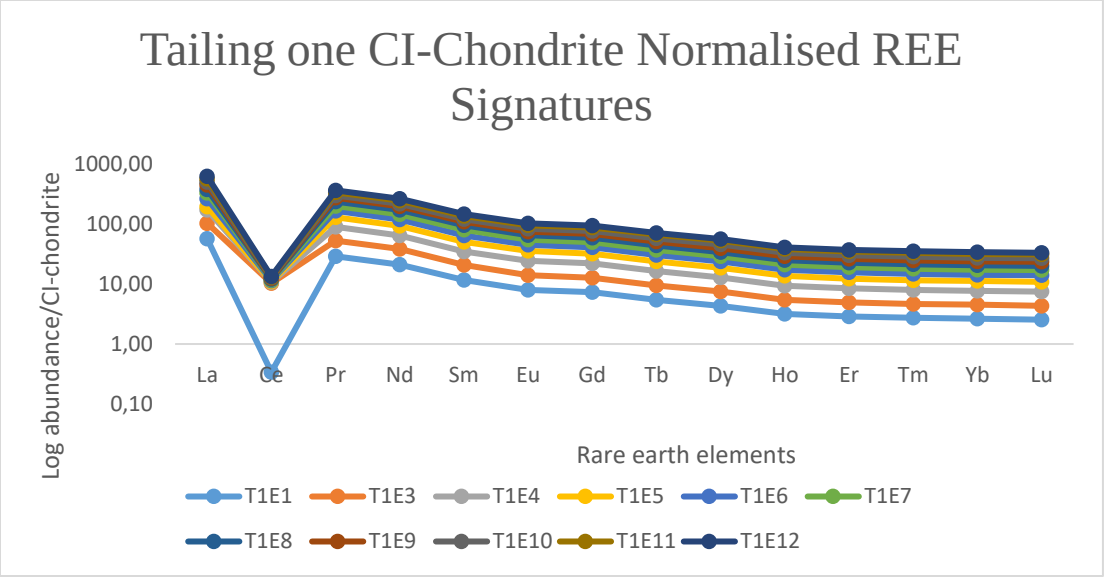


**Figure 7:** CI-chondrite normalized (Anders and Grevesse, 1989) REE pattern of tailing one from a South African uranium mine.

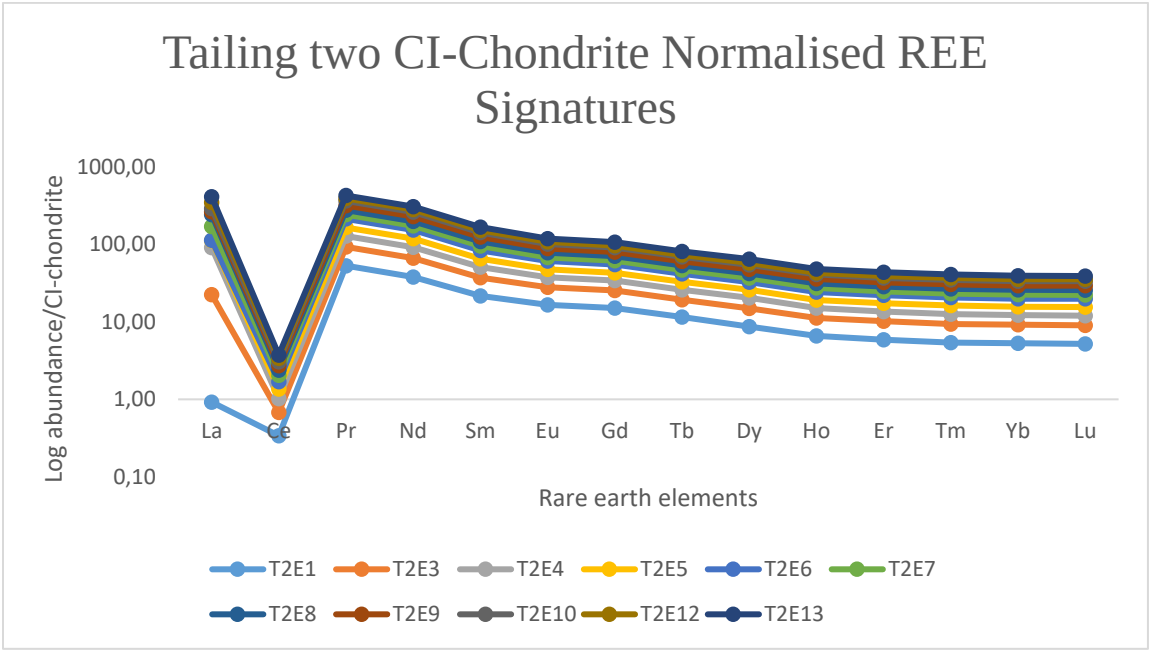


**Figure 8:** CI-chondrite normalized (Anders and Grevesse, 1989) REE pattern of tailing two from a South African uranium mine.

**Determination of REE concentrations from a Namibian uranium mine**

Table 3 and Table 4 provide REE concentrations of the analyzed tailings in Namibia. The REE concentration of mine tailing and underground water samples were distinguished. Mine tailing had REE (∑REE) concentrations, which were significantly lower compared to underground water, with the total number of REE (∑REE) of mine tailing, which were ranging between 0.434 and 0.644 ppm and for underground water it ranged between 3.630 and 29.370 ppm. All these are lower than the coarse and fine sediments reported by (Silva et al., 2016), which consists of ∑REE ranging between 48.35 to 95.23 ppm and 125.38 to 320.81 ppm respectively. These values were also lower than the fine sand and coarse sand which ranges from 12.5 to 63.6 ppm and 126.2 to 877.6 ppm reported by (Sako et al., 2009). The sum of the LREEs (∑LHREE) and HREEs (∑HREE) ranged between 0.388 to 0.582 and 0.046 to 0.064 ppm respectively for mine tailings and for underground water it ranged between 3.140 to 28.150 and 0.490 to 3.120. LREE (∑LHREE) contributed about 89.22% while HREE (∑HREE) contributed 10.78% of the total REEs for the mine tailings. For underground water, LREE (∑LHREE) contributed about 87.46% while HREE (∑HREE) contributed 12.54% of the total REEs.

The REE patterns were enriched with LREE, as the LaN/YbN ratio for mine tailings varied from 5.484 to 7.048 ppm and 1.511 to 3.936 ppm for underground water, see Table 3 and 4. These values were consistence with the ones reported by (Silva, Pinto et al. 2016). The GdN/YbN ratios ranged from 1.470 to 1.730 ppm for mine tailings and between 1.202 to 1.748 ppm for underground water. Mine tailings and underground water exhibited HREE patterns that were almost flat with no fractionation. All the samples displayed consistently negative Eu anomalies with an exception of underground water which also exhibited a positive Ce anomaly with Ce/Ce* ratios ranging between 1.424 and 1.625, this Ce/Ce* ratio is greater than 1 (>1) and it indicates a positive anomaly. Eu/Eu* ratios ranging between 0.456 to 0.609 for underground water and 0.436 to 0.555 for mine tailings, the Eu/Eu* ratio is less than 1 (<1) and this is an indication of a negative anomaly. As mentioned in chapter 2 a decrease in the solubility of Cerium with oxygen and its precipitates results in a positive Cerium which is then used as a tool to identify the origin of samples. Depletion of Eu (negative anomaly) and enrichment of Ce (positive anomaly) also acts a tool for this identification of geological location of samples as discussed in Chapter 2.

**Table 3:** REE concentrations for mine tailings (NAM-T) in ppm.

| Sample ID | La | Ce | Pr | Nd | Sm | Eu | Gd | Tb | Dy | Ho | Er | Tm | Yb | Lu | ∑REE | ±∑REE | LaN/YbN | GdN/YbN | ∑LREE | ∑HREE | Eu/Eu* |
|---|---|---|---|---|---|---|---|---|---|---|---|---|---|---|---|---|---|---|---|---|---|
| **NAM-T-1** | 0.081 | 0.179 | 0.022 | 0.087 | 0.018 | 0.003 | 0.018 | 0.003 | 0.020 | 0.004 | 0.011 | 0.002 | 0.010 | 0.002 | 0.461 | 0.050 | 5.484 | 1.470 | 0.409 | 0.052 | 0.555 |
| **NAM-T-2** | 0.106 | 0.231 | 0.029 | 0.114 | 0.023 | 0.004 | 0.024 | 0.004 | 0.026 | 0.005 | 0.013 | 0.002 | 0.012 | 0.002 | 0.597 | 0.065 | 5.967 | 1.612 | 0.532 | 0.064 | 0.550 |
| **NAM-T-3** | 0.089 | 0.161 | 0.024 | 0.096 | 0.020 | 0.003 | 0.020 | 0.004 | 0.023 | 0.004 | 0.012 | 0.002 | 0.011 | 0.002 | 0.472 | 0.048 | 5.564 | 1.516 | 0.415 | 0.057 | 0.522 |
| **NAM-T-4** | 0.120 | 0.255 | 0.031 | 0.123 | 0.025 | 0.004 | 0.025 | 0.004 | 0.025 | 0.005 | 0.013 | 0.002 | 0.012 | 0.002 | 0.644 | 0.072 | 7.048 | 1.730 | 0.582 | 0.061 | 0.448 |
| **NAM-T-5** | 0.077 | 0.170 | 0.021 | 0.082 | 0.018 | 0.003 | 0.017 | 0.003 | 0.019 | 0.003 | 0.009 | 0.001 | 0.009 | 0.001 | 0.434 | 0.048 | 5.855 | 1.589 | 0.388 | 0.046 | 0.436 |
| **NAM-T-6** | 0.084 | 0.181 | 0.022 | 0.091 | 0.019 | 0.003 | 0.019 | 0.003 | 0.021 | 0.004 | 0.011 | 0.002 | 0.010 | 0.002 | 0.471 | 0.051 | 5.593 | 1.512 | 0.418 | 0.052 | 0.553 |
| **NAM-T-7** | 0.091 | 0.206 | 0.025 | 0.099 | 0.020 | 0.004 | 0.021 | 0.004 | 0.023 | 0.004 | 0.012 | 0.002 | 0.011 | 0.002 | 0.524 | 0.058 | 5.666 | 1.541 | 0.466 | 0.058 | 0.540 |
| **NAM-T-8** | 0.086 | 0.183 | 0.023 | 0.092 | 0.019 | 0.003 | 0.019 | 0.003 | 0.021 | 0.004 | 0.011 | 0.002 | 0.010 | 0.002 | 0.477 | 0.052 | 5.852 | 1.550 | 0.424 | 0.052 | 0.544 |
| **NAM-T-9** | 0.084 | 0.180 | 0.022 | 0.090 | 0.018 | 0.003 | 0.018 | 0.003 | 0.020 | 0.004 | 0.010 | 0.002 | 0.010 | 0.002 | 0.466 | 0.051 | 6.002 | 1.565 | 0.416 | 0.049 | 0.515 |
| **NAM-T-10** | 0.098 | 0.221 | 0.026 | 0.106 | 0.021 | 0.004 | 0.022 | 0.004 | 0.023 | 0.004 | 0.012 | 0.002 | 0.011 | 0.002 | 0.555 | 0.062 | 6.335 | 1.675 | 0.498 | 0.057 | 0.519 |
| **Average** | 0.092 | 0.197 | 0.025 | 0.098 | 0.020 | 0.003 | 0.020 | 0.004 | 0.022 | 0.004 | 0.011 | 0.002 | 0.011 | 0.002 | 0.510 | 0.056 | 5.936 | 1.576 | 0.455 | 0.055 | 0.518 |
| **STD** | 0.013 | 0.030 | 0.003 | 0.013 | 0.002 | 0.000 | 0.002 | 0.000 | 0.002 | 0.000 | 0.001 | 0.000 | 0.001 | 0.000 | 0.068 | 0.008 | 0.465 | 0.079 | 0.063 | 0.006 | 0.043 |
| **STD ERR** | 0.043 | 0.068 | 0.022 | 0.042 | 0.016 | 0.008 | 0.017 | 0.007 | 0.016 | 0.006 | 0.011 | 0.004 | 0.009 | 0.004 | 0.095 | 0.035 | 0.191 | 0.063 | 0.094 | 0.024 | 0.059 |
| **Min** | 0.077 | 0.161 | 0.021 | 0.082 | 0.018 | 0.003 | 0.017 | 0.003 | 0.019 | 0.003 | 0.009 | 0.001 | 0.009 | 0.001 | 0.434 | 0.048 | 5.484 | 1.470 | 0.388 | 0.046 | 0.436 |
| **Max** | 0.120 | 0.255 | 0.031 | 0.123 | 0.025 | 0.004 | 0.025 | 0.004 | 0.026 | 0.005 | 0.013 | 0.002 | 0.012 | 0.002 | 0.644 | 0.072 | 7.048 | 1.730 | 0.582 | 0.064 | 0.555 |

**Table 4:** REE concentrations for underground water (UDW) in ppm.

| SAMPLE ID | | La | Ce | Pr | Nd | Sm | Eu | Gd | Tb | Dy | Ho | Er | Tm | Yb | Lu | ∑REE | ±∑REE | LaN/YbN | GdN/YbN | ∑LREE | ∑HREE | Ce/Ce* | Eu/Eu* |
|---|---|---|---|---|---|---|---|---|---|---|---|---|---|---|---|---|---|---|---|---|---|---|---|
| **UDW-1** | | 0.610 | 25.350 | 0.230 | 1.280 | 0.280 | 0.050 | 0.350 | 0.080 | 0.490 | 0.090 | 0.260 | 0.040 | 0.230 | 0.030 | 29.370 | 6.700 | 1.836 | 1.258 | 28.150 | 1.220 | 16.225 | 0.485 |
| **UDW-2** | | 0.480 | 1.710 | 0.150 | 0.650 | 0.150 | 0.030 | 0.170 | 0.030 | 0.220 | 0.050 | 0.120 | 0.010 | 0.100 | 0.020 | 3.890 | 0.451 | 3.323 | 1.405 | 3.340 | 0.550 | 1.528 | 0.571 |
| **UDW-3** | | 0.910 | 3.560 | 0.320 | 1.340 | 0.310 | 0.060 | 0.370 | 0.070 | 0.430 | 0.080 | 0.220 | 0.030 | 0.190 | 0.030 | 7.920 | 0.938 | 3.316 | 1.610 | 6.870 | 1.050 | 1.582 | 0.538 |
| **UDW-4** | | 2.430 | 9.910 | 0.900 | 3.750 | 0.940 | 0.190 | 1.100 | 0.220 | 1.300 | 0.250 | 0.660 | 0.090 | 0.520 | 0.080 | 22.340 | 2.602 | 3.236 | 1.748 | 19.220 | 3.120 | 1.607 | 0.567 |
| **UDW-5** | | 0.470 | 1.580 | 0.150 | 0.610 | 0.140 | 0.030 | 0.160 | 0.030 | 0.200 | 0.040 | 0.110 | 0.010 | 0.090 | 0.010 | 3.630 | 0.419 | 3.616 | 1.469 | 3.140 | 0.490 | 1.427 | 0.609 |
| **UDW-6** | | 1.080 | 3.870 | 0.360 | 1.500 | 0.330 | 0.070 | 0.380 | 0.070 | 0.450 | 0.090 | 0.240 | 0.030 | 0.190 | 0.030 | 8.690 | 1.026 | 3.936 | 1.653 | 7.590 | 1.100 | 1.488 | 0.600 |
| **UDW-7** | | 0.630 | 2.530 | 0.240 | 1.020 | 0.300 | 0.050 | 0.370 | 0.080 | 0.530 | 0.100 | 0.250 | 0.040 | 0.220 | 0.040 | 6.400 | 0.657 | 1.983 | 1.390 | 5.140 | 1.260 | 1.560 | 0.456 |
| **UDW-8** | | 1.950 | 6.940 | 0.700 | 2.940 | 0.780 | 0.150 | 0.910 | 0.190 | 1.210 | 0.230 | 0.590 | 0.080 | 0.480 | 0.070 | 17.220 | 1.830 | 2.813 | 1.567 | 14.370 | 2.850 | 1.424 | 0.541 |
| **UDW-9** | | 1.520 | 6.670 | 0.570 | 2.420 | 0.660 | 0.120 | 0.690 | 0.140 | 0.910 | 0.170 | 0.430 | 0.060 | 0.360 | 0.050 | 14.770 | 1.744 | 2.923 | 1.584 | 12.650 | 2.120 | 1.718 | 0.540 |
| **UDW-10** | | 0.480 | 1.770 | 0.170 | 0.770 | 0.220 | 0.040 | 0.320 | 0.070 | 0.480 | 0.090 | 0.250 | 0.040 | 0.220 | 0.030 | 4.950 | 0.459 | 1.511 | 1.202 | 3.770 | 1.180 | 1.485 | 0.458 |
| **Average** | | 1.056 | 6.389 | 0.379 | 1.628 | 0.411 | 0.079 | 0.482 | 0.098 | 0.622 | 0.119 | 0.313 | 0.043 | 0.260 | 0.039 | 11.918 | 1.683 | 2.849 | 1.489 | 10.424 | 1.494 | 3.004 | 0.536 |
| **STDEV** | | 0.692 | 7.210 | 0.259 | 1.063 | 0.279 | 0.055 | 0.314 | 0.064 | 0.386 | 0.073 | 0.187 | 0.027 | 0.147 | 0.022 | 8.743 | 1.906 | 0.812 | 0.175 | 8.221 | 0.904 | 4.646 | 0.055 |
| **STD ERR** | | 0.674 | 2.853 | 0.421 | 0.833 | 0.436 | 0.197 | 0.453 | 0.206 | 0.489 | 0.211 | 0.334 | 0.129 | 0.288 | 0.111 | 2.533 | 1.469 | 0.481 | 0.144 | 2.546 | 0.740 | 2.681 | 0.074 |
| **Min** | | 0.470 | 1.580 | 0.150 | 0.610 | 0.140 | 0.030 | 0.160 | 0.030 | 0.200 | 0.040 | 0.110 | 0.010 | 0.090 | 0.010 | 3.630 | 0.419 | 1.511 | 1.202 | 3.140 | 0.490 | 1.424 | 0.456 |
| **Max** | | 2.430 | 25.350 | 0.900 | 3.750 | 0.940 | 0.190 | 1.100 | 0.220 | 1.300 | 0.250 | 0.660 | 0.090 | 0.520 | 0.080 | 29.370 | 6.700 | 3.936 | 1.748 | 28.150 | 3.120 | 16.225 | 0.609 |

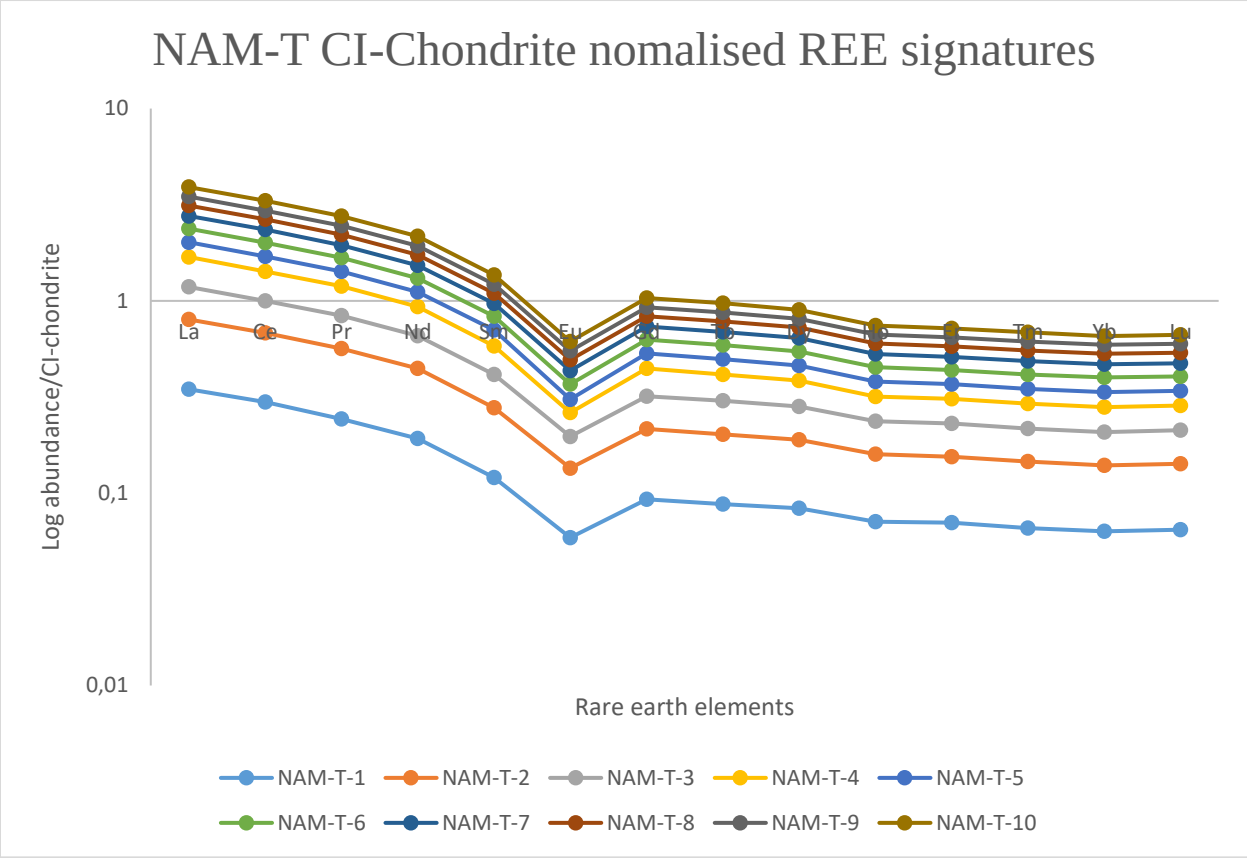


**Figure 9:** CI-chondrite normalized (Anders and Grevesse, 1989) REE pattern of mine tailing from a Namibian uranium mine.

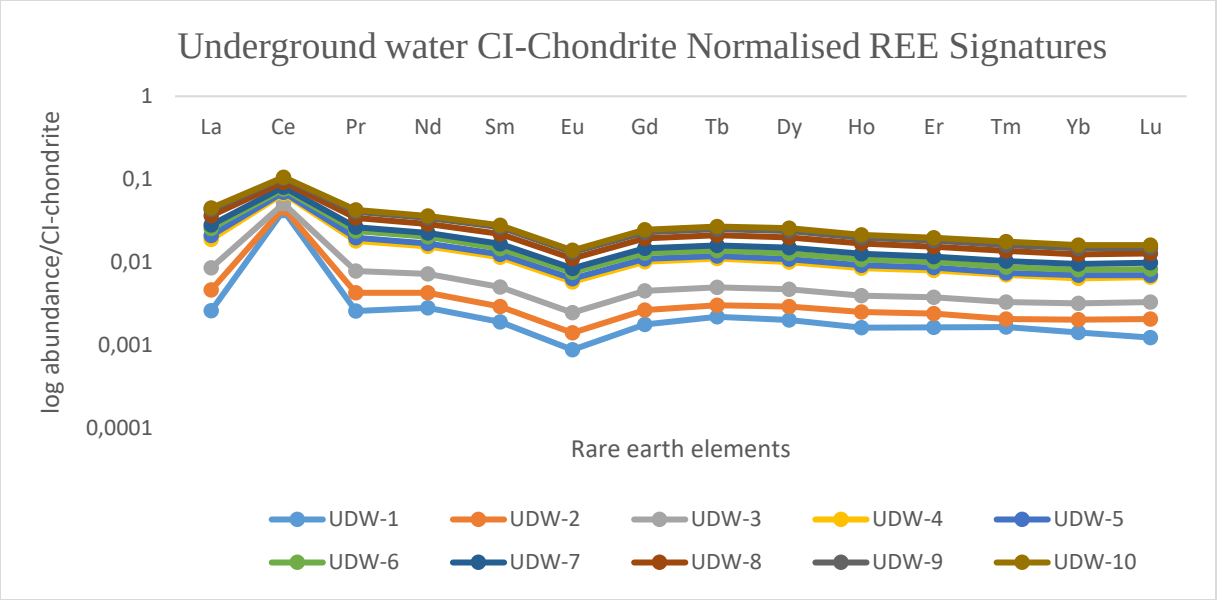


**Figure 10:** CI-chondrite normalized (Anders and Grevesse, 1989) REE pattern of underground water from a Namibian uranium mine.

**REE pattern of samples taken from Namibia**

Three REEs were found to be a fingerprint on both the mine tailing and underground water. These were La, Ce and Nd. The mine tailing ad underground water both had higher concentrations of Ce than all other REEs. This indicated an enrichment of the LREEs, indicating a large concentration of uranium.

Samples of this mine tailing shown in Figure 9 and 10 exhibited a strong negative Eu anomaly, showing no HREE (Tb-Lu) fractionation and LREE (La-Gd) fractionation. This is possibly due to the geo-tectonic activity related with the mining area. The HREE were flat clearly indicating that the uranium processing or geological factors did not change them. The LREE exhibited La, Ce, Pr, Nd and Sm enrichment with an exception of Eu. A negative Eu anomaly is an identification of a quartz-pebble conglomerate (Varga et al., 2010b), which is due to REE mineralizing fluids associated with granitic melt or weathered granitic deposits. Figure 10 also indicates a positive Ce anomaly. The chondrite normalized REE patterns observed from Figure 9 and Figure 10 strongly agrees with the REE pattern obtained from Rossing uranium mine in Namibia, reported by (Krajko, 2016), which exhibited a negative Eu anomaly.

## 4.2 Determination of nuclear forensic signature lead isotopic ratios

Isotopic fingerprinting depends on the precise variation in isotopic abundance in order to identify the certain sources of Pb present in the samples. The isotopic ratios of Pb are analyzed using mass spectrometry, with either thermal ionization (TIMS) or with inductively coupled plasma (ICP-MS) as the ion source (Cheng and Hu, 2010). To calibrate the mass spectrometers and normalize the measured ratios of the four Pb isotopes, a standard reference material (such as NIST SRM-981) is required. In this study, ICP-MS (Perkin Elmer NexION 2000C) was used to measure lead isotopic ratios and the following national institute of standards and technology (NIST SRM 981) values with errors based on 95% confidence levels were used:

- Atomic abundance Ratio, $^{204}Pb/^{206}Pb = 0.059042 \pm 0.000037$
- Atomic abundance Ratio, $^{207}Pb/^{206}Pb = 0.91464 \pm 0.00033$
- Atomic abundance Ratio, $^{208}Pb/^{206}Pb = 2.1681 \pm 0.0008$
- Atomic abundance Ratio, $^{206}Pb/^{204}Pb = 16.9416$
- Atomic abundance Ratio, $^{207}Pb/^{204}Pb = 15.4998$
- Atomic abundance Ratio, $^{208}Pb/^{206}Pb = 36.7249$

**Determination of lead isotopic ratios of samples from South Africa**

All four lead isotopic ratios were identified using the isotopic method on ICP using the NIST standard as reference. The results were analysed using excel by plotting $^{207}Pb/^{206}Pb$ vs $^{204}Pb/^{206}Pb$ and $^{208}Pb/^{204}Pb$ vs $^{206}Pb/^{204}Pb$. The difference between these lead ratios in this study is higher than the NIST lead ratios this means that the uranium and thorium content in the uranium is higher (see Chapter 2).

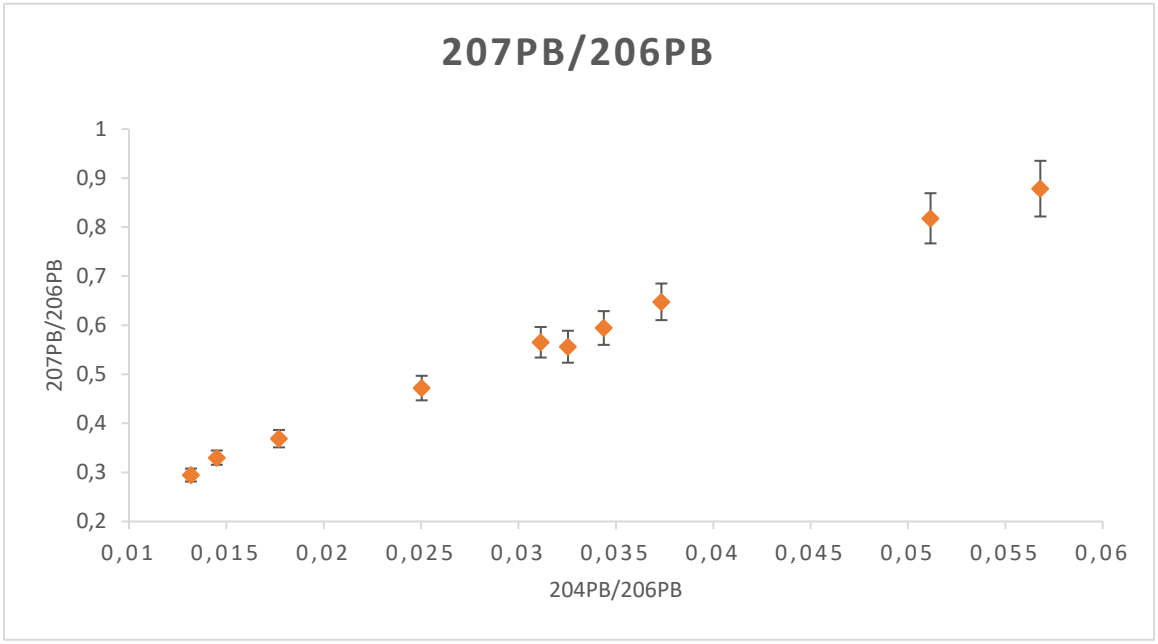


**Figure 11:** $^{207}Pb/^{206}Pb$ vs $^{204}Pb/^{206}Pb$ ratios of mine T1.

The values in Figure 11 varies from 0.013 to 0.056 for $^{204}Pb/^{206}Pb$, which were less than the NIST SRM 981 value of 0.059042. Figures 11 & 12 shows similarities for these plots, thus providing a signature for the mine. However, Figure 11 plots were distributed in linear form and in an increasing order across $^{206}Pb/^{204}Pb$. The $^{207}Pb/^{206}Pb$ content of Figure 11 and 12 were also lower than the NIST values; this could be because the $^{235}U$ content was very low in this sample.

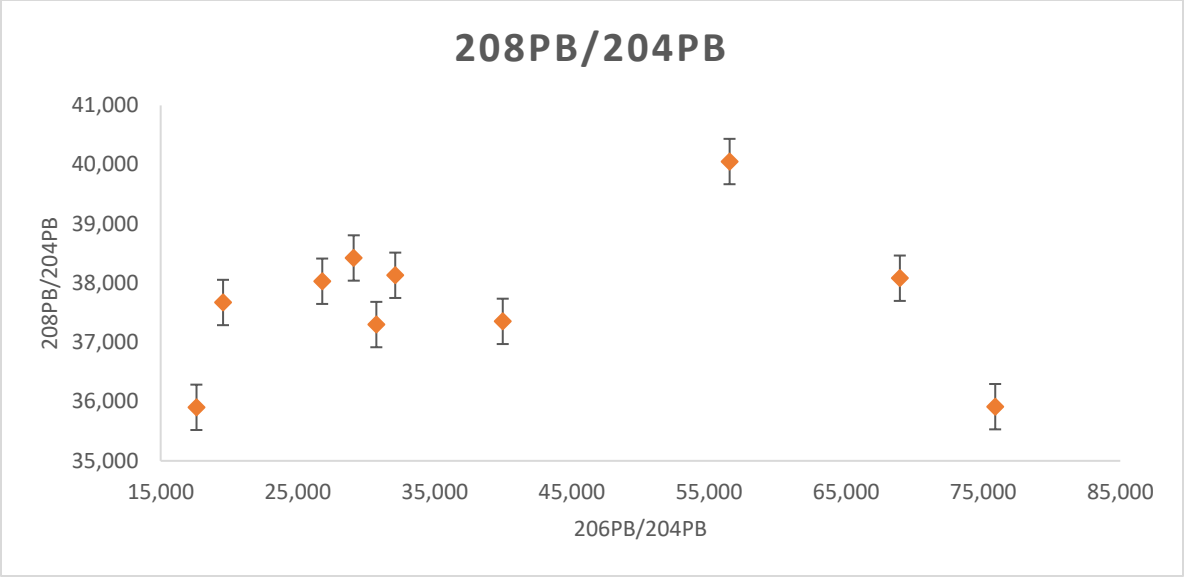


**Figure 12:** $^{208}Pb/^{204}Pb$ vs $^{206}Pb/^{204}Pb$ ratios of mine T1.

The lead ratios plotted in Figure 12 indicates the geological provenance of the deposit. There was a highly radiogenic isotopic composition of $^{206}Pb/^{204}Pb$ that was greater than 20, which could be due to Pb emanating from uranium ore. The abundance of isotopic compositions of radiogenic Pb means that the Pb in tailing one were derived from a Pb-rich ore. An isotopic composition is less radiogenic when it has $^{206}Pb/^{204}Pb$ less than 17.6 and this indicates poor uranium content in the deposit. Consequently, the three points in Figure 6 were due to the higher value of $^{206}Pb$, which implies a higher content rich in uranium ($^{238}U$). Since $^{206}Pb/^{204}Pb$ is greater than 20, these deposits are of radiogenic origin.

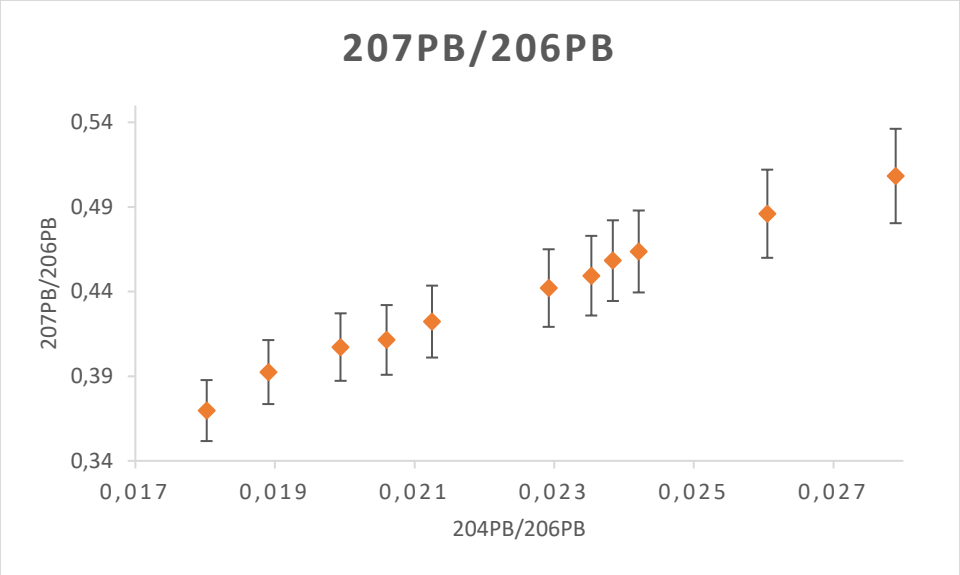


**Figure 13:** $^{207}Pb/^{206}Pb$ vs $^{204}Pb/^{206}Pb$ ratios of mine T2.

The values were distributed in a linear order along $^{204}Pb/^{206}Pb$ from 0.018 to 0.028, which was less than the NIST SRM 981 value of 0.059 for $^{204}Pb/^{206}Pb$. Figure 13 shows the content of $^{235}U$ which is less than 0.59 (NIST recommended limit). This means that this uranium was not enriched since its content was low. Similarities between Figures 13 and 14 were found and could be used as another signature for this mine. Mine T1 and T2 were from the same mine and therefore, display the same trend of having $^{204}Pb/^{206}Pb$ values that were lower than the NIST values, and both display a linear trend of $^{207}Pb/^{206}Pb$ versus $^{204}Pb/^{206}Pb$. The signature found in tailings one and two determines the origin of the mine.

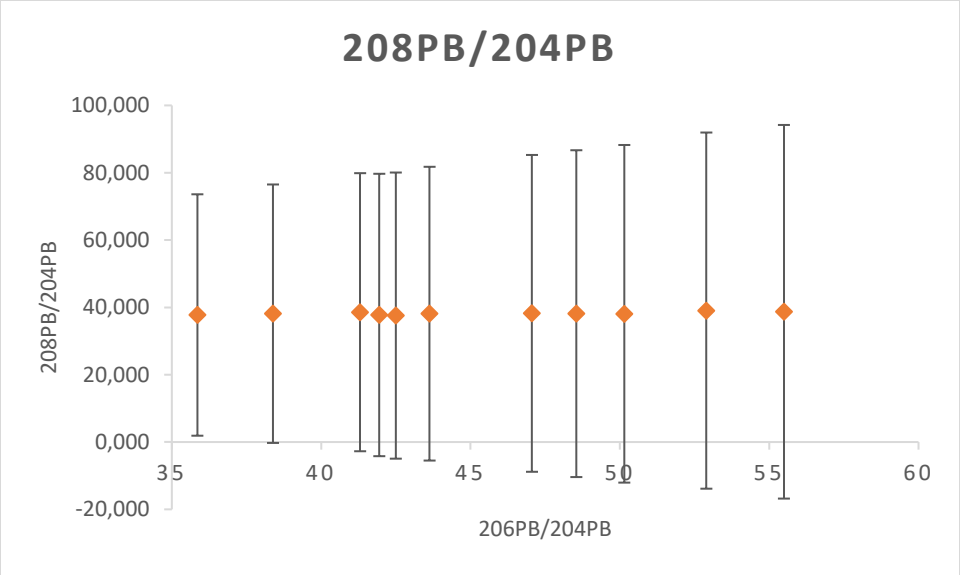


**Figure 14:** $^{208}Pb/^{204}Pb$ vs $^{206}Pb/^{204}Pb$ ratios of mine T2.

**Determination of lead isotopic ratios of samples from Namibia**

The values shown in the Figure 15 are set at 0.020 to 0.025, which was less than the NIST value of 0.059. This means that the sample contains a low $^{204}Pb$ content. There was a low $^{207}Pb/^{206}Pb$, which means that the sample contains a poor $^{235}U$ content.

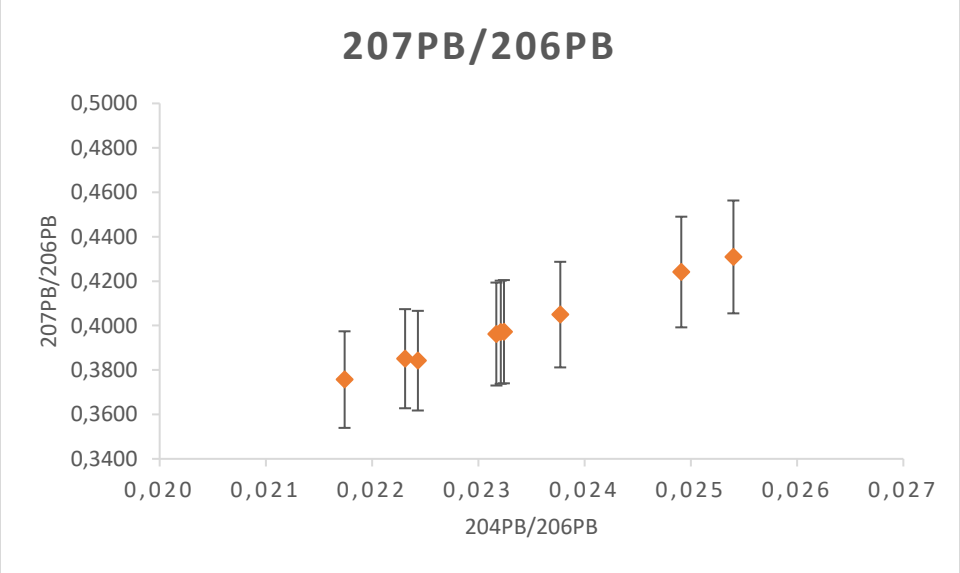


**Figure 15:** $^{207}Pb/^{206}Pb$ vs $^{204}Pb/^{206}Pb$ ratios of NAM-T.

In Figure 16, the $^{206}Pb/^{204}Pb$ was grouped between 39.37 and 45.99. This isotopic ratio was higher than 20, which indicates that this sample is of radiogenic origin and originated from a uranium rich ore deposit (see Figure 15). (Varga et al., 2009) obtained a value of 36.730 for the $^{208}Pb/^{206}Pb$ ratio, which was consistent to the NIST acceptable value of 36.7249. However; these values were not consistent with the ones obtained in this study because they were higher than the recommended value.

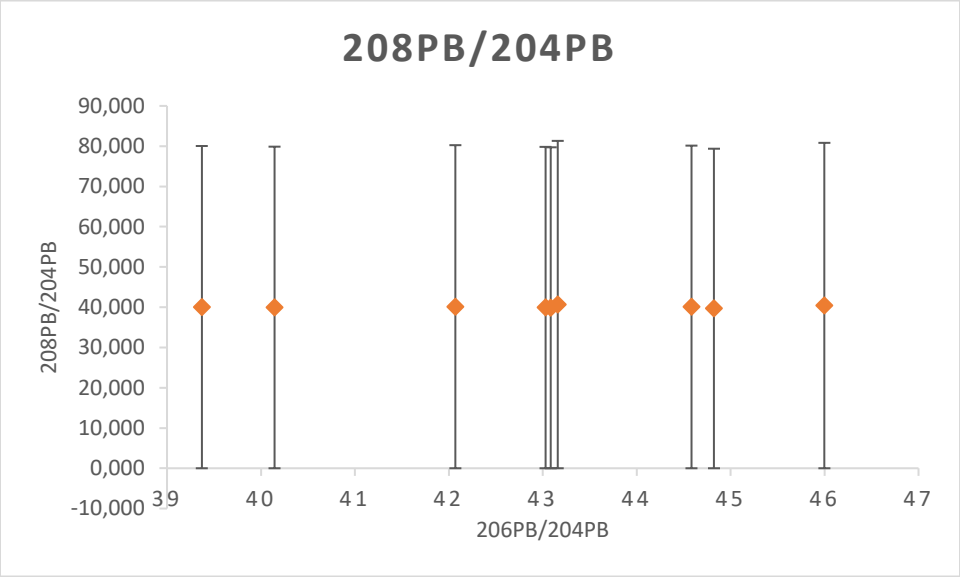


**Figure 16:** $^{208}Pb/^{204}Pb$ vs $^{206}Pb/^{204}Pb$ ratios of NAM-T.

Figure 17 was in accordance with the agreed value of NIST SRM 981 because the ratio of $^{206}Pb/^{204}Pb$ was distributed around the value of 0.059. Figures 17 and 18 displayed similarities, thus providing a signature for this mine. The $^{207}Pb/^{206}Pb$ content was also in agreement with the NIST values apart from two samples which were above 0.91, these background levels were expected since this underground water was not contaminated with nuclear materials.

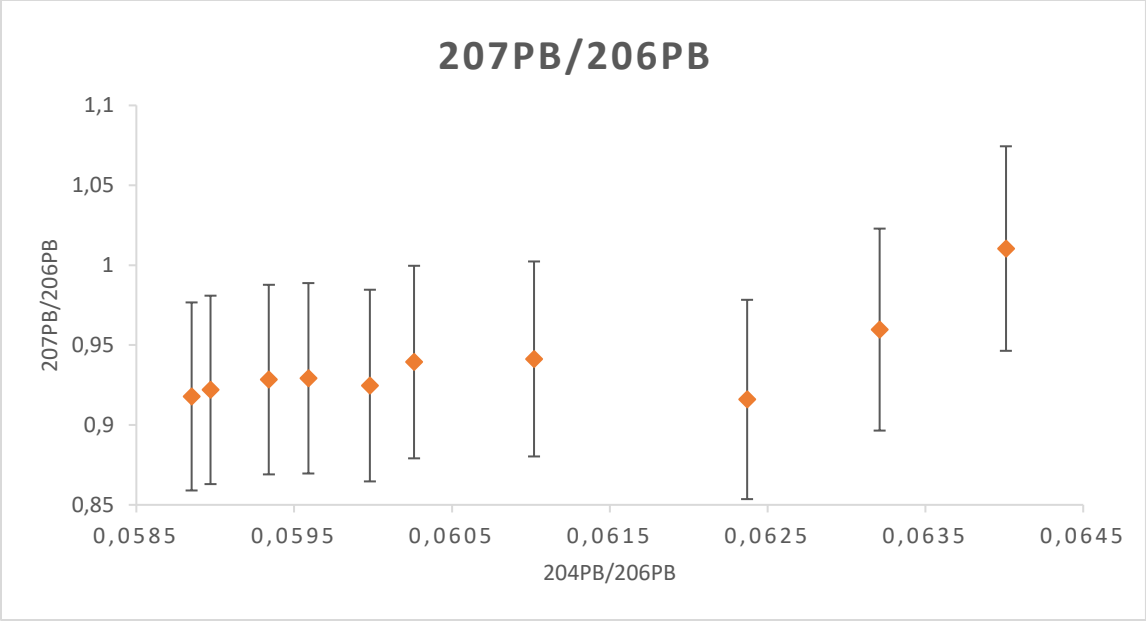


**Figure 17:** $^{207}Pb/^{206}Pb$ vs $^{204}Pb/^{206}Pb$ ratios of UDW.

Sample represented in Figure 18 below indicated that the sample was not radiogenic because $^{206}Pb/^{204}Pb$ was below 20. This means that the deposit had a low uranium content of $^{238}U$. This could be because this borehole sample was collected a distance (≥ 5 km) away from the mine and it shows that mining process did not contaminate it. An isotopic composition is non radiogenic when it has a $^{206}Pb/204Pb$ ratio less than 17.6 and this indicates poor uranium content in the deposit. Figure 18 shows the natural lead ratios and from the results, all the lead ratios were distributed at 35 which is slightly lower than the NIST values. Since the decay product of $^{232}Th$ is $^{208}Pb$, this implies that thorium content in this sample was very low.

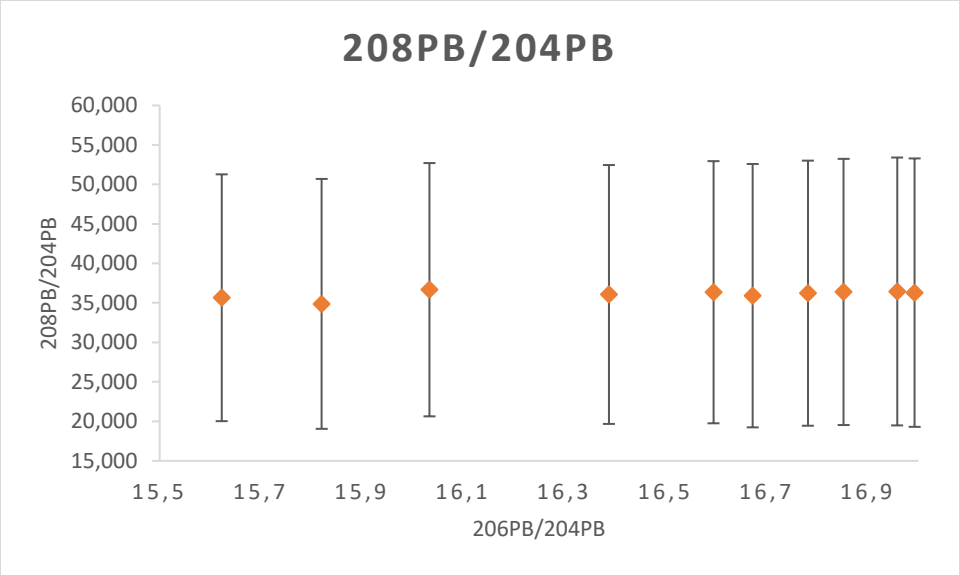


**Figure 18:** $^{208}Pb/^{204}Pb$ vs $^{206}Pb/^{204}Pb$ ratios of UDW.

Figures 19, 20 and 21 displayed the latest natural ratios of $^{206}Pb/^{204}Pb$, $^{207}Pb/^{204}Pb$ and $^{208}Pb/^{204}Pb$. The greater the radiogenic lead variation from the natural lead composition, the greater the deposit age and the greater the uranium and thorium content in the source rock. The lead isotopic composition of ore concentrates in most cases differs vastly from that of the typical natural lead and the ratios varied over a wide range. The lack of consistency of $^{206}Pb/^{204}Pb$, $^{207}Pb/^{204}Pb$ and $^{208}Pb/^{204}Pb$ ratios between samples of different origins is several orders of magnitude. The broad range of inconsistency is highly beneficial and can be used to differentiate ore concentrate and to validate the origin of the uranium ore by comparing with a standard sample of known origin. As can be seen from replicate samples from South Africa (mine T1 and T2) and Namibia (Nam-T and UDW), the difference in lead isotopic ratio in samples derived from the same mine can be very large and can lead to false assumptions. The difference of the lead isotopic is the result of two effects in the duplicate samples: the non-uniformity of the isotopic composition of lead in the ore body and the steady depletion of the radiogenic lead by chemical separation and its persistent dilution of the isotope with natural lead due to the contamination of reagents during the milling stage.

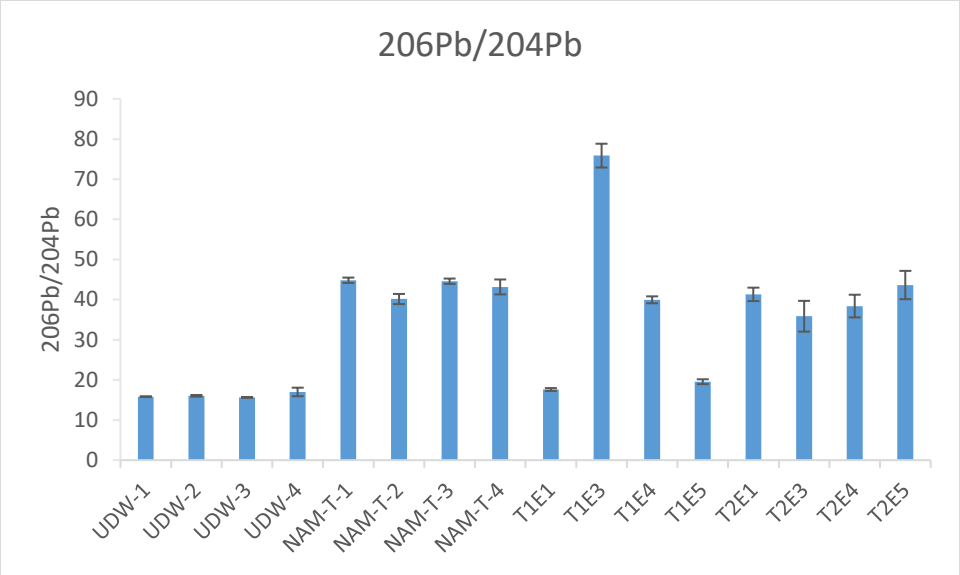


**Figure 19:** The $^{206}Pb/^{204}Pb$ isotope ratios for uranium mines along with the standard error around the mean n=3 for all measured samples.

The ratios of $^{207}Pb/^{204}Pb$, $^{206}Pb/^{204}Pb$ and $^{208}Pb/^{204}Pb$ ranged from (16-23), (15-75) and (36-43) respectively, were higher than the permissible NIST values of 15.4998, 16.9416 and 36.7249. In the determination of origin, the $^{208}Pb$ content plays an important role because this isotope is the daughter of $^{232}Th$ decay sequence found in uranium ore (Varga et al., 2009). Figure 21 below shows a high level of $^{208}Pb$ (for Nam-T, mine T1 and T2) and this indicates a deposit of quartz-pebble conglomerate that is distinguished by a high thorium content. Mine T1 and T2 (South Africa) and NAM-T (Namibia) could be distinguished by this isotopic pattern (Varga et al., 2009).

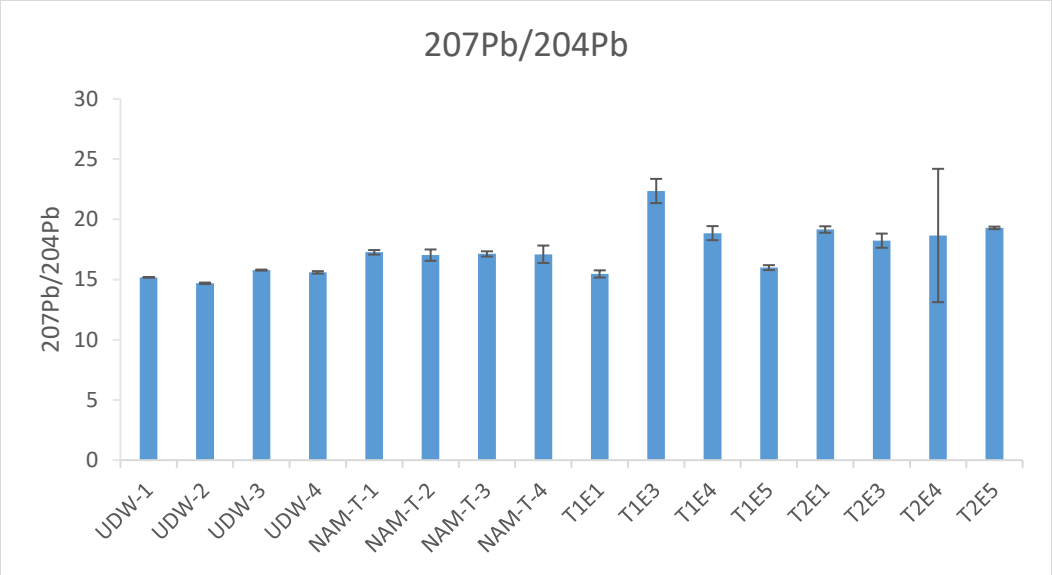


**Figure 20:** The $^{207}Pb/^{204}Pb$ isotope ratios for uranium mines along with the standard error around the mean n=3 for all measured samples.

The isotopic ratio of $^{206}Pb/^{204}Pb$ shown in Figure 19 ranged between 15.6225 and 75.8725. As reported by (Bellucci et al., 2013), a ratio of $^{206}Pb/^{204}Pb$ greater than 20 suggests that the Pb examined originated from uranium ore, whereas a ratio of less than 20 suggests a Pb-rich ore. In Figure 19, the $^{206}Pb/^{204}Pb$ isotope ratios were greater than 20, which suggests that these samples were from uranium-rich ores with the exception of UDW, T1E1 and T1E5, which were lower than 20. Zircon, monazite and apatite are the uranium-bearing products related to the higher radiogenic Pb material.

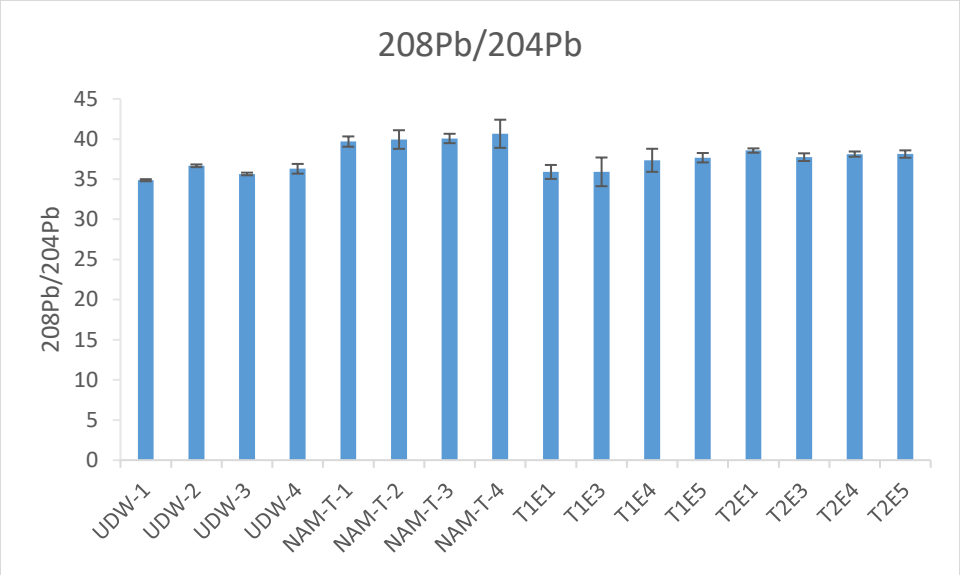


**Figure 21:** The $^{208}Pb/^{204}Pb$ isotope ratios for uranium mines along with the standard error around the mean n=3 for all measured samples.

According to (Vecchia et al., 2017), the standard ranges of the Pb isotopic ratio contained in natural materials, including ores and rocks are 14-30 for $^{206}Pb/^{204}Pb$, 15-17 for $^{207}Pb/^{204}Pb$ and 35-50 for $^{208}Pb/^{204}Pb$, although values beyond these ranges are not rare. The isotopic ratios shown in Figures 20 and 21 varied from 14.6857 to 19.2879 and 34.872 to 40.657 for $^{207}Pb/^{204}Pb$ and $^{208}Pb/^{204}Pb$ respectively. $^{206}Pb/^{204}Pb$ was higher than the range stipulated above, but it was not an unusual range for natural ores.

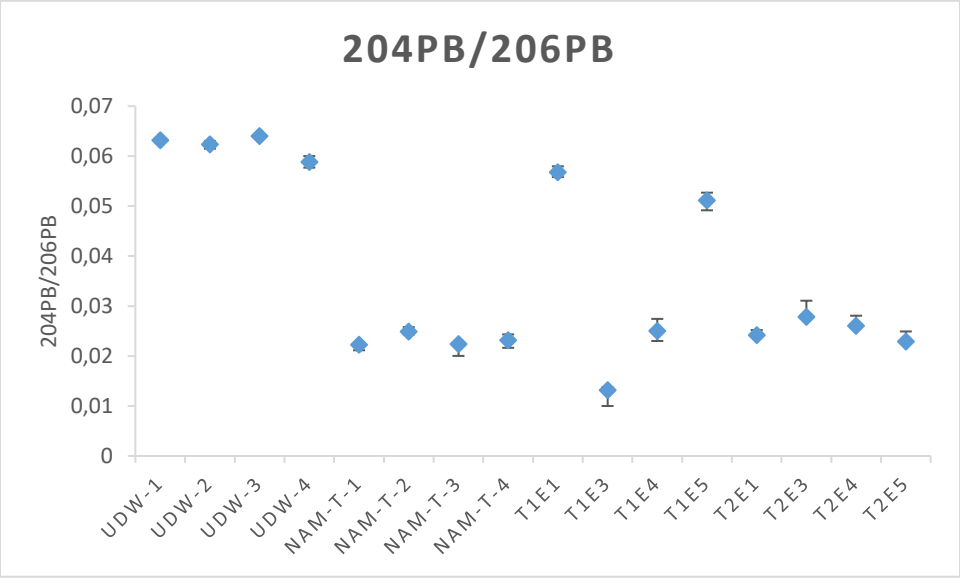


**Figure 22:** Radiogenic isotopic ratio of $^{204}Pb/^{206}Pb$ for all measured samples.

Figures 22, 23 and 24 as shown; exhibited the same pattern although the isotopic ratios were different. This could be as a result of the varying abundance percentages of lead isotopes. $^{208}$Pb is more abundant than other isotopes and that is the reason why its ratio is higher than $^{206}$Pb relative to the other ratios. It may also be due to the enrichment of $^{232}$Th. The isotope ratio of $^{204}$Pb/$^{206}$Pb has the lowest ratio since a small 1.4% percentage of $^{204}$Pb is found in the Earth's crust. $^{207}$Pb is slightly lower than $^{206}$Pb and thus the ratio of $^{207}$Pb/$^{206}$Pb in Figure 23 was moderate relative to other isotopic ratios (Varga et al., 2009, Reimann et al., 2012).

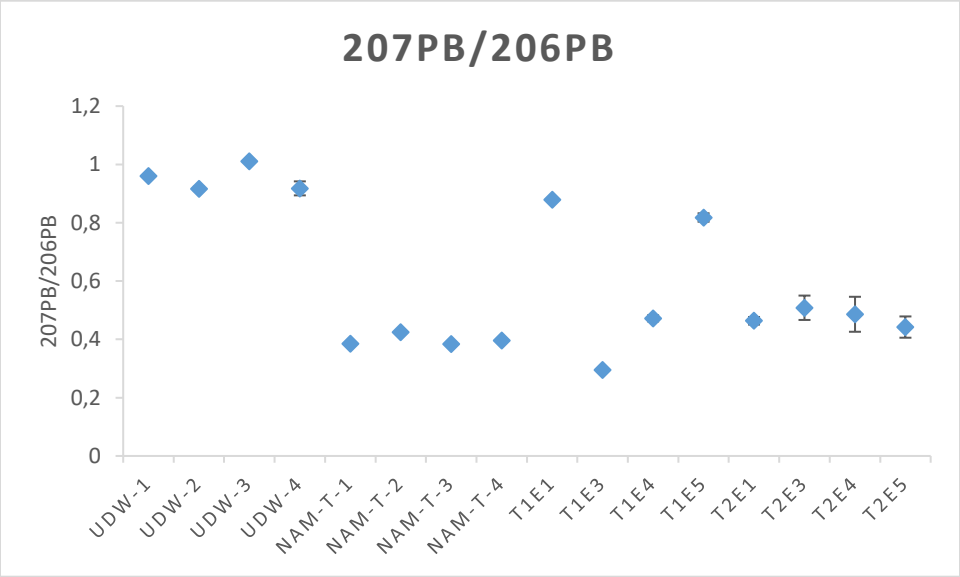


**Figure 23:** Radiogenic isotopic ratio of $^{207}$Pb/$^{206}$Pb for all measured samples.

Radiogenic Pb isotopic ratios were shown in Figures 22, 23 and 24 are for the uranium ore and water samples. Depending on the geological age and uranium or thorium content, the lead contained in the sample may contain varying quantities of natural and radiogenic lead. The overall uncertainty in the data is too small to be seen for samples with a very low $^{204}$Pb content thus; the samples with a high primordial lead content have a high uncertainty, which can be visible.

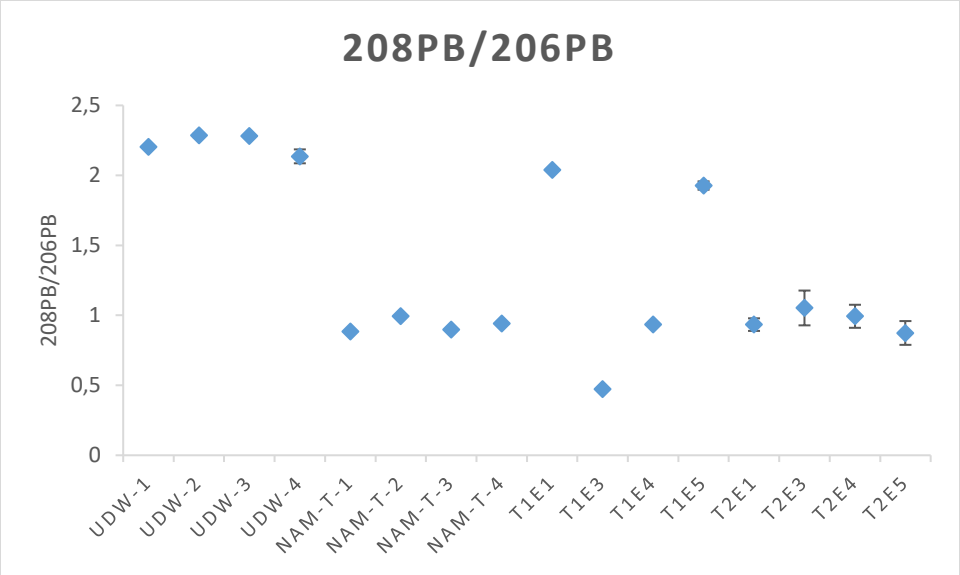


**Figure 24:** Radiogenic isotopic ratio of $^{208}Pb/^{206}Pb$ for all measured samples.

## 4.3 LIBS data analysis

**REEs of tailing one (mine T1)**

The range of spectra acquired was 250 - 850 nm, obtained without argon gas ambient. Because of the density number, some interference lines were observed from the spectrum. The main neutral and ionic lines of the rare earth elements have been identified within the specified wavelength range. The following rare earth elements were not detected; La, Sm, Eu, Tb, Ho and Lu. According to Palleschi 2019, LIBS is not highly sensitive to most of the elements of interest, this explains why some elements were not detected (Palleschi, 2019). Arab (2014) compared the USB 4000 spectrometer with the Maya 2000 Pro spectrometer from Ocean Optics and found that Maya 2000 obtained better results with more high peaks as the limit of detection (LOD) was lower than the USB4000. The USB4000 is in the same group as the USB2000+ spectrometer used in this study. The USB series has a high limit of detection (LOD) and thus shows low spectral resolution compared to the spectral resolution of the Maya spectrometer (Arab et al., 2014). Any element with a wavelength below the detection limit cannot be detected. This may be the explanation why certain elements have not been identified. However, we have detected a number of rare earth elements such as Ce, Pr, Nd, Gd, Dy, Er, Tm and Yb. LREEs peaks were most dominant in this

sample relative to HREEs. The spectrum is dominated by rare earth element Ce, Gd, Tm and Dy LREEs and HREEs respectively.

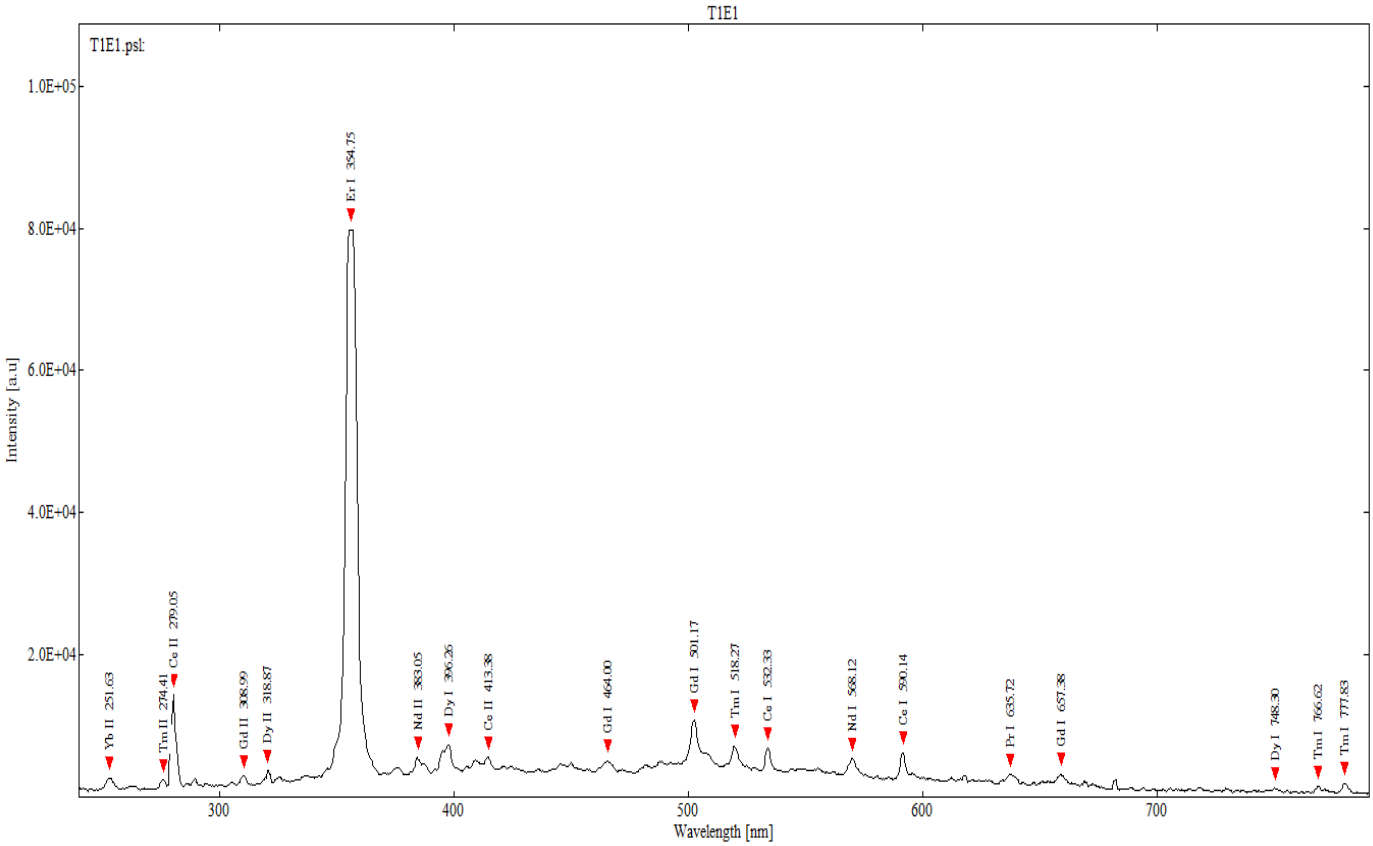


**Figure 25:** REE spectrum of T1E1.

Most peaks lie in the range between 0 to $2x10^4$ intensity and the highest peaks between $8x10^4$ to $1x10^5$ intensity. Er I (354.75 nm), Ce II (279.05 nm), Gd I (501.17 nm) and Nd I (532.08 nm) recorded the highest peaks as shown in Figure 25**.** In addition, the strongest emission lines of Yb II 251.63 nm, Gd II 308.99 nm, Nd II 383.05 nm, Ce II 413.38 nm and Ce II 532.33 nm described in the NIST database were also observed in this spectrum. The total number of REEs observed in Figure 25 is 19.

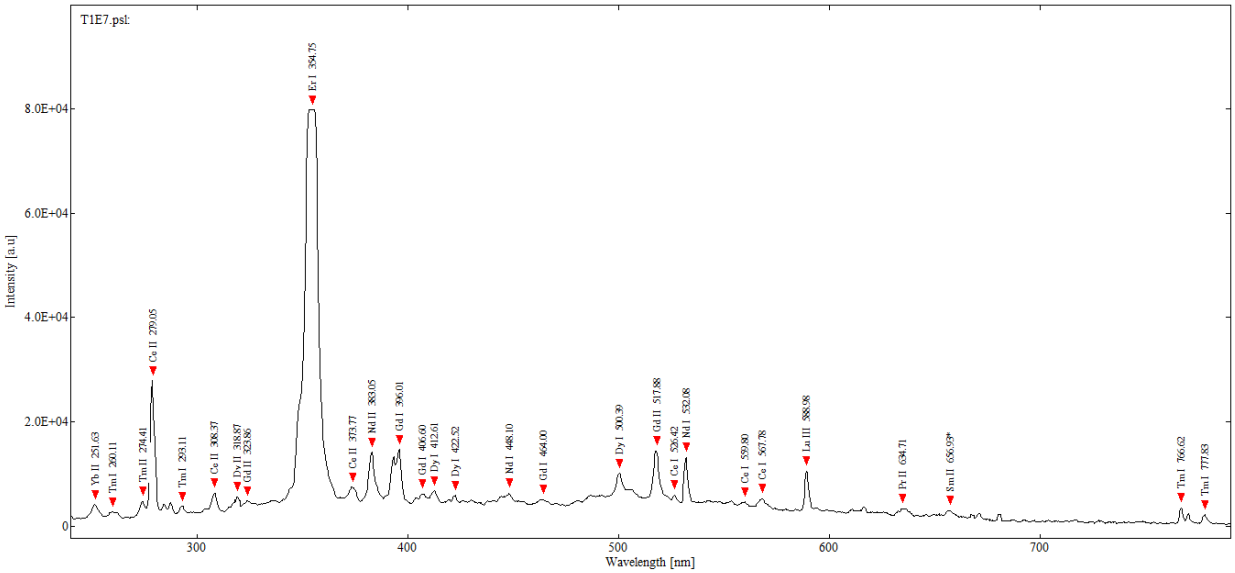


**Figure 26:** REE spectrum of T1E7.

The emission of Er I 354.75 nm interferes with the Tm I 354.21 nm emission line. This may be caused by a lack of ambient argon gas during analysis of the sample. In addition, several interferences affected the results of the LIBS and most of this were discussed in Chapter 2. Figure 26 was dominated by LREE in contrast with HREE. The highest peaks were observed in the following emission lines; Er I 354.75 nm, Ce II 279.05 nm, Nd I 385.05 nm, Gd I 396.01 nm, Gd II 517.88 nm, Nd I 532.08 nm and Lu III 588.98 nm. There were the highest peaks in LREE. Ce, Gd, Tm and Dy mostly populated the spectra. Most peaks ranged from 0 to 2 x $10^4$, apart from Ce II 279.05 and Er I 354.75 nm, which ranged from 2 x $10^4$ to 4 x $10^4$and 8 x $10^4$ respectively. The following strong emission lines Ce I 567.78 nm, Nd II 383.05 nm and Dy I 422.52 nm were in agreement with those acquired from the NIST database. About 28 REEs were identified in Figure 26.

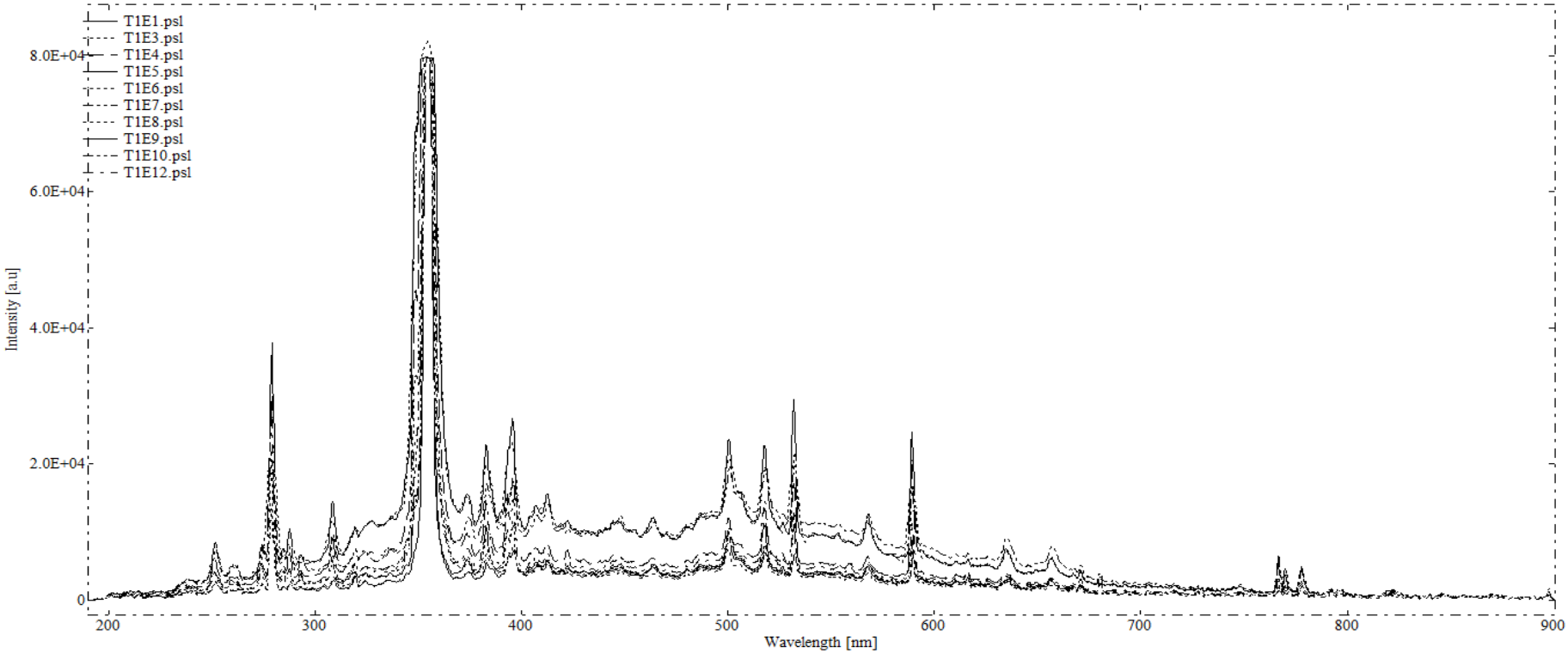


**Figure 27:** Overlay spectra of mine T1.

The full spectra of all samples examined in one mine tailing is shown in Figure 27 above. Samples T1E1 and T1E7 showed similar spectral patterns. This pattern could be seen from the above overlay spectra. This overlay spectra showed the signature of the tailing of the mine. Since these samples showed the same pattern, it could be inferred that they might be of the same geological origin. All samples showed Ce, Gd, Tm and Dy occurred often.

Elements with relatively low ionization energy have a high emission and can be detected at very low abundance. High ionization energy elements can be expected to have low emissions and can be observed at very high abundances. Since REE has a low ionization energy, there is therefore a high emission and a very small abundance can be detected. In detail, most of the spectral lines of useful and high intensity were around the 250 - 590 nm range. At the same time, LIBS spectra provided a significantly lower intensity and stable pattern at 590 - 800 nm (Yu et al., 2016).

**REEs of tailing two**

Figure 28 showed a distinct REE fingerprint from the other samples. Ce II 279.05, Er I 354.75, Nd II 383.05, Gd I 393.01, Nd I 532.08 and Yb II 589.72 nm were the lines with the highest peaks in the spectra. Most of the highest peaks were occupied by LREEs relative to HREES. This may be because the ionization energy on the periodic table increases from left to right, resulting in the elements on the left having low ionization energy. As mentioned, a low ionization energy implies low spectral emission and a very small abundance. The lines of Gd, Ce, Pr, Nd, Tm, Er, and Yb occurred frequently. Tailing two samples also revealed a similar tendency to have more LREEs than HREE, thereby exhibiting a similar characteristic trend for tailing one and two. This characteristic was observed as a signature for these two tailings.

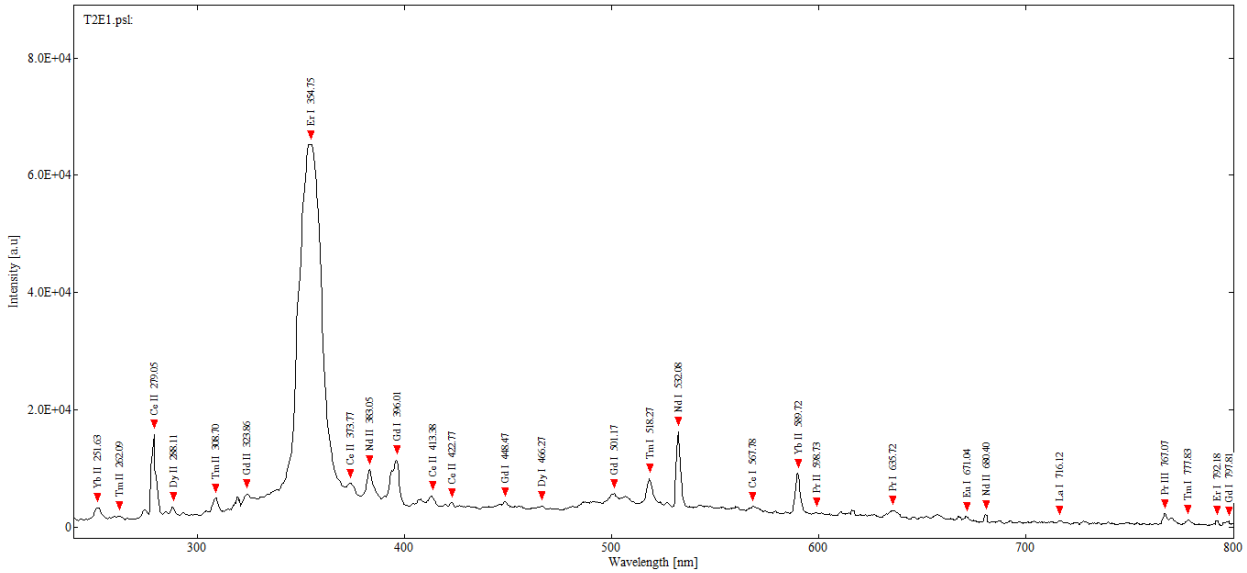


**Figure 28:** REE spectrum of T2E1.

The highest peak (Er I 354.75 nm) ranged from 6 x $10^4$ to 8 x $10^4$, while the other high peaks ranged from 0 - 2 x $10^4$. Figure 28 had emission peaks comparable to tailing one, both of which showed Ce II 279.05, Nd II 383.05 and Nd I 532.05 nm. The distinction is that a few samples contain Pr at 598.73, 635.73 and 767.707 nm in tailing two and some samples showed Er as one of the HREE's dominant peaks, and this was not observed in tailing one.

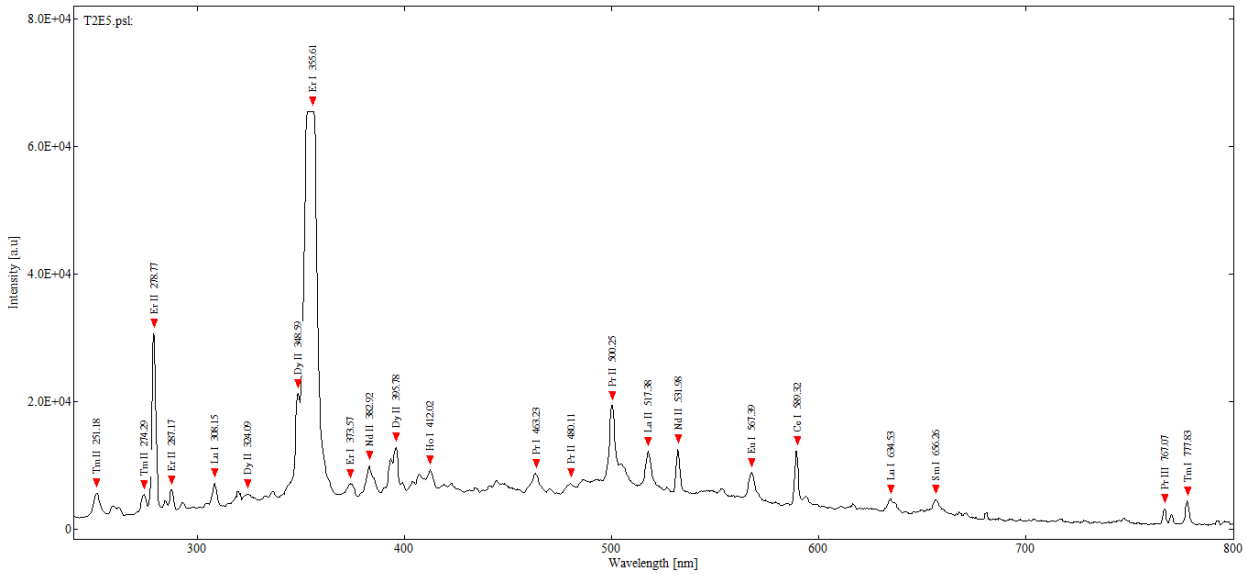


**Figure 29:** REE spectrum of T2E5.

In Figure 29, approximately 22 emission lines were detected and only 13 were HREE and 14 LREE were detected. This means that LREE were more predominant in this spectrum relative to HREEs. The most elements occurring frequently in the spectrum were Pr and Nd for LREEs and Er, Tm and Dy for HREEs. Most rare earth elements have been detected, except for Gd, Tb and Yb. The highest peaks were located at 355.61, 278.77, 348.59, 500.25, 517.38, 531.98, and 589.32 nm. In comparison to the other samples, the emission line of 279.05 nm Ce II was not observed in the spectra. According to the NIST database, the strongest lines are Ho I 412.02, Dy II 395.78, Nd II 382.92 and Pr I 463.23 nm, these lines were also observed in Figure 29.

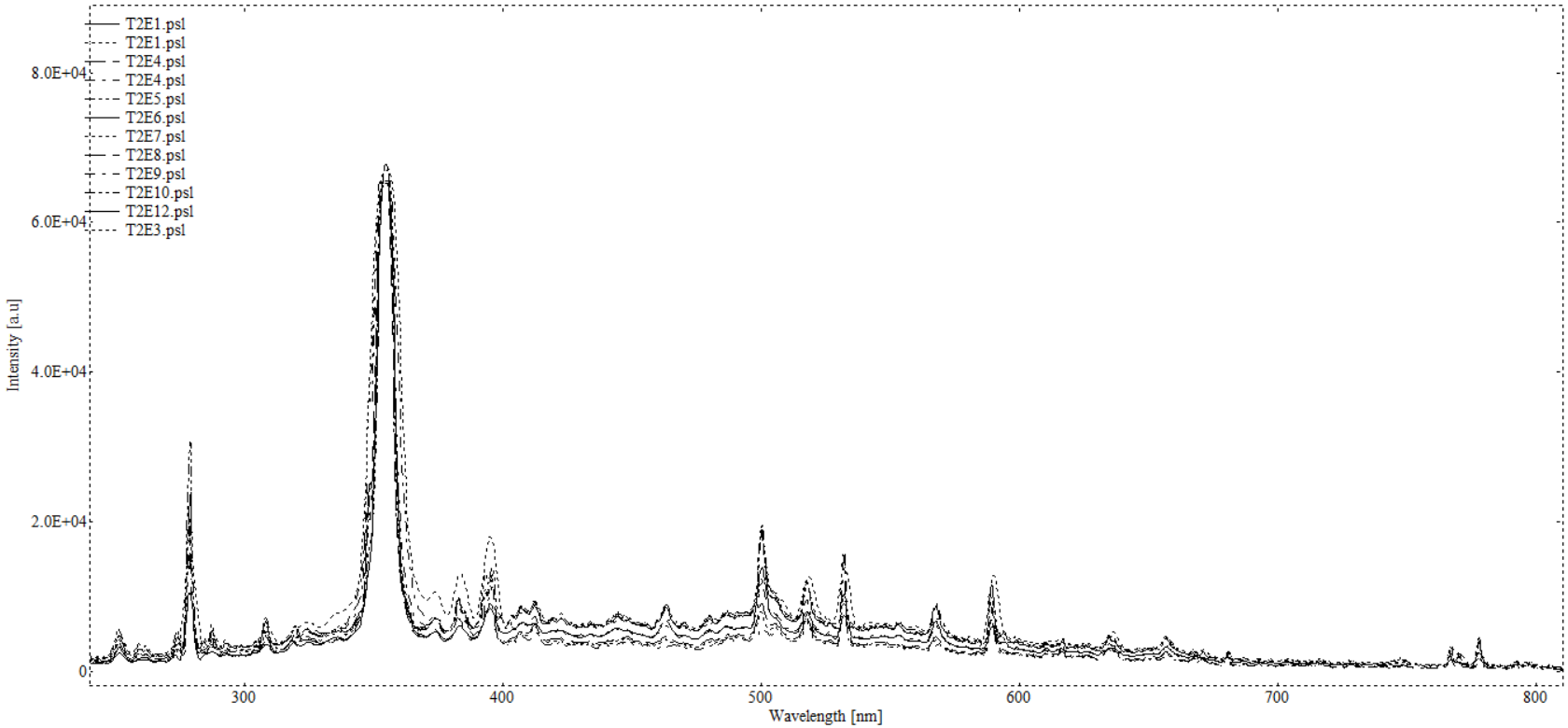


**Figure 30:** Overlay spectra of T2.

LREE were the predominant ones in all samples except for only one sample. Tailing two overlay revealed the fingerprint of the mine. The pattern of tailing one looked different from the tailing one overlay. The overlay consisted of 11 samples from the same mine. Since these samples showed the same pattern, it can be inferred that they might have been of the same geological origin. All samples showed that Ce, Gd, Tm and Dy appeared continually. Most of the spectral lines of useful and high intensity were around the 250 - 590 nm range. At the same time, the LIBS spectra provided a significantly lower intensity and stable pattern at 590 - 800 nm.

**REEs of NAM-T**

There were 19 REE found in this sample, of which 12 were LREE and the rest HREE. Ce, Nd, Dy and Tm were classified as the most predominant in the spectrum. Tm I 354.21 nm appeared to be saturated, which suggested that the obtained plasma light was more than the detector could count. The highest peaks were recorded at Tm I 354.21 nm, Yb II 589.72 nm, Nd I 532.08 nm and Ce II 279.05 nm at intensities between (6 x $10^4$- 8 x $10^4$), (4 x $10^4$- 6 x $10^4$), (2 x $10^4$- 4 x $10^4$) and (0 - 2 x $10^4$) respectively. A few REE emission lines observed in Figure 31 were listed in the NIST as the lines with the strongest emission lines. Those lines are Ce II 422.77 nm, Ce I 569.29 nm, Tm I 354.21 nm, Dy I 396.26 nm and Nd II 383.05 nm.

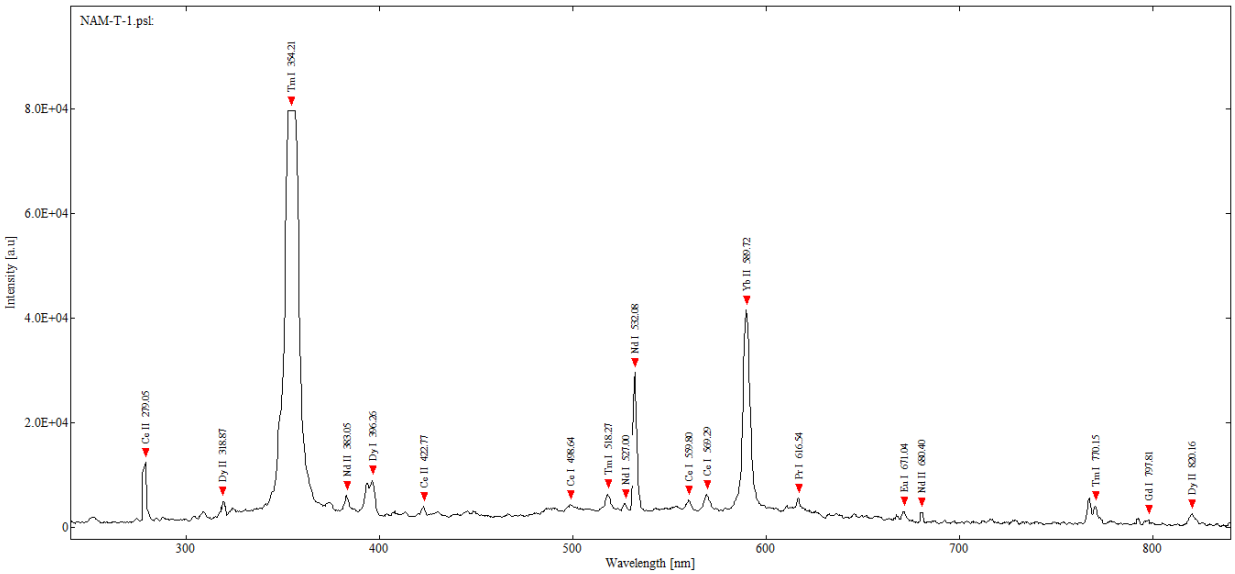


**Figure 31:** REE spectrum of NAM-T-1.

The intensity of Figure 32 varies from 0 to 8 x $10^4$ a.u. There were three highest peaks present in this spectrum; Tm I 354.21 nm, Ce I 589.32 nm, Ce II 279.05 nm with intensities between 2 x $10^4$-8 x $10^4$, 1.5 x $10^4$ - 2 x $10^4$ and 1 x $10^4$ – 1.5 x $10^4$ a.u. Since the height of a peak can be determined as a dominant factor in the spectra, these three peaks were the dominant ones in this spectrum. Several REEs found in Figure 32. Approximately 31 LREE and HREE were detected in this sample. All LREE and HREE were detected, but some were detected several times more than others such as Gd, Ce, Nd, Eu, Tm, Dy and Er. For the first time, Yb IV 214.48 nm, Gd III 237.43 nm, Tm III 266.30 nm, Lu I 636.60 and Yb III 840 nm were detected in the sample in Figure 32. There was no saturation of the detector in this spectrum. The emission lines were scattered across spectral wavelengths of 250 to 700 nm. Ce I 559.80 nm, La I 578.92 nm, Nd II 373.28 nm, Eu I 429.87 nm, Eu II 382.67 nm, Gd I 407.87 nm, Dy II 303.83 nm, Dy I 393.01 nm, Dy 422.52 nm, Tm I 317.36 nm and Tm I 354.21 nm observed were identified as the strongest in the NIST database.

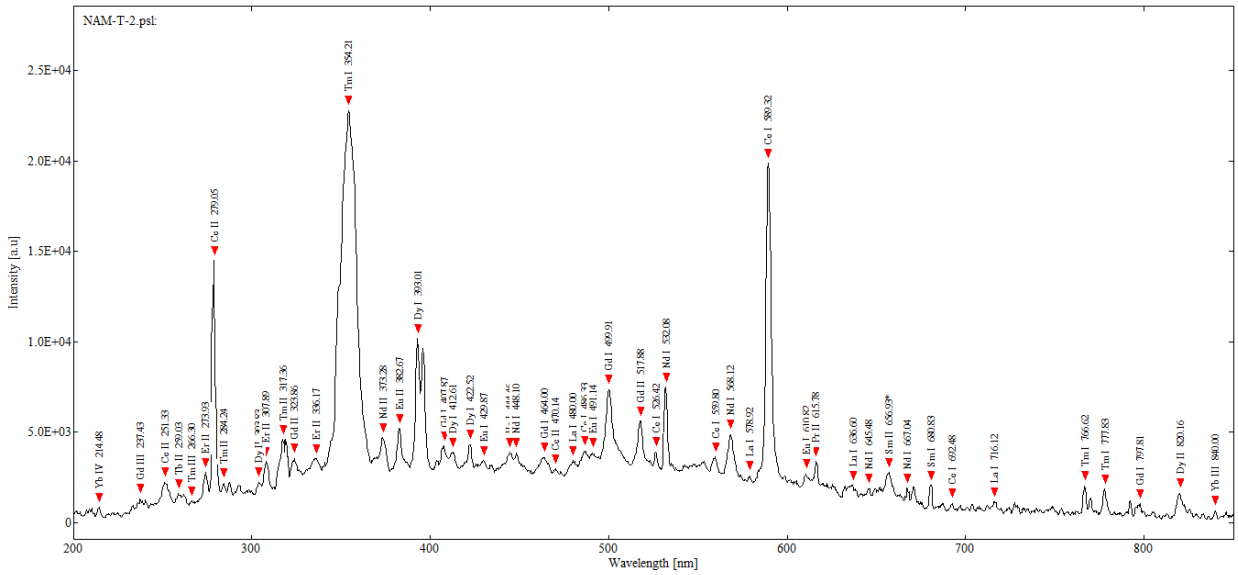


**Figure 32:** REE spectrum of NAM-T-2.

.

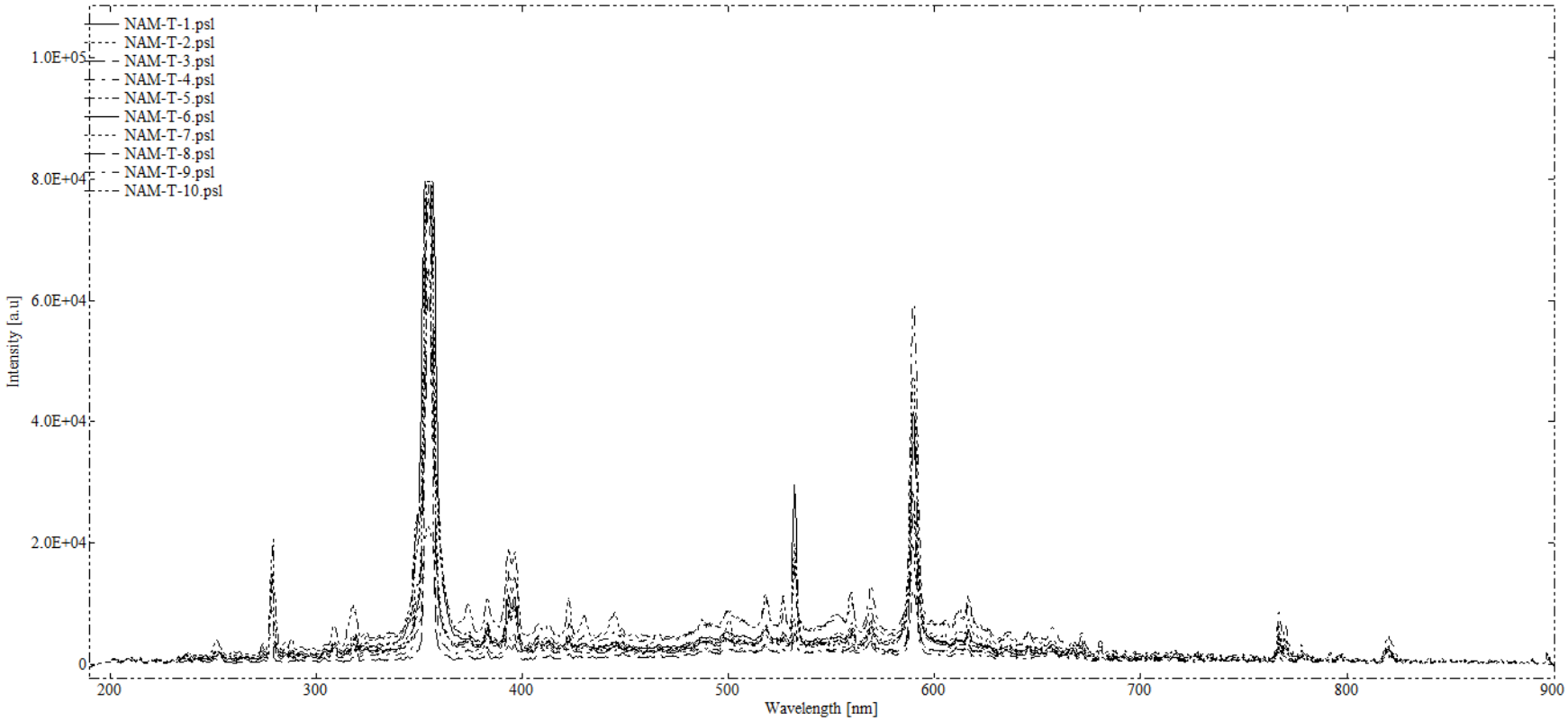


**Figure 33:** An overlay spectra of NAM-T.

The overlay consisted of all 10 samples from the Namibian tailings mine. The pattern in Figure 33 showed the fingerprint of this mine. This overlay showed a distinct pattern from the overlay of the other tailings. Each spectrum in this tailing looked identical, although some of the samples had more REE than others. Interferences were found, most of which were due to the reasons mentioned in Chapter 2 under the LIBS section.

**REEs of underground water**

There were several emission lines present in this spectrum, which were identified as the strongest lines in the NIST database, such as Tm I 287.84 nm, Tm II 324.15 nm, Er II 336.67 nm, Tm I 354.21 nm, Er I 385.59 nm, Er I 390.40 nm, Gd II 434.22 nm, Ce I 567.78 nm and Pr I 598.73 nm. The spectra shown in Figure 34 had 28 REE detected with 14 LREE and HREE. There was also an equal amount of LREE and HREE in this sample. Ce, Tm and Er occurred more than once in the Figure 34. The emission lines with the highest peaks were: Tm I 354.21 nm, Ce I 506.40 nm, Dy I 412.61 nm, Tm II 287.84 nm, Ce II 251.33 nm, Er I 385.59 nm and Pr II 634.71 nm with intensities between 6 x $10^4$ -8 x $10^4$ for Tm I 354.21 nm and 2 x$10^4$ – 4 x$10^4$ for the rest of the peaks. Most of the emission lines were between 250 - 670 nm wavelengths.

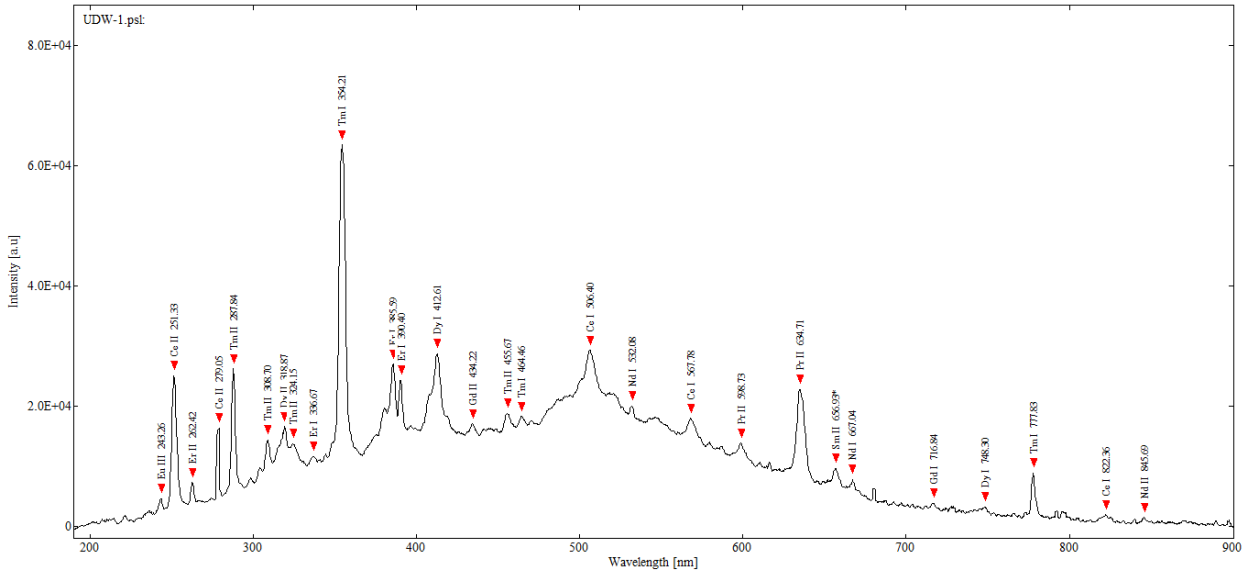


**Figure 34:** REE spectrum of UDW-1.

Only 14 REE were measured with few LREE (6) relative to HREE (8), so this spectrum was dominated by HREE. The elements that occurred more than once were Tm, Er, Ce and Nd. The highest peaks occurring in this spectrum were Er I 354.75 and Ce II 279.05 nm with intensities between (5 x $10^4$ – 6 x $10^4$) and (1 x $10^4$ – 2 x $10^4$) respectively. Many REEs were clustered between 250 - 530 nm wavelengths. In Figure 35, Tb, Ho, Lu, Yb, La, Pr, Sm, Eu and Gd were not measured by the spectrometer.

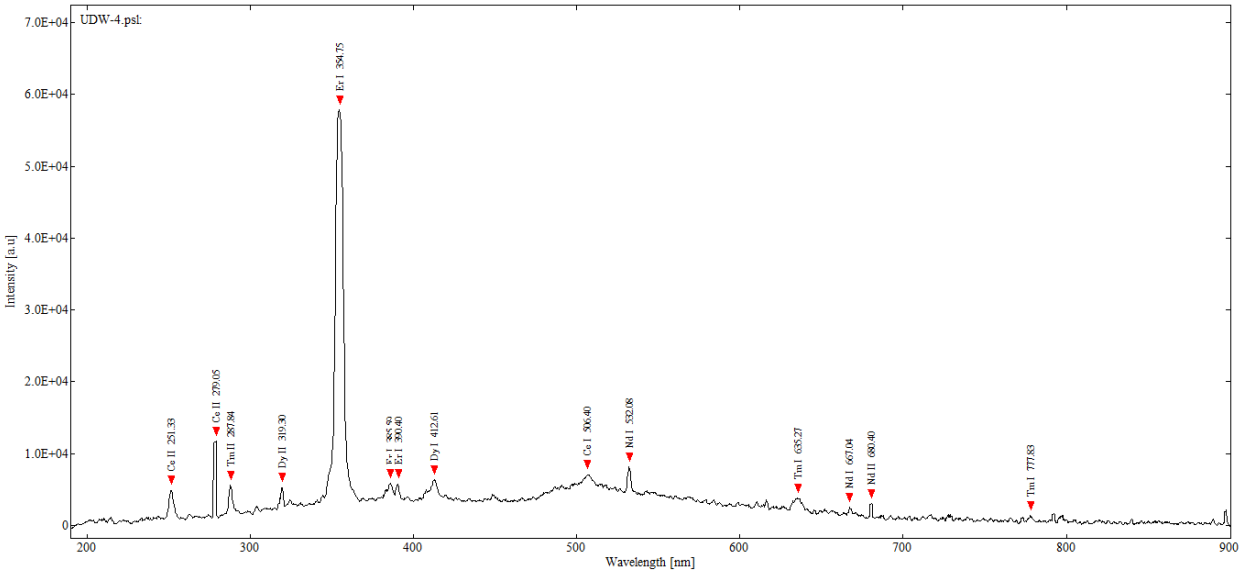


**Figure 35:** REE spectrum of UDW-4.

Most of the peaks were grouped from 250-650 nm. This overlay also depicted the fingerprint of the underground water (UDW). The pattern was different from the mine tailings (NAM-T) although they were from the same area (Namibia). The overlay spectrum consisted of all 10 samples taken from underground water.

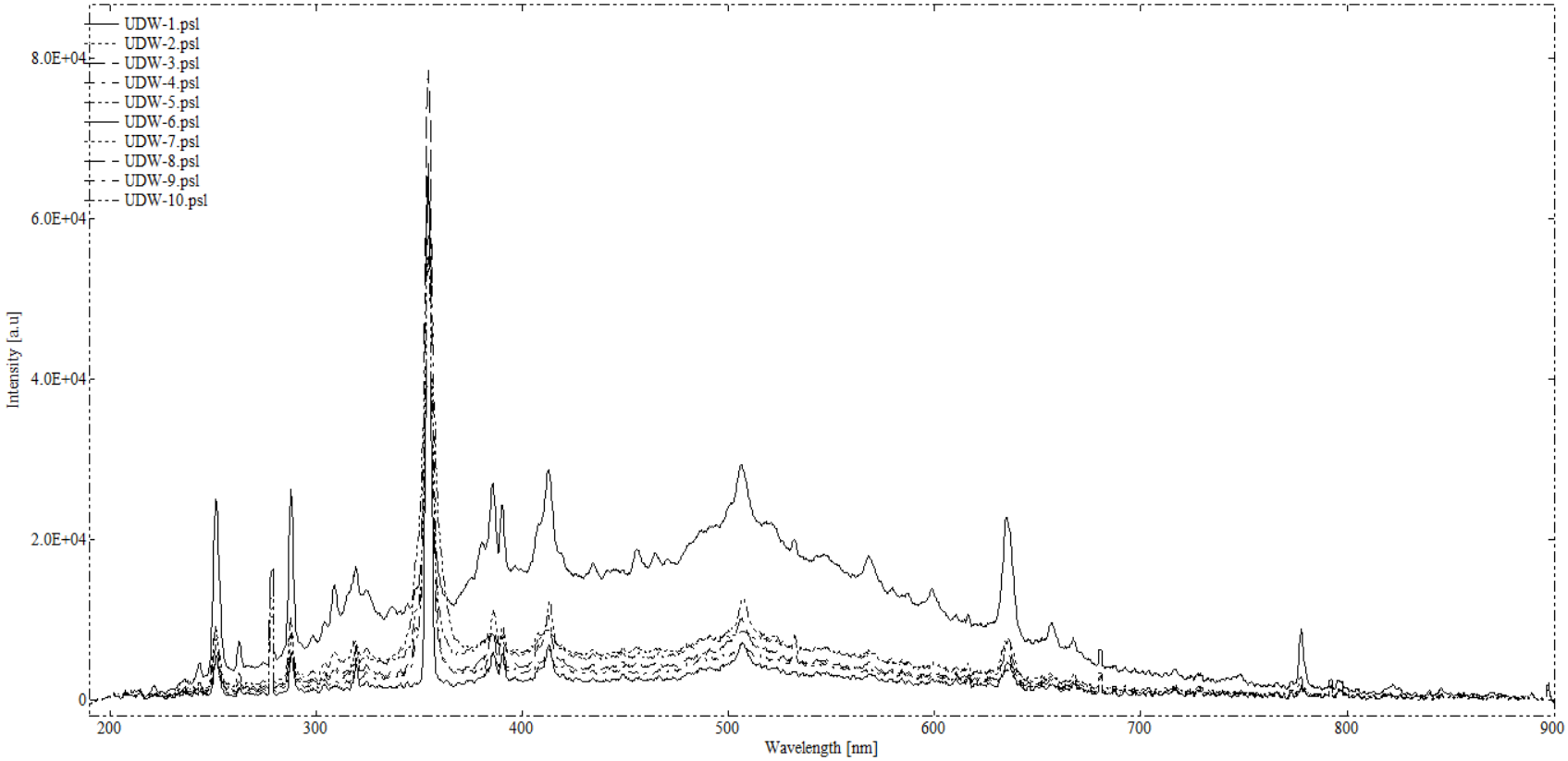


**Figure 36:** Overlay spectra of UDW.

## 4.3 Comparison of ICP-MS and LIBS

In this section, the REE signatures obtained from ICP-MS were compared with those obtained from LIBS. All REEs were detected by ICP-MS as shown in Figures 7 to 10, however. LIBS was unable to detect some of the REE in all the tailings. This may be because their intensity was too small to be detected by the spectrometer or because the spectrometer's resolution was not high enough and because the spectrometer's wavelength used cannot reach ranges below 250 nm and above 850 nm. Although LIBS is said to be the most sensitive instrument to detect elemental compositions, it has not been able to measure all REEs present in the sample.

The ability of LIBS to detect REEs was mainly affected by interference. This can be resolved by using the argon gas ambient in the experiment, calibrating the spectrometer using a high-pressure Hg (mercury) lamp or Hg-Ar (mercury-argon) lamp for wavelength correction and using a high-resolution spectrometer with a wavelength range of 100 -1100 nm. The patterns observed from the overlay spectra can be used as REE signatures for the various mines.

REEs from ICP-MS indicated that mine T1 and T2 from a South African uranium mine had a negative cerium anomaly with flat HREEs and no fractionation, whereas NAM-T and UDW (from the Namibian uranium mine) had a negative europium anomaly with enriched LREEs and a flat HREEs. LREEs were found to dominate the spectrum on the LIBS analysis, indicating that they were enriched, therefore, the LIBS results agree with the ICP-MS. REEs collected from LIBS indicated that T1 and T2 (South African uranium mine) had more identified REEs than NAM-T and UDW (Namibia uranium mine). Ce, Nd, Gd, Tm and Dy dominated the spectra of T1, T2, Nam-T and UDW.

### 4.3.1 Dendrogram cluster analysis

There are three clusters contained in Figure 37. There were some cases in which cluster analysis grouped samples from different geo-locations into one cluster. Cluster analysis was unable to group samples from the same mine as those showing similarities, instead only samples showing similarities were grouped regardless of the origin from which they came. Figure 37 provided illustrations of this. The first group comprised samples from South Africa (tailing one and Namibia (NAM-T). The second and third comprised underground water (UDW) from Namibia.

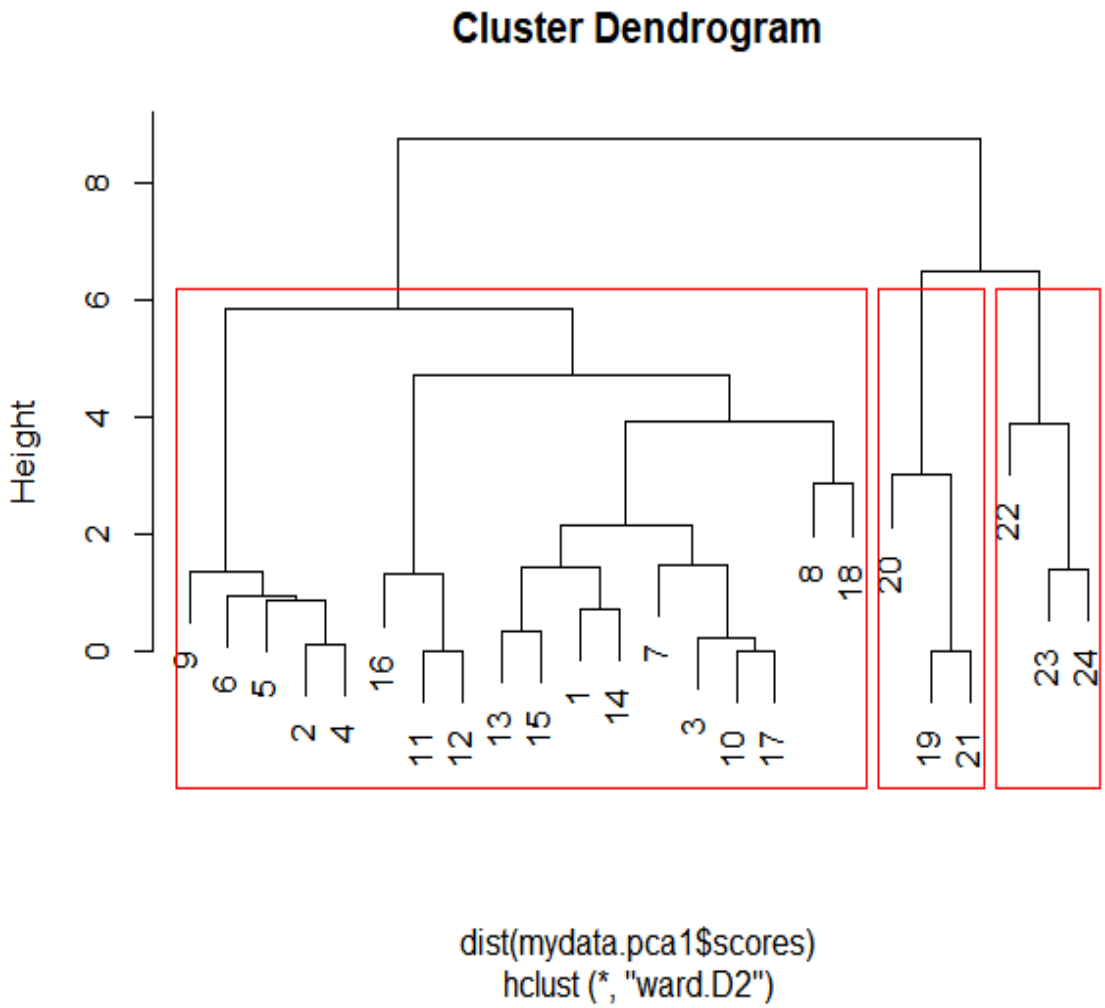


**Figure 37:** Dendrogram showing clusters of T1, NAM-T and UDW. First cluster (mine T1), second clusters (NAM-T) and third cluster (UDW).

Figure 37 displayed the outcome of the cluster analysis in the form of a dendrogram for twenty-four samples. Ce, Nd, Gd, Dy and Tm were the common elements present in all samples. Mine T2 was not included in the clustering analysis because it did not have all the elements common to mine T1, NAM-T and UDW. Because of this factor, it was generating errors. Only samples from T1, NAM-T and UDW were included in this analysis. This selection was intentional, since it results in a conservative analysis of similarities.

### 4.3.2 Principal component analysis (PCA)

The plot provides insight into the spectral characteristics, which primarily affect the various principal components. The positive loads represent the magnification of the resulting principal component.

Clustering was observed when adding the uranium ore and water to the plot in Figure 38. A rough categorization of mine T1, NAM-T and UDW suggested that mine T1 and NAM-T were positioned in the right quadrant (predominantly in the top right with positive PC1 and positive PC2 values). On the side of PC1, the LIBS uranium ore spectra were differentiated, although some spectra appeared to be on the positive side of PC2. There was a small overlap that indicated that there was a clear distinction between the three clusters.

The findings of the dendrogram were consistent with the results obtained from the PCA. Figure 37 displays three clusters clustered in the same way as Figure 38. The spectral line with less interference was chosen to achieve accurate analysis (Yang et al., 2017). PCA was used to distinguish spectral differences between similar types of samples (Harmon et al., 2017). PCA provided a valuable tool to evaluate whether the samples are the same or different and which variables were responsible for the possible differences (Gottfried et al., 2009).

PCA was carried out to display any variation between the 3 samples using the LIBS spectra on the selected characteristic lines. Each point represented one spectrum in the scatter plot.

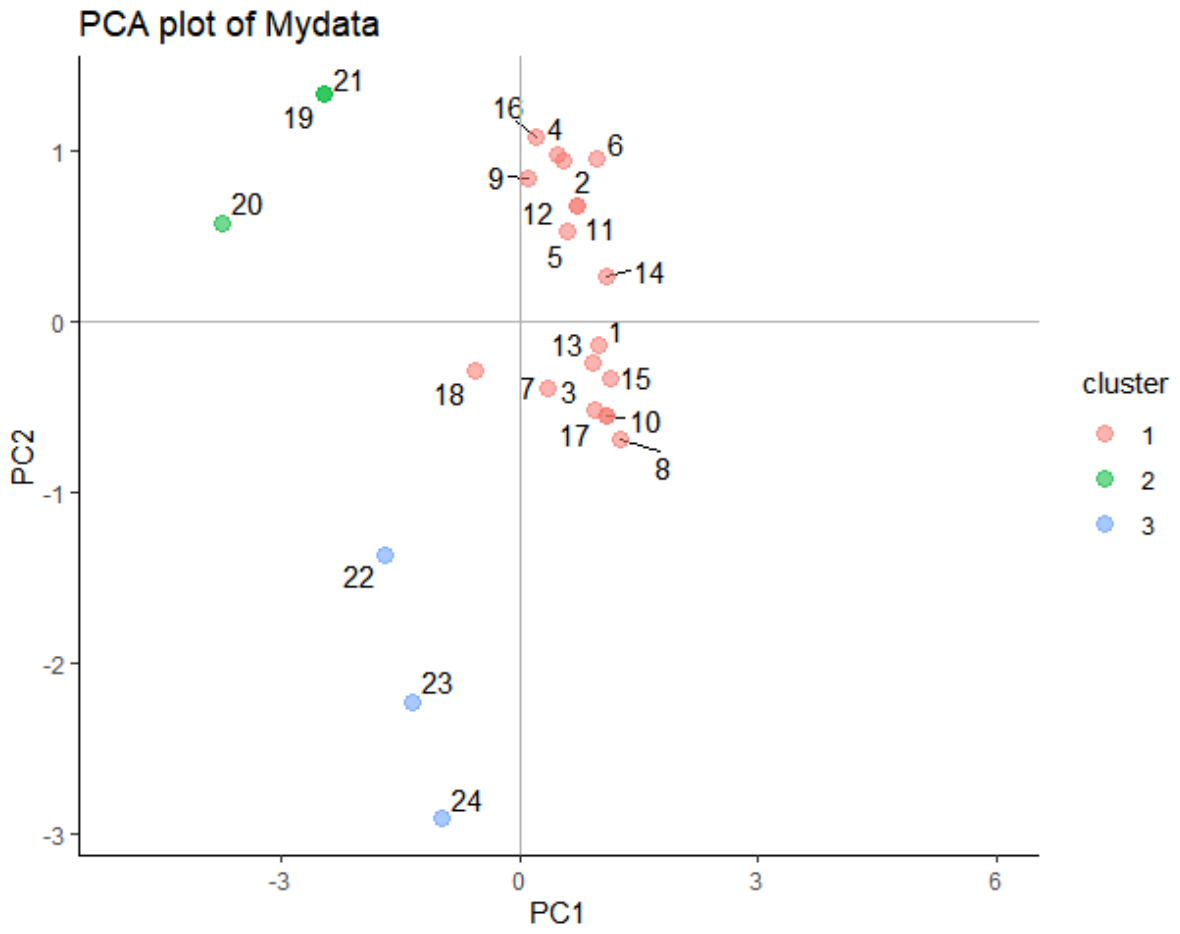


**Figure 38:** Principal component analysis for sample mine T1, NAM-T and UDW obtained from LIBS.

Figure 39 shows three clusters displayed in dots of three different colors, pink, green and blue. Cluster 1-18 reflects tailing one, (mine T1) and mine tailings (NAM-T) samples which were grouped into one cluster and plotted between -1 and +1. Tailing two was not part of the PCA clusters as in the dendrogram simply because it had distinct elements and emission lines from other samples. Mines T1 and NAM-T both formed one cluster, while UDW was divided into two distinct clusters, from19-21 on positive PC2 and 22-24 on negative PC2 clusters. The results showed that tailing one and NAM-T mine tailings exhibited identical patterns and UDW showed a distinct trend relative to mine T1 and NAM-T. This mean that mine T1 and NAM-T had identical rare earth patterns compared to UDW.

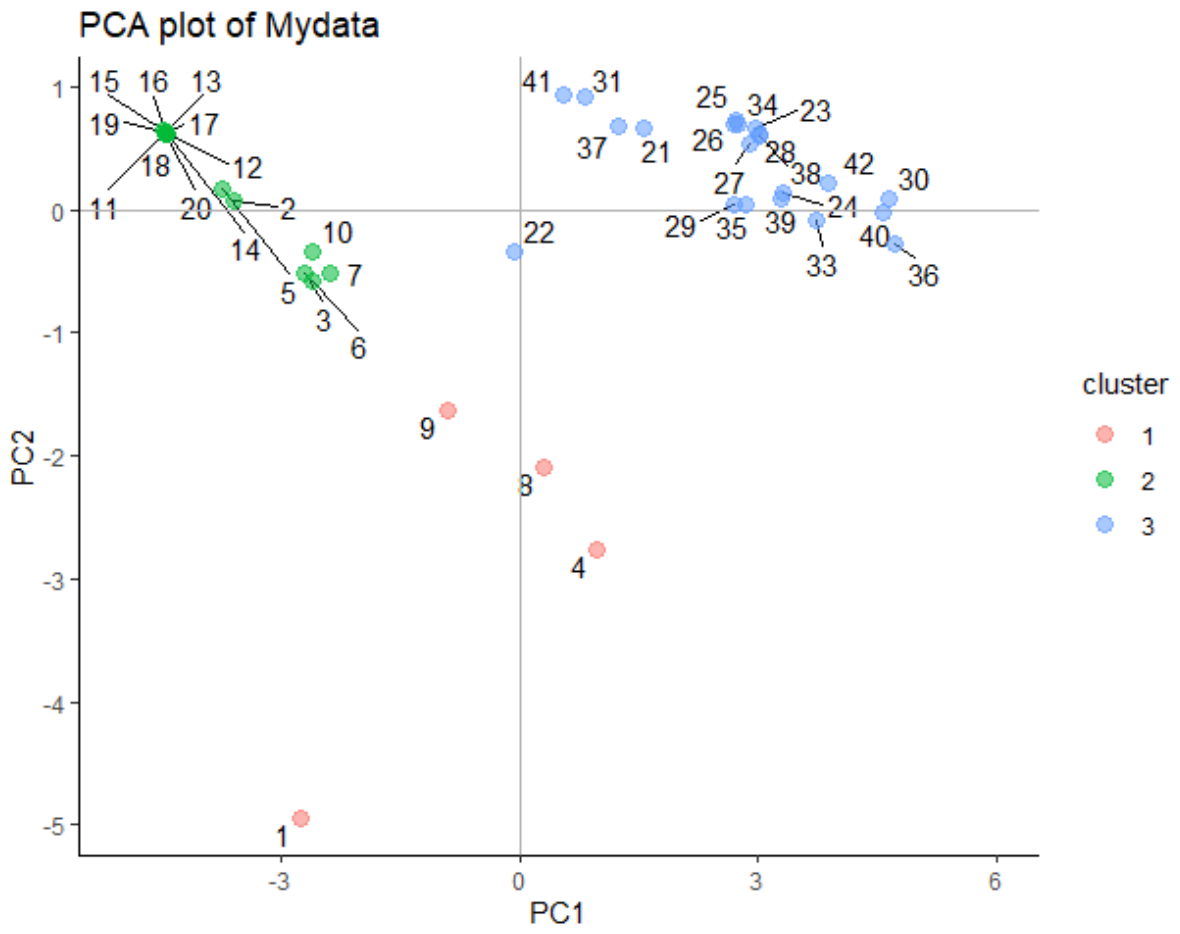


**Figure 39:** PCA analysis of samples obtained from ICP-MS.

Figure 39 displays the PCA results obtained from the ICP-MS and presents three clusters. This plot consisted of all samples from mines T1, T2, NAM-T and UDW. From the diagram, mines T1 and T2 transformed into one cluster, and NAM-T and UDW transformed into another cluster, with the exception of a few samples of UDW-1, UDW-3, UDW-4 and UDW-9, which formed a separate cluster as shown by pink dots. This similarity was expected because mines T1 and T2 were from the same geological area and the same applies to NAM-T and UDW, they were of the same origin but NAM-T was uranium ore, while UDW was underground water.

This PCA plot indicates that samples with similar trend originated from the same area, while the LIBS PCA plot does not indicate that samples with the same trend originated from the same location.

## Chapter 5: Conclusion and recommendation

The goal of this study was to identify nuclear forensic signatures from lead isotopic ratios and rare earth elements in uranium ore samples from the Namibian and South African uranium mines. Namibia and South Africa are major uranium ore exporters. These countries are also at risk of nuclear material being stolen for malicious purposes, and the nuclear forensic signatures produced in this study will promote and improve nuclear security and safety in the fight against theft of nuclear material, thereby promoting the non-violent use of nuclear material. That is why nuclear forensic signatures of uranium or nuclear materials need to be established and stored in a nuclear forensic library database.

This research examined the REE signatures and lead isotopic ratios in 32 uranium ore samples and 10 groundwater samples (22 samples of uranium from South Africa and 10 samples of uranium ore and 10 samples of groundwater both from Namibia). The REE signatures were developed using ICP-MS and LIBS techniques for the mines under investigation. REE found to be prevalent were Ce, Nd, Gd, Tm, Er and DY from LIBS and from ICP-MS the REEs found to be abundant for T1 and T2 were La, Ce and Nd whereas for NAM-T and UDW, La, Pr, Nd and Dy were found. Based on the LaN/YbN ratio, LREE was found to dominate the South African mine and there was a negative cerium anomaly. It was found that LREE dominated the Namibian mine and a negative europium anomaly was observed. Based on this ratio, LREE of underground water were also found to dominate water samples. Therefore, enriched LREEs and depleted HREEs, were exhibited in both samples analyzed by LIBS and ICP-MS.

These findings were consistent with the ones obtained from LIBS because the mine was also dominated by LREE in both samples from South Africa and Namibia. The LIBS results showed that most of the emission lines and high intensities that were useful or strongest were in the range of 300 - 590 nm. The differences and similarities or trend on the clusters between samples from different mines were observed in the principal component analysis of ICP-MS and LIBS, which can be used as signatures for these mines.

The principal component analysis displayed identical patterns within the mines for samples analyzed using ICP-MS whereas distinct patterns were observed from samples analyzed using LIBS.

The lead isotopic fingerprints plotted relative to $^{206}Pb$ did not comply with the reference values for NIST SRM 981, which are as follows: 0.059, 0.9146 and 2.168 respectively for $^{204}Pb/^{206}Pb$, $^{207}Pb/^{206}Pb$ and $^{208}Pb/^{206}Pb$. The lead isotopic concentrations of underground water, however, were in line with the NIST values. It was found that the $^{206}Pb/^{204}Pb$ plotted exceeded the NIST reference values and that marks a rich uranium or lead ore because they are higher than 20. All samples exhibited that they were from an ore rich in uranium excluding underground water that is located a distance away from the Namibian mine, which means that the uranium content in water was poor, so it contained natural uranium/lead content. Lead isotopic ratios from South Africa exhibited a very rich uranium ore content compared to the lead ratios from Namibia.

This research therefore determined the nuclear forensic signatures from lead isotopic ratios and the REE of uranium ore and water samples and the characteristics found could be used as a fingerprint in promoting nuclear safety.

All the objectives of this study were achieved, with the exception of the second last objective which states that the nuclear forensic library will be established for Namibia and South Africa. This occurred because of time constraints and because there were few samples examined for both countries and which were not enough to build a forensic library. In addition, collecting more results for both countries would have a great benefit in developing such a library.

The limitations encountered in this research were: lack of laser resources, such as the unavailability of a laser operating at a wavelength of 1064 nm at CARST laboratory, the lack of a high resolution spectrometer with wavelengths ranging from 100 to 1100 nm, not having a high-pressure mercury-argon lamp at CARST laboratory for wavelength calibration and the lack of argon atmospheric gas during the experiment. This research could be improved by increasing the sample size and availability of resources for the LIBS experiment.

**Recommendations and future work**

In order to make well informed decisions of the nuclear forensic signatures, a reasonable set of samples should be collected and analyzed. A high resolution spectrometer is recommended since it would be difficult to measure wavelengths within the vacuum UV wavelength range (i.e. about 100 – 250 nm). An argon gas is recommended during the experiment to avoid absorption of other emission lines.

Future work must include a huge number of samples covering all the uranium mines in South Africa and Namibia. In order to observe the signatures and make a decisive conclusion on the origin. This information from the samples would then be put in a nuclear forensic database to help in safeguarding nuclear materials in both countries. A well-established laser laboratory is necessary to make explicit conclusions on the results.

# References


ABEDIN, K., HAIDER, A., RONY, M. & KHAN, Z. 2011. Identification of multiple rare earths and associated elements in raw monazite sands by laser-induced breakdown spectroscopy. *Optics & Laser Technology,* 43**,** 45-49.

AGGARWAL, S. K. 2016. Nuclear forensics: what, why and how? *Current Science***,** 782-791.

ALBRIGHT, D. 1994. South Africa's secret nuclear weapons. *Isis Report,* 1**,** 15.

ANDERS, E. & GREVESSE, N. 1989. Abundances of the elements: Meteoritic and solar. *Geochimica et Cosmochimica acta,* 53**,** 197-214.

ARAB, M., BIDIN, N., RIZVI, Z., SAFIE, S. & ALSAEDI, M. 2014. Comparison study of two commercial spectrometers for heavy metal analysis of laser induced breakdown spectroscopy (LIBS). *Photonic Sensors,* 4**,** 63-69.

ARAGÓN, C. & AGUILERA, J. 2008a. Spatial and temporal scaling and common apparent excitation temperature of laser-induced plasmas generated at constant irradiance with different pulse energies. *Journal of Applied Physics,* 103**,** 013310.

ARAGÓN, C. & AGUILERA, J. A. 2008b. Characterization of laser induced plasmas by optical emission spectroscopy: A review of experiments and methods. *Spectrochimica Acta Part B: Atomic Spectroscopy,* 63**,** 893-916.

ARNOLD, L. 2003. The history of nuclear weapons: The Frisch-Peierls memorandum on the possible construction of atomic bombs of February 1940. *Cold War History,* 3**,** 111-126.

BELLUCCI, J. J., SIMONETTI, A., WALLACE, C., KOEMAN, E. C. & BURNS, P. C. 2013. Lead isotopic composition of trinitite melt glass: evidence for the presence of Canadian industrial lead in the first atomic weapon test. *Analytical chemistry,* 85**,** 7588-7593.

BUTTON, P., HEALEY, G. & CHIPLEY, D. Change in impurities observed during the refining and conversion processes. ESARDA Symposium, Bruges, 2013.

CHENG, H. & HU, Y. 2010. Lead (Pb) isotopic fingerprinting and its applications in lead pollution studies in China: a review. *Environmental pollution,* 158**,** 1134-1146.

CHEONG, C.-S., KIM, N., YI, K., JO, H. J., JEONG, Y.-J., KIM, Y., KOH, S. M. & IIZUKA, T. 2015. Recurrent rare earth element mineralization in the northwestern Okcheon Metamorphic Belt, Korea: SHRIMP U–Th–Pb geochronology, Nd isotope geochemistry, and tectonic implications. *Ore Geology Reviews,* 71**,** 99-115.

CHINNI, R. C., CREMERS, D. A., RADZIEMSKI, L. J., BOSTIAN, M. & NAVARRO-NORTHRUP, C. 2009. Detection of uranium using laser-induced breakdown spectroscopy. *Applied spectroscopy,* 63**,** 1238-1250.

CONNELLY, D. 2008. Uranium processing. *International mining***,** 58-61.

CREMERS, D. A. & RADZIEMSKI, L. J. 2006. History and fundamentals of LIBS. *Laser Induced Breakdown Spectroscopy: Fundamentals and Applications***,** 9-16.

DE HOFFMANN, E. & STROOBANT, V. 2007. Tandem mass spectrometry. *Mass spectrometry principles and applications, 3rd Edition, John Wiley & Sons Ltd., West Sussex, England***,** 189-215.

DONARD, A., POTTIN, A.-C., POINTURIER, F. & PÉCHEYRAN, C. 2015. Determination of relative rare earth element distributions in very small quantities of uranium ore concentrates using femtosecond UV laser ablation–SF-ICP-MS coupling. *Journal of Analytical Atomic Spectrometry,* 30**,** 2420-2428.

EDWARDS, C. & OLIVER, A. 2000. Uranium processing: a review of current methods and technology. *Jom,* 52**,** 12-20.

EL-DEFTAR, M. M. A. 2014. *Evaluation of Laser-Induced Breakdown Spectroscopy (LIBS) for the Elemental Profiling of Forensic Evidence.* University of Canberra.

EMMERT, L. A., CHINNI, R. C., CREMERS, D. A., JONES, C. R. & RUDOLPH, W. 2011. Comparative study of femtosecond and nanosecond laser-induced breakdown spectroscopy of depleted uranium. *Applied optics,* 50**,** 313-317.

EPPICH, G. R., WILLIAMS, R. W., GAFFNEY, A. M. & SCHORZMAN, K. C. 2013. 235 U–231 Pa age dating of uranium materials for nuclear forensic investigations. *Journal of Analytical Atomic Spectrometry,* 28**,** 666-674.

FAHEY, A., RITCHIE, N., NEWBURY, D. & SMALL, J. 2010. The use of lead isotopic abundances in trace uranium samples for nuclear forensics analysis. *Journal of radioanalytical and nuclear chemistry,* 284**,** 575-581.

FEDCHENKO, V. 2015. *The new nuclear forensics: analysis of nuclear materials for security purposes*, Oxford university press.

FUCHS, S., WILLIAMS-JONES, A. & PRZYBYLOWICZ, W. 2016. The origin of the gold and uranium ores of the Black Reef Formation, Transvaal Supergroup, South Africa. *Ore Geology Reviews,* 72**,** 149-164.

GEHRKE, R., EAST, L. & HARKER, Y. 2000. Information in spectra from sources containing "aged" 241Am as from TRU waste. *Waste Management,* 20**,** 555-559.

GLOSSARY, I. S. 2002. edition, Nuclear Verification Series No. 3. IAEA/NVS/3.

GOTTFRIED, J. L., HARMON, R. S., DE LUCIA JR, F. C. & MIZIOLEK, A. W. 2009. Multivariate analysis of laser-induced breakdown spectroscopy chemical signatures for geomaterial classification. *Spectrochimica Acta Part B: Atomic Spectroscopy,* 64**,** 1009-1019.

HARMON, R. S., HARK, R. R., THROCKMORTON, C. S., RANKEY, E. C., WISE, M. A., SOMERS, A. M. & COLLINS, L. M. 2017. Geochemical Fingerprinting by Handheld Laser-Induced Breakdown Spectroscopy. *Geostandards and Geoanalytical Research,* 41**,** 563-584.

HO, D. M. L. 2015. *Study on the applicability of structural and morphological parameters on selected uranium compounds for nuclear forensic purposes.*

HUTCHEON, I., KRISTO, M. & KNIGHT, K. 2013. Uranium-Cradle to Grave.

IAEA 2006. Nuclear Forensics Support. *Nuclear Security Series No.2.* Vienna: International Atomic Energy Agency.

IAEA 2009. *Nuclear Fuel Cycle Information System,* Vienna, INTERNATIONAL ATOMIC ENERGY AGENCY.

IAEA 2011. Division of Nuclear Fuel Cycle and Waste Technology. *In:* AGENCY, I. A. E. (ed.). Vienna.

IAEA 2015. International Atomic Energy Agency, Nuclear forensics in support of investigations. *IAEA Nuclear Security Series (2-G)*.

IAEA 2015a. Activities of the international atomic energy agency relevant of article III of the treaty on the non-proliferation of nuclear weapons: background paper prepared by the secretariat of the international atomic energy agnecy, review conference of the parties to the treaty on the non-proliferation of nuclear weapon. . *NPT/CONF.2015/13.*

IAEA 2018. Development of a national nuclear forensic library: A system for the identification of nuclear or other radioactive material out of regulatory control. Vienna.

IAEA 2019. Incident and trafficking databae (ITDB).

INITIATIVE, N. T. 2016. CNS Global Incidents and Trafficking Database. Online database. Washington, DC.

KAMUNDA, C. 2017. *Human health risk assessment of environmental radionuclides and heavy metals around a gold mining area in Gauteng province, south Africa.* North-West University (South Africa) Mafikeng Campus.

KEEGAN, E., KRISTO, M. J., COLELLA, M., ROBEL, M., WILLIAMS, R., LINDVALL, R., EPPICH, G., ROBERTS, S., BORG, L. & GAFFNEY, A. 2014. Nuclear forensic analysis of an unknown uranium ore concentrate sample seized in a criminal investigation in Australia. *Forensic Science International,* 240**,** 111-121.

KEEGAN, E., KRISTO, M. J., TOOLE, K., KIPS, R. & YOUNG, E. 2016. Nuclear forensics: scientific analysis supporting law enforcement and nuclear security investigations. ACS Publications.
KEEGAN, E., RICHTER, S., KELLY, I., WONG, H., GADD, P., KUEHN, H. & ALONSO-MUNOZ, A. 2008. The provenance of Australian uranium ore concentrates by elemental and isotopic analysis. *Applied Geochemistry,* 23**,** 765-777.
KHUMALO, N. & MATHUTHU, M. 2018. Determination of trace elements and lanthanide (REE) signatures in uranium mine products in South Africa by means of inductively coupled plasma mass spectrometry. *Journal of Geochemical Exploration,* 186**,** 235-242.
KRAJKO, J. 2016. Isotopic signatures for origin assessment of natural uranium samples.
KRISTO, M. J., GAFFNEY, A. M., MARKS, N., KNIGHT, K., CASSATA, W. S. & HUTCHEON, I. D. 2016. Nuclear forensic science: analysis of nuclear material out of regulatory control. *Annual review of earth and planetary sciences,* 44**,** 555-579.
LOBATO, L. M., PIMENTEL, M. M., CRUZ, S. C., MACHADO, N., NOCE, C. M. & ALKMIM, F. F. 2015. U–Pb geochronology of the Lagoa Real uranium district, Brazil: Implications for the age of the uranium mineralization. *Journal of South American Earth Sciences,* 58**,** 129-140.
MANGUM, S. & SHELTON, C. 2015. Uranium isotope ratio measurements with the NexION ICP-MS. *Perkin Elmer Inc Shelton, CT application note: ICP-mass spectrometry***,** 1-4.
MATHUTHU, M. & KHUMALO, N. 2017. Developing Nuclear Forensics Signatures and National Nuclear Forensics Libraries for the African Continent: A Case Review for South Africa. *International Journal of Applied Science-Research and Review,* 4**,** 1-3.
MATHUTHU, M., UUSHONA, V. & INDONGO, V. 2020. Radiological safety of groundwater around a uranium mine in Namibia. *Physics and Chemistry of the Earth, Parts A/B/C***,** 102915.
MAYER, K. & GLASER, A. 2015. Nuclear Forensics. Chapter 18. Univ. of Michigan, Ann Arbor, MI (United States).
MAYER, K., WALLENIUS, M., LÜTZENKIRCHEN, K., GALY, J., VARGA, Z., ERDMANN, N., BUDA, R., KRATZ, J., TRAUTMANN, N. & FIFIELD, K. Nuclear forensics: a methodology applicable to nuclear security and to non-proliferation. Journal of Physics: Conference Series, 2011. IOP Publishing, 062003.
MAYER, K., WALLENIUS, M. & RAY, I. 2005. Nuclear forensics—a methodology providing clues on the origin of illicitly trafficked nuclear materials. *Analyst,* 130**,** 433-441.
MCMAHON, G. 2020. *ICP-MS instrumentation, ICP-MS analysis strengths and limitations* [Online]. Available: https://www.technologynetworks.com/analysis/articles/icp-ms-icp-ms-instrumentation-icp-ms-analysis-strengths-and-limitation-341882 [Accessed].
MERCADIER, J., CUNEY, M., LACH, P., BOIRON, M. C., BONHOURE, J., RICHARD, A., LEISEN, M. & KISTER, P. 2011. Origin of uranium deposits revealed by their rare earth element signature. *Terra Nova,* 23**,** 264-269.
MEYERS, L. A. 2013. *Investigations of Nuclear Forensic Signatures in Uranium Bearing Materials.* University of Cincinnati.
MIZIOLEK, A. W., PALLESCHI, V. & SCHECHTER, I. 2006. *Laser induced breakdown spectroscopy*, Cambridge university press.
MOODY, K. J., GRANT, P. M. & HUTCHEON, I. D. 2014. *Nuclear forensic analysis*, CRC Press.
MORGENSTERN, A., APOSTOLIDIS, C. & MAYER, K. 2002. Age determination of highly enriched uranium: separation and analysis of 231Pa. *Analytical Chemistry,* 74**,** 5513-5516.
MUTUA, J.-M. 2015. Uranium yellowcake trafficking incidents in Africa: Proliferation threat or non-proliferation opportunity? *African Security Review,* 24**,** 162-189.
NJINGA, R. L., TSHIVHASE, M. V., KGABI, N. A. & ZIVUKU, M. 2016. Hazards index analysis of Gamma emitting radionuclides in selected areas around the Uranium Mine sites at Erongo Region, Namibia.

NUCLEAR, K. L. 2001. Radiochemistry-Fundamentals and Applications Second, Revised Edition. WILEY-VCH Verlag GmbH. Weinheim, Germany.

PACE, D. M. D., BERTUCCELLI, G. & D'ANGELO, C. A. Characterization of laser–induced plasmas by atomic emission spectroscopy. Journal of Physics: Conference Series, 2011. IOP Publishing, 012076.

PALLESCHI, V. 2019. Seven Common Errors to Avoid in LIBS Analysis. ADVANSTAR COMMUNICATIONS INC 131 W 1ST STREET, DULUTH, MN 55802 USA.

PASCHOTTA, R. 2008. *Encyclopedia of laser physics and technology*, Wiley Online Library.

PATHAK, A. K., KUMAR, R., SINGH, V. K., AGRAWAL, R., RAI, S. & RAI, A. K. 2012. Assessment of LIBS for spectrochemical analysis: a review. *Applied Spectroscopy Reviews,* 47**,** 14-40.

PELLE, M. B. 2008. *An investigation of the molecular properties of 1, 1, 1-trichloro methyl silane using laser spectroscopy.* North-West University.

RAMEBÄCK, H., NYGREN, U., TOVEDAL, A., EKBERG, C. & SKARNEMARK, G. 2012. Uncertainty assessment in gamma spectrometric measurements of plutonium isotope ratios and age. *Nuclear Instruments and Methods in Physics Research Section B: Beam Interactions with Materials and Atoms,* 287**,** 56-59.

READING, D. G. 2016. *Nuclear forensics: determining the origin of uranium ores and uranium ore concentrates via radiological, elemental and isotopic signatures.* University of Southampton.

READING, D. G., CROUDACE, I. W., WARWICK, P. E. & CIGLIANA, K. A. 2016. Applying multivariate statistics to discriminate uranium ore concentrate geolocations using (radio) chemical data in support of nuclear forensic investigations. *Journal of environmental radioactivity,* 162**,** 172-181.

REED, T. C. & STILLMAN, D. B. 2010. *The nuclear express: A political history of the bomb and its proliferation*, Zenith Press.

REIMANN, C., FLEM, B., FABIAN, K., BIRKE, M., LADENBERGER, A., NÉGREL, P., DEMETRIADES, A., HOOGEWERFF, J. & TEAM, T. G. P. 2012. Lead and lead isotopes in agricultural soils of Europe–The continental perspective. *Applied Geochemistry,* 27**,** 532-542.

RÜHLMANN, M., BÜCHELE, D., OSTERMANN, M., BALD, I. & SCHMID, T. 2018. Challenges in the quantification of nutrients in soils using laser-induced breakdown spectroscopy–A case study with calcium. *Spectrochimica Acta Part B: Atomic Spectroscopy,* 146**,** 115-121.

SAKO, A., MILLS, A. J. & ROYCHOUDHURY, A. N. 2009. Rare earth and trace element geochemistry of termite mounds in central and northeastern Namibia: Mechanisms for micro-nutrient accumulation. *Geoderma,* 153**,** 217-230.

SARKAR, A., ALAMELU, D. & AGGARWAL, S. K. 2008. Determination of thorium and uranium in solution by laser-induced breakdown spectrometry. *Applied Optics,* 47**,** G58-G64.

SARKAR, A., ALAMELU, D. & AGGARWAL, S. K. 2012. Gallium quantification in solution by LIBS in the presence of bulk uranium. *Optics & Laser Technology,* 44**,** 30-34.

SARKIS, J. & ROSA, D. 2011. Rare earth elements in uranium compounds and important evidence for nuclear forensic purposes.

SILVA, M. M. V. G., PINTO, M. M. C. & CARVALHO, P. C. S. 2016. Major, trace and REE geochemistry of recent sediments from lower Catumbela River (Angola). *Journal of African Earth Sciences,* 115**,** 203-217.

SIRVEN, J.-B., PAILLOUX, A., M'BAYE, Y., COULON, N., ALPETTAZ, T. & GOSSE, S. 2009. Towards the determination of the geographical origin of yellow cake samples by laser-induced breakdown spectroscopy and chemometrics. *Journal of Analytical Atomic Spectrometry,* 24**,** 451-459.

SKOOG, D., HOLLER, F. J. & CROUCH, S. 2007. Principles of Instrumental Analysis. Thomson Brooks. *Cole, Canada*.

STANLEY, F. E., STALCUP, A. & SPITZ, H. 2013. A brief introduction to analytical methods in nuclear forensics. *Journal of Radioanalytical and Nuclear Chemistry,* 295**,** 1385-1393.

STRAUB, M. D., ARNOLD, J., FESSENDEN, J. & KIPLINGER, J. L. 2020. Recent Advances in Nuclear Forensic Chemistry. *Analytical Chemistry*.
ŠVEDKAUSKAITĖ-LE GORE, J. 2008. Development and validation of a method for origin determination of uranium-bearing material.
ŠVEDKAUSKAITE-LEGORE, J., MAYER, K., MILLET, S., NICHOLL, A., RASMUSSEN, G. & BALTRUNAS, D. 2007. Investigation of the isotopic composition of lead and of trace elements concentrations in natural uranium materials as a signature in nuclear forensics. *Radiochimica Acta,* 95**,** 601-605.
ŠVEDKAUSKAITĖ-LEGORE, J., RASMUSSEN, G., ABOUSAHL, S. & VAN BELLE, P. 2008. Investigation of the sample characteristics needed for the determination of the origin of uranium-bearing materials. *Journal of Radioanalytical and Nuclear Chemistry,* 278**,** 201-209.
SWEET, L. E., BLAKE, T. A., HENAGER, C. H., HU, S., JOHNSON, T. J., MEIER, D. E., PEPER, S. M. & SCHWANTES, J. M. 2013. Investigation of the polymorphs and hydrolysis of uranium trioxide. *Journal of Radioanalytical and Nuclear Chemistry,* 296**,** 105-110.
TELLE, H. H., UREŅA, A. G. & DONOVAN, R. J. 2007. *Laser chemistry: spectroscopy, dynamics and applications*, John Wiley & Sons.
THOMAS, R. 2013. *Practical guide to ICP-MS: a tutorial for beginners*, CRC press.
UNSCR. 2004. *Security council resolution 1540 [concerning weapons of massive destruction* [Online]. UN Security Council. Available: https://www.refworld.org/docid/411366744.html [Accessed 12 December 2020].
VARGA, Z., KATONA, R., STEFÁNKA, Z., WALLENIUS, M., MAYER, K. & NICHOLL, A. 2010a. Determination of rare-earth elements in uranium-bearing materials by inductively coupled plasma mass spectrometry. *Talanta,* 80**,** 1744-1749.
VARGA, Z., NICHOLL, A., WALLENIUS, M. & MAYER, K. 2012. Development and validation of a methodology for uranium radiochronometry reference material preparation. *Analytica chimica acta,* 718**,** 25-31.
VARGA, Z. & SURÁNYI, G. 2007. Production date determination of uranium-oxide materials by inductively coupled plasma mass spectrometry. *Analytica chimica acta,* 599**,** 16-23.
VARGA, Z., WALLENIUS, M. & MAYER, K. 2010b. Origin assessment of uranium ore concentrates based on their rare-earth elemental impurity pattern. *Radiochimica Acta,* 98**,** 771-778.
VARGA, Z., WALLENIUS, M., MAYER, K. & HRNECEK, E. 2011. Alternative method for the production date determination of impure uranium ore concentrate samples. *Journal of Radioanalytical and Nuclear Chemistry,* 290**,** 485-492.
VARGA, Z., WALLENIUS, M., MAYER, K., KEEGAN, E. & MILLET, S. 2009. Application of lead and strontium isotope ratio measurements for the origin assessment of uranium ore concentrates. *Analytical chemistry,* 81**,** 8327-8334.
VECCHIA, A. M. D., RODRIGUES, P. C. H., RIOS, F. J. & LADEIRA, A. C. Q. 2017. Investigations into Pb isotope signatures in groundwater and sediments in a uranium-mineralized area. *Brazilian Journal of Geology,* 47**,** 147-158.
VESTERLUND, A. 2016. *Gamma Spectrometric Measurements of Nuclear Material for Nuclear Forensic Purposes.* Chalmers Tekniska Hogskola (Sweden).
VESTERLUND, A. 2019. *Method Development for Signatures in Nuclear Material for Nuclear Forensic Purposes.* Chalmers University of Technology.
VILTA, M. 2016. NexION 300 ICP-MS instruments animation. Perkin Elmer Inc. Shelton.
WALLENIUS, M., LÜTZENKIRCHEN, K., MAYER, K., RAY, I., DE LAS HERAS, L. A., BETTI, M., CROMBOOM, O., HILD, M., LYNCH, B. & NICHOLL, A. 2007. Nuclear forensic investigations with a focus on plutonium. *Journal of Alloys and Compounds,* 444**,** 57-62.
WALLENIUS, M., MAYER, K. & RAY, I. 2006. Nuclear forensic investigations: two case studies. *Forensic science international,* 156**,** 55-62.

WILLIAMS, A. N. 2016. *Measurement of Rare Earth and Uranium Elements Using Laser-Induced Breakdown Spectroscopy (LIBS) in an Aerosol System for Nuclear Safeguards Applications*, Virginia Commonwealth University.

WINDE, F. & STOCH, E. 2010. Threats and opportunities for post-closure development in dolomitic gold mining areas of the West Rand and Far West Rand (South Africa)–a hydraulic view Part 1: Mining legacy and future threats. *Water SA,* 36.

YANG, X., HAO, Z., YI, R., LI, J., YU, H., GUO, L., LI, X., ZENG, X. & LU, Y. 2017. Simultaneous determination of La, Ce, Pr, and Nd elements in aqueous solution using surface-enhanced laser-induced breakdown spectroscopy. *Talanta,* 163**,** 127-131.

YU, K.-Q., ZHAO, Y.-R., LIU, F. & HE, Y. 2016. Laser-induced breakdown spectroscopy coupled with multivariate chemometrics for variety discrimination of soil. *Scientific reports,* 6**,** 1-10.

ZAKARIYA, N. I. 2016. *Development of nuclear-radiological facility monitoring system.* Cape Peninsula University of Technology.

ZSIGRAI, J., NGUYEN, T. C. & BERLIZOV, A. 2015. Gamma-spectrometric determination of 232U in uranium-bearing materials. *Nuclear Instruments and Methods in Physics Research Section B: Beam Interactions with Materials and Atoms,* 359**,** 137-144.

ZWANE, T. 2018. *Nuclear Terrorism as a possible threat to Africa.* University of Pretoria.